Dissertations   UMSL Graduate Works

6-20-2014

Spatial Mapping of Macular Pigment Optical Density and Its Relationship to Contrast Sensitivity and Glare Disability

Christopher Michael Putnam
University of Missouri-St. Louis

Follow this and additional works at: https://irl.umsl.edu/dissertation

Part of the Optometry Commons

Spatial Mapping of Macular Pigment Optical Density and Its Relationship to Contrast Sensitivity and Glare Disability

Christopher Putnam
O.D., Optometry, Pacific University, 2005
B.S., Biology, South Dakota State University, 2000

A Dissertation submitted to The Graduate School at the University of Missouri-St. Louis in partial fulfillment of the requirements for the degree Doctor of Philosophy in Vision Science

June 2014

Dissertation Committee
Carl Bassi, PhD
Chairperson

Erwin Wong, OD, PhD

Gary Bachman, OD, MS

William McAlister, OD, MA, MPH

ACKNOWLEDGEMENTS

TABLE OF CONTENTS

LIST OF FIGURES

LIST OF TABLES

Abstract

Macular pigment (MP) is the shared term for three xanthophyllic- carotenoids: lutein, zeaxanthin, and meso-zeaxanthin, which, relative to human serum concentrations, are highly concentrated in the central macula. The term macular pigment optical density (MPOD) refers to a quantifiable (typically in log units) value of the peak optical absorption density of MP in the central retina. MP alters the spectral composition of incident light due to its anatomic position relative to the photoreceptors. In addition to its short wavelength filtering properties, MP also exhibits potent antioxidant properties that have become the subject of interest for a wide range of retinal conditions, most notably, age-related macular degeneration.

Recently, a number of studies have focused their efforts on the spectral properties of MP and its relationship with visual performance. These studies have demonstrated a correlation between central MPOD and visual performance measures including contrast sensitivity (Hammond et al., 2012 and Loughman et al., 2012), glare disability (Hammond et al., 2012 and Loughman et al., 2010), temporal sensitivity function (Renzi et al., 2010), glare discomfort (Stringham et al., 2011), and photostress recovery time (Stringham et al., 2007 and 2008). All of these visual performance metrics were measured at central fixation.

No published studies have examined the relationship between visual performance and MPOD at parafoveal locations where MP levels are lower. The

objectives of this project were to explore the relationship of the MPOD spatial profile with measures of contrast sensitivity, specifically glare sensitivity, at foveal as well as parafoveal locations out to 6^0 of eccentricity in order to better understand the role of the MPOD spatial profile on measures of visual performance.

In pursuit of demonstrating the parafoveal relationship of MPOD and visual performance, a novel device capable of measuring MPOD across the central 16^0 of retina along 8 principle meridians using customized heterochromatic flicker photometry (cHFP) to determine MPOD (e.g., Bone et al., 2004) at foveal eccentricities of 0°, 2°, 4°, 6° and 8° using a 1° stimulus diameter was built. MPOD was calculated as five different values: [1] Stimulus center discrete value, [2] Stimulus center integrated across 1°, [3] Stimulus point at highest retinal sensitivity integrated across 1°, [4] area under the curve (AUC) using stimulus center across 16° and [5] AUC using stimulus point at highest retinal sensitivity across 16°.

Visual performance was assessed as contrast sensitivity (CS), glare disability (GD), relative glare disability (RGD) and intraocular scatter. CS was measured using vertical grating stimuli presented at foveal eccentricities of 0°, 2°, 4°, 6° and 8° using a 1° stimulus diameter. GD was calculated as a difference in CS between glare and no glare conditions ($CS_{No\ Glare} - CS_{Glare}$) using the same vertical grating stimuli presented at the same foveal eccentricities. RGD [($CS_{No\ Glare} - CS_{Glare}$) / $CS_{No\ Glare}$] was calculated to isolate the glare attenuation effects

of MPOD by controlling for CS variability among the subject sample. Intraocular scatter was assessed through a direct compensation method using a commercially available device. Statistical analysis of the discrete and integrated MPOD associations with CS, GD, RGD and intraocular scatter were evaluated.

Macular Pigment Spatial Distribution

The cHFP identified reliable MPOD spatial distribution maps demonstrating a 1st order exponential decay curve as a function of increasing eccentricity with a r^2 value of 0.886 when fit to stimulus center and a r^2 value of 0.907 when fit to stimulus point at highest retinal sensitivity. Correlation values at each foveal eccentricity were highly significant (2° r = 0.955-0.968, p<0.001 / 4° r = 0.928-0.947, p<0.001 / 6° r = 0.875-0.929, p<0.001) suggesting symmetrical MPOD distribution along the four measured meridians. OriginPro9 software was used to create a Lorentzian distribution across the 16° macula for each subject. Individual Lorentzian distributions were also integrated across the 1° stimulus diameter at each measured retinal loci and across the 16° macula assuming both stimulus center and stimulus point of highest retinal sensitivity. Kurtosis calculations for each MPOD spatial distribution were calculated showing a range of -0.763 (highly platykurtic) to 7.154 (highly leptokurtic). Although overall MPOD spatial distribution shows a Lorentzian distribution, substantial variability exists among individual distributions.

Contrast Sensitivity and Glare Disability across the Macula

CS and GD were measured and RGD was calculated at 0°, 2°, 4° and 6° of foveal eccentricity for vertical grating stimuli of 3, 6 and 9 cycles per degree (cpd) along nasal, temporal, superior and inferior meridians. CS for all three spatial frequencies showed consistent trends as a function of eccentricity. Stimuli at 3cpd showed the highest CS with the lowest variability at all retinal loci measured. Stimuli at 9cpd showed the lowest CS with the highest variability at all retinal loci measured. Among all spatial frequencies measured, significant differences between horizontal and vertical meridians were identified. GD showed a general trend with increasing foveal eccentricity. At each spatial frequency, GD increased as a function of increased foveal eccentricity with more subjects following the expected trend using 9cpd stimuli (25 of 33 subjects) than 3cpd stimuli (21 of 33 subjects). When glare attenuation effects were isolated by calculating RGD, the trend of increasing RGD as a function of increased foveal eccentricity was higher using 9cpd stimuli (28 of 33 subjects) than 3cpd stimuli (24 of 33 subjects) supporting a possible influence of spatial frequency on resulting RGD.

Relationship between MPOD, CS, GD and Intraocular Scatter

Overall, no significant correlation between MPOD and CS was demonstrated using 3, 6 or 9cpd stimuli. Quartile analysis of CS at 0°, 2°, 4° and 6° using 3, 6 and 9cpd stimuli showed non-significant differences between the highest and lowest peak foveal MPOD values.

Using 3cpd stimuli, non-significant correlations were demonstrated between peak foveal measures of MPOD and both GD and RGD at 0°, 2°, 4° and 6° of foveal eccentricity. Non-significant correlations were also found between corresponding retinal loci of calculated MPOD and both GD and RGD (i.e. 2° MPOD vs. 2° GD and RGD). However, quartile analysis found significant differences at 2° and 4° RGD between the highest and lowest peak foveal MPOD values.

Using 6cpd stimuli, significant correlations were demonstrated between peak foveal measures of MPOD and RGD at 0° and 2° of foveal eccentricity. Non-significant correlations were found between corresponding retinal loci of calculated MPOD and both GD and RGD. Quartile analysis found significant differences 0°, 2° and 4° RGD between the highest and lowest peak foveal MPOD values.

Using 9cpd stimuli, significant correlations were demonstrated between peak foveal MPOD measures and GD at 0° and 2° foveal eccentricities and RGD at 0°, 2° and 4° foveal eccentricities. Significant correlations were also identified between corresponding retinal loci of calculated MPOD measures and both GD and RGD at 2° and 4° foveal eccentricities. Quartile analysis found significant differences 0°, 2° and 4° GD and RGD between the highest and lowest peak foveal MPOD values.

Intraocular scatter correlations between peak foveal MPOD measures and integrated MPOD across 16° macula demonstrated non-significant values. However, quartile analysis of intraocular scatter showed a significant difference (t = -2.715, p=0.015) between the highest and lowest peak foveal MPOD measures.

In summary, peak foveal MPOD revealed the highest correlation coefficients with RGD using 9cpd stimuli. These results possibly support a spatial frequency association on the glare attenuation effects of MP. Further support of a spatial frequency association may be seen form the significant correlations between corresponding parafoveal MPOD measures and both GD and RGD at 2° and 4° of foveal eccentricity. Additionally, all calculated measures of peak foveal MPOD shared similar significant correlation coefficients with both GD and RGD using 6cpd and 9cpd stimuli. These results indicate that discrete and integrated measures of MPOD are similar in regards to their association with glare attenuation effects across the macula. Intraocular scatter resulting from incident light is primarily induced at the cornea and lens before reaching the retina. The ocular media influences prior to absorption by MP are the likely explanation for non-significant correlations between peak foveal MPOD measures and 16° integrated measure across the macula with intraocular scatter. However, the significant differences in intraocular scatter values between the highest and lowest peak foveal quartiles indicate MPOD may minimize scattered intraocular short-wavelength light albeit to a lesser degree than the cornea and lens.

I. MACULAR PIGMENT

A. Composition and Anatomic Location

Macular pigment (MP) is the shared name for 3 isomeric carotenoids: lutein (L), zeaxanthin (Z), and meso-zeaxanthin (MZ) which characterizes roughly 36%, 18%, and 18% of total retinal carotenoid content, respectively (Beatty et al., 1999). The remaining 28% of macular carotenoids are comprised of metabolic isomers including 3'-oxolutein and 3-methoxyzeaxanthin (Landrum et al., 1997). The level of carotenoids comprising MP within the retina rises more than 1000X above levels found in serum (Landrum et al., 1997), suggesting a specific role in human vision.

MP is distributed across the retina with a peak density in the central 1^0 of the macula with an exponential decay function falling to optically undetectable levels around 8° of foveal eccentricity (Hammond et al., 1997). Trieschmann et al. (2008) found that the density and distribution of MP differs among individuals and that spatial distribution measurements did not show a significant relationship with peak MP density found at the fovea. This finding may underscore the importance that any MP measurement method must account for the density of foveal MP levels as well as the spatial distribution profile.

Within the retina, L and Z are localized predominantly in the outer and inner plexiform layers of the retina (Snodderly et al., 1984) and in the outer segments of the photoreceptors (Sommerberg et al., 1999 and Rapp et al., 2000). MP

location and distribution within the retina was later confirmed by Trieschmann et al. (2008): L and Z are incorporated at the location of the fovea within the outer plexiform layer, or Henle fiber layer, which is comprised of cone receptor axons and in the parafovea within the inner plexiform layer of the retina. Gass et al. (1999) postulated that a layer of Müller glial cells exists between the internal limiting membrane and the Henle fiber layer specifically at the base of the foveal depression. Recently, work performed by Reichenbach et al. (2013) identified a relationship between Müller glial functions and MP deposition and transport within the central macula. A paper published by Westrup et al. (2014) posited that it is an association between Müller glial cells in the foveola and cone axons in the fovea extending to the macula which produces the spatial distribution pattern of MP.

L is found in greater levels within the peripheral retina as the ratio of L:Z changes from approximately 1:2.4 at the fovea to 1.8:1 in the parafovea to 2.7:1 in the peripheral retina (Bone et al., 1988 and Bone et al., 1997). The inversion of the L:Z ratio with eccentricity parallels the rod:cone ratio demonstrated by Osterberg (1935) and Curcio et al. (1990) suggestive of a possible underlying process which promotes structure-specific accumulation (Bone et al., 1988). Bone et al. (2007) suggested that MP spatial distribution is highly correlated with cone photoreceptor distribution possibly indicating a role in cone function. Nolan et al. (2008) proposed that foveal anatomical structure directly influences L and Z distribution. Their results found that foveal levels of MP integrated under the

spatial distribution curve shared a significant relationship with foveal width measured as both foveal crest to foveal crest (r = 0.32, p <0.05) and absence of nerve fiber layer (r = 0.41, p<0.01). Westrup et al. (2014) hypothesized that the density differences of photoreceptor axons at the foveal center versus the parafovea underlies the spatial distribution pattern of MP. Their findings support that the foveal peak of MP is due to the Müller glial cells and the spatial distribution decline of MP is a result of the higher density of photoreceptor axons within the Henle fiber layer creating an integration of two structures incorporating L and Z: Müller glial cells in the foveal center and the Henle fiber layer in the parafovea producing a monotonous, exponential decline with eccentricity.

Proposed xanthophyll-binding proteins demonstrating a presence in cones as well as rods were explored by Handelman et al. (1991). Their findings supported a L and Z specific deposition process within primate retinal tissue using high performance liquid chromatography techniques compared against microdensitometry. Bhosale et al. (2004) confirmed a selective biologic mechanism in Z integration within the retina. Their work demonstrated the pi-isoform of glutathione *S*-transferase (GSTP1) as a Z-specific binding protein showing the highest levels within the outer and inner plexiform layers of the human retina. Bhosale et al. (2009) identified and later confirmed by Li et al. (2011), a membrane-associated lutein-binding protein (StARD3) and showed specific presence of this lutein-binding protein within the rod and cone inner segments along with an increased occurrence within the Henle fiber layer.

The only other xanthophyll existing at substantial levels within the macula region is meso-zeaxanthin (MZ) (Bone et al., 1993 and Landrum et al., 2001). MZ is a stereoisomer of zeaxanthin that is not found in significant amounts within a traditional Western diet and is not readily detectable in the serum through conventional HPLC assays. Bone et al. (1997) proposed that a process may be found in cone axons which may allow L to undergo isomeric conversion to MZ and was later confirmed by Bhosale et al. (2007) demonstrating that MZ is a metabolic isomer of L in primate models. This pathway may help to explain the prevalence of Z relative to L at the fovea supported by a nearly 1:1 foveal:peripheral ratios of (L+MZ)/Z originally identified by Bone et al. (1997).

L and Z are not produced *de novo* and therefore only available through dietary intake. The bioavailability of xanthophyllic carotenoids depends on their chemical matrix within the dietary source and ester bonds at xanthophyll hydroxyl groups (Schalch et al., 2007). A number of studies have evaluated the MP response to oral supplementation with L and Z (Bone et al., 2003, Schalch et al. 2007, Trieschmann et al., 2007, Richer et al., 2011). Although serum levels of L and Z generally correlated with MP, differences in retinal L and Z concentrations within the population may offer further support of specific physiologic pathways that regulate the retinal uptake of L and Z. For example, L is the dominant xanthophyll relative to Z in almost all food sources with only a few rare exceptions including orange and red peppers (Perry et al., 2009). However, studies have shown that this abundance of dietary L is almost never reflected within central retinal

measures of MP (Bone, 1997). It is likely that individual metabolic processes such as specific protein binding, serum lipoprotein profiles and body composition account for the L and Z levels of MP distribution.

B. Function

Proposed functions of MP are derived from the anatomical characteristics and the specific biochemical structure of L and Z. The effects of L and Z on short wavelength (SW) visible light absorption and their respective antioxidant properties have been investigated in a number of studies. Within the realm of current literature, three primary roles for the function of MP have been described: Protection, Optical, and Neural Efficiency. All three proposed functions derived their hypotheses directly from structural attributes and physiological characteristics MP.

1. Protection Hypothesis

The proposed protective hypothesis of MP depends upon its chemical structure as well as its spectral absorption properties. Carotenoids in general are recognized for their antioxidant and free radical scavenging properties (Krinsky, 1989). The exact pathogenesis of age related macular degeneration remains uncertain although current models implicate a combination of cumulative damage from reactive oxygen intermediates (ROIs) created through metabolic processes and high energy, short wavelength light and chronic inflammation (Hollyfield et al., 2008). O'Connell et al. (2006) provided a review of the two primary roles of

macular carotenoids of specific importance in terms of their recognized tissue protective effects: 1) Antioxidant function and 2) SW light filtration.

Antioxidant Function

Carotenoids, including L and Z, have demonstrated the ability to reduce singlet oxygen (Krinsky et al., 1989), moderate ROIs (DiMacio et al., 1989), inhibit cell membrane perioxidation (Lim et al., 1992) and reduce lipofuscin formation (Sundelin et al., 2001). The presence of L and Z within the photoreceptor outer segments and retinal pigmented epithelium offers further support of the ROI and singlet oxygen reducing properties of MP (Sommerburg et al., 1999 and Rapp et al., 2000).

Khachik et al. (1997) were able to provide the first evidence of oxidative products of MP within retinal tissue indicating metabolic oxidation-reduction events. These results showed definitive L and Z antioxidant activity within retinal tissue. L and Z antioxidant properties are derived from their ability to quench singlet oxygen and inhibit peroxyl radicals (Paiva et al., 1999). These antioxidant functions are based on the number of conjugated double bonds and hydroxyl end groups. L and Z have been confirmed to inhibit light-induced oxidative damage within retinal tissue (Beatty et al., 1999). Their study showed that metabolic oxidative products including singlet oxygen, free peroxyl radicals, and ROIs are attenuated in the presence of L and Z.

Krinsky et al. (2003) and Stahl et al. (2003) further explored the antioxidant

mechanism of L and Z. They identified various free radicals are created under

oxidative stress conditions found in retinal tissue and of these, xanthophyllic

carotenoids show the greatest efficiency with reactions involving peroxyl radicals.

These peroxyl radicals are the result of lipid peroxidation and the free radical

scavenging abilities of L and Z attenuates the progression of damage to lipophilic

structures (Landrum, 2013). In a number of animal models, SW light exposure

may lead to the development of ROIs which have the potential to damage

biologic tissues at a molecular level and negatively affect subcellular structures,

cells and tissues (Polidori et al., 2001 and Krutmann, 2000).

Carotenoids can quench the destructive properties of free radicals by either

providing an electron to the free radical itself or incorporating the free radical into

its own molecular structure through a covalent bond to pair the single electron.

The molecular nature of the carotenoid structure attracts free radicals ultimately

providing protection from oxidative damage to cellular lipids, proteins, and DNA

(Stahl et al., 2003).

Yeum et al. (2004) furthered the understanding of the antioxidant efficacy of

xanthophyllic carotenoids. Their study, along with results from Semba et al.

(2003), identified the polar end-groups of L and Z as a primary source of their

effectiveness. These polar end-groups project outside the cell membrane into

both the intracellular and extracellular plasma allowing enhanced interaction with

ROIs. This unique membrane insertion enhances the antioxidant properties of L

and Z within the photoreceptor outer segment which has a significant membrane

surface area subject to oxidative reactions (Semba et al., 2003). L and Z show a

high affinity to lipid containing structures and, along with their efficiency in peroxyl

radical mitigation, carotenoids may serve a critical role in cell membrane

protection and oxidative damage (Stahl et al., 2005).

Short Wavelength Light Filtration

SW light damage at high intensity within the retinal tissue has been extensively

documented (Ham et al., 1976). At wavelengths of 450nm, nearly 100X less

energy is required to produce retinal injury compared to wavelengths greater

than 590nm. Ham et al. (1979) demonstrated the severity of light-induced injury

to retinal cells. Their work revealed that the severity of retinal damage caused by

high energy, SW light can be expressed as a function of wavelength. They

described an exponential increase in the severity of retinal damage as the

wavelength of the source decreased. Ham et al. (1984) and Noell (1980)

evaluated a bandwidth for visible SW light induced retinal damage. Their studies

identified increased risk of retinal injury at wavelengths between 400-450nm.

This action spectrum bandwidth for SW induced damage shows considerable

overlap with the previously established absorption spectrum of MP of 400-

500nm.

SW light generated by an intraocular operating biomicroscope has been recognized to create retinal lesions that demonstrate a lesser degree of injury in affected areas corresponding to higher levels of MP (Michels et al., 1992) and identified macular sparing from light-induced retinal lesions relative to surrounding non-macular retinal tissue (Jaffe et al., 1988).

Snodderly et al., (1984a) proposed three reasons that L and Z are capable of providing an optical filter of SW visible light: 1) the absorbance spectrum of macular pigment has a peak at 460nm which falls within the short wavelength portion of the visible light spectrum. 2) MP is at its highest levels within the cone axon layers (primarily Henle's fiber layer) of the retina. This prereceptoral anatomic location allows MP to employ its absorptive properties on SW visible light prior to incidence on the photoreceptors. 3) MP is found not only within the axon layers of the retina but also within the outer segments of the photoreceptor membrane itself. The presence of MP within the photoreceptor membranes may provide additional SW light optical filtration to adjacent cells as a result of the anatomic path followed by the axon projection to more anterior layers (Whitehead et al., 2006). Using the absorbance formula applied with spectroscopy measurements [$A=\log_{10}(I_o/I)$], Snodderly et al. (1984b) postulated that macular carotenoids are capable of decreasing incident blue light by approximately 40%, assuming their study sample mean central MPOD.

Sujak et al. (1999) demonstrated that L and Z are incorporated into the liposome bilayer at different orientations. Z was identified in a vertical orientation with respect to the membrane layer while L was incorporated in both a vertical and horizontal orientation. Differences in both SW absorption and antioxidant properties may be attributed to these differences in orientation. Junghans et al. (2001) identified L as a superior filter of SW light relative to Z. They posited that the higher optical filtration efficiency of L was a result of the both parallel and perpendicular orientations found within photoreceptor membranes compared to Z which has only a perpendicular membrane orientation. A likely result of the two orthogonal orientations of L within the lipid membrane is an improved capture of incident SW light. L and Z are located in an anatomically ideal location to attenuate incident SW light and may preclude the photosensitization of retinal tissue and the formation of ROIs. The SW attenuation provided by L and Z can be viewed as an indirect protective function (Bernstein et al., 2010).

The Protection Hypothesis is comprised of two primary elements: antioxidant functions and SW light filtration. These two elements are not mutually exclusive and likely act in a synergistic fashion. Clinical conditions resulting in annular maculopathy including maculopathy resulting from use of photosensitizing drugs are described by central retinal degeneration in an annular pattern which surrounds but spares the 1° foveal region corresponding to the diameter of highest MPOD (Weiter et al., 1988). Foveal sparing may be a result of the free radical scavenging and oxidative damage inhibition properties demonstrated by

MP. Foveal sparing has also been documented in advanced cases geographic atrophy associated with AMD (Schatz et al., 1989 and Sunness et al., 1999).

Haegerstrom-Portnoy (1988) published results documenting a loss of SW cone sensitivity with age. Their study identified less SW sensitivity loss in the fovea where MP is at the highest levels compared to non-foveal areas. Hammond et al. (1998) also found photopic sensitivity was related to MP in subjects aged 60-84 years. Their study demonstrated a significant relationship for both 550nm ($p < 0.01$) and 440nm ($p < 0.001$). However, older individuals (ages 60-84) with the highest levels of MP had visual sensitivity levels that were not significantly different from younger individuals (ages 24-36). Older individuals with the lowest levels of MP had significantly different visual sensitivity levels than younger subjects. Their results support a visual sensitivity relationship and suggest that potential retinal protection may be offered by MP.

A case-control study performed by Bone et al. (2001) utilized donor retinas from 56 individuals diagnosed with age-related macular degeneration (AMD) and 56 control donors without evidence of AMD. Three concentric regions of retina, an inner region of 0° to 5°, a middle region of 5° to 19° and a peripheral region of 19° to 38° were analyzed for L and Z concentration using high performance liquid chromatography (HPLC). The differences in L and Z content between controls and AMD donors were greatest at the inner region and decreased with eccentricity. A logistic regression analysis showed that individuals with the

highest levels of L and Z concentrations had an 82% risk reduction for AMD than those with the lowest levels when controlling for both age and gender. The Lutein Antioxidant Supplementation Trial (LAST) (Richer et al., 2004) was one of the first large scale prospective placebo controlled trials to identify a significant link between AMD, lutein supplementation, and visual performance. Treatment groups received one of three possible conditions: lutein, lutein plus antioxidants or a placebo. MPOD measured at the end of a 12-month trial showed a mean increase of nearly 0.09 optical density units from baseline measurements and improved visual acuity as well as contrast sensitivity. The NIH-sponsored Age-Related Eye Disease Study 2 (AREDS2) is the largest multi-center, longitudinal, placebo-controlled, randomized clinical trials performed using lutein and zeaxanthin supplementation. The study encompasses 2 of the 3 hypotheses of MP by using a primary outcome measure as rate of progression to advanced AMD (Protection Hypothesis) and a secondary outcome measure of cognitive function (Neural Hypothesis). Results for the AREDS2 indicated a 10% reduction in progression to advanced AMD when L and Z were added to the original AREDS formula. When L and Z were substituted in place of β-carotene, results identified an18% risk reduction in advanced AMD within 5 years and a 22% risk reduction in neovascular AMD within 5 years. The authors of AREDS2 acknowledged that a potential competitive inhibition of carotenoids may have occurred when both beta-carotene and L and Z were incorporated within the original AREDS formulation.

Growing evidence indicates that the Protection Hypothesis is better supported by the shape of the MP spatial distribution rather than the MP peak density (Wenzel et al., 2006 and Stringham et al., 2010). Peak MPOD is typically measured at the fovea or central 1^0 of retina. Large variations in spatial distribution across the remaining macula are not reported in foveal measurements which may overlook important differences in a total integrated MP versus a single peak MP value. As both an antioxidant and SW visible light filter incorporated into the photoreceptor axon membrane, L and Z would likely confer greater benefits distributed across the macula as opposed to a single, central, isolated peak. Evidence of an association between MPOD spatial distribution and an increased risk of age-related macular degeneration has been described in the literature (Kirby et al., 2010). The characteristics of L and Z that confer protective benefits in retinal disease may be the same characteristics that are able to confer optical benefits to both foveal and parafoveal areas.

2. Optical Hypotheses

The origins of the Optical Hypothesis were first posited by Walls and Judd (1933) in reference to 'oil-droplet filters of a carotenoid nature' which were associated with cone photoreceptors. The ellipsoid containing the oil droplet is located at the distal end of the inner segment which covers the outer segment. This positioning allows a majority of incident light to pass through it before reaching the visual pigment. Later, Nussbaum et al. (1981) advanced the Optical Hypothesis in

which MP is specifically referenced. Both summaries shared common ideas for the principle functions of an "Optical Hypothesis". These principle functions are:

1) The improvement visual acuity by a reduction of chromatic aberration

2) The promotion of comfort by a reduction of glare

3) The improvement of detail by atmospheric blue-haze absorption

4) The enhancement of contrast by selective short wavelength light attenuation

Separate, but not mutually exclusive from the Protection Hypothesis, the Optical Hypothesis posits MP filters SW visible light causing an attenuation of chromatic aberrations and SW light scatter. Related to the SW attenuation properties, MP has been described as a dichroic filter exhibiting selective absorption of plane polarized light.

The primary focus of the Optical Hypothesis is the theory that MP enhances visual potential through optical filtration effects due to its pre-receptoral location within the inner layers of the macula. The multi-faceted theory of the Optical Hypothesis of MP encompasses several mutually dependent physiological and optical roles. In general, the Optical Hypothesis can be broken down into separate, interrelated components: the Acuity Hypothesis, the Glare Hypothesis, and the Visibility Hypothesis.

i. Acuity Hypothesis

Engles et al. (2007) provided a review of the origins of the Optical Hypothesis. First formally proposed in 1866 by German anatomist Max Schultze, the Optical Hypothesis postulated that MP may enhance visual acuity by facilitating a reduction of short wavelength aberrations through absorptive properties. Schultze contended that the selective wavelength absorption of MP helped to limit chromatic aberration. Discussed as the "Acuity Hypothesis" by Wooten et al. (2002), it was been proposed that MP improves acuity by screening both scattered and aberrated SW visible light that would otherwise degrade image quality.

The first empiric measurements to review Shultze's theory were conducted by Reading and Weale (1974). They initially calculated the resulting blur circle due to the chromatic aberration of natural sunlight. Using the derived aberration data, they were able to derive the spectral transmission of an ideal filter that would diminish the SW portion of visible light to near threshold levels at the same time maximizing remaining light transmission. The resulting transmission characteristics closely resembled the spectral absorption of MP. Reading and Weale then used the resulting filter combined with psychophysical data associated with chromatic aberration and visual thresholds. From this, they determined levels of macular pigment sufficient to decrease the violet (SW) portion of a white disc to subthreshold levels and theoretically improve visual acuity.

Campbell and Gubisch (1966) also measured visual acuity using broadband light versus monochromatic light under photopic conditions and found that chromatic aberration accounts for ~50% of the variance between physical and psychophysical assessments of the human eye's optical quality. Yoon and Williams (2002) repeated the Campbell and Gubisch experiment using strict controls and measuring acuity as well as contrast sensitivity. Their results demonstrated that at spatial frequency greater than 6cpd, using narrow-band light increased acuity measurements by a factor of approximately 1.2-1.5. However, neither experiment measured associated MPOD. Therefore, if normal optical density of a subject is assumed, the initial contention of Reading and Weale (1974) is supported and any additional reduction in SW visible light would be largely superfluous and additional improvement in visual acuity would be non-significant. This same interpretation has been documented in numerous studies that document specific bandwidth filters (e.g. yellow filters) in general, may improve contrast sensitivity and decrease glare but do not improve spatial resolution (Wooten et al., 2002 and Eperjesi et al., 2002).

Engles et al. (2007) reviewed chromatic aberration effects and summarized that refractive error with a wavelength dependence will affect retinal image quality of a polychromatic stimulus to the greatest degree at wavelengths below 500nm. The authors cited Howarth et al. (1986) which stated SW light defocus can reach 1.6D at 420nm and approximately 1.2D defocus at 460nm. The characteristics of chromatic aberration are wavelength dependent image degradation (e.g.

longitudinal chromatic aberration) and wavelength dependent image position (e.g. lateral chromatic aberration). Each of these components decreases the retinal image quality, however; longitudinal chromatic aberration tends to be the dominant component in a typical eye. Empirical studies performed by Kaiser (1988) show that for each additional diopter of retinal image degradation, visual acuity falls by a factor of nearly two.

Engles et al. (2007) created an empiric evaluation of the Acuity Hypothesis by direct comparison of macular pigment optical density and both resolution acuity and hyperacuity. Previous studies (Yoon et al., 2002 and Wooten et al., 2002) had evaluated resolution acuity but Engles et al. extended the hypothesis to include hyperacuity. The authors' position to include hyperacuity was that it characterizes the highest level of spatial discrimination and may be the first to exhibit improvements with the elimination of image degradation. Their study utilized solid black targets presented on a white background with a peak wavelength of 460nm or a yellow background with a peak wavelength of 570nm. Results revealed no significant correlations between MP and acuity, either resolution or hyperacuity, in either background condition. Engles et al. also evaluated a standard observer's V(λ) curve as it related to optical defocus centered on 565nm. They found only a 12% difference in defocus of greater than 0.25D in the 430nm to 510nm region. The authors concluded that macular pigment is not related to resolution acuity or hyperacuity.

ii. Glare Hypothesis

The human visual system is adept at detecting at luminance levels that span approximately 8 orders of magnitude (e.g. Pokorny et al., 2006). Retinal adaptation adjusts the range of visual sensitivity to prevailing luminance. Perceptual difficulties occur when the visual system must adapt to changes across this range. Glare is caused by light entering the eye that does not aid vision and is most commonly luminance that is too intense or variable across the visual field (Mainster et al., 2012). Glare can be evaluated as three distinct forms: disability glare, discomfort glare and dazzling glare. Vos (2003) provides a comprehensive review of the types of glare.

Disability Glare

Disability glare has been defined as loss of retinal image contrast resulting from veiling illuminance or intraocular scatter. Decreased visual performance follows the loss of retinal image contrast as a consequence of increased forward scatter within the eye. Diminution in visual potential may result from both veiling illuminance that reduces the object contrast as well as photopigment depletion and regeneration rates. The origins of disability glare support a dependence on the overall luminance and wavelength created by a glare source (Aslam et al., 2007). Forward scattering or straylight is not the primary cause of disability glare symptoms in all cases. At smaller angles of incidence, neural inhibition at the level of the retina can add to disability glare through retinal gain models (van den Berg et al. 1991).

Increased MPOD will not affect glare disability when the wavelength of the stimulus and the wavelength of the background are the same (Stringham et al., 2007). If MP absorbs SW light from the stimulus and background in equivalent amounts, the ratio will remain comparable regardless of the MP density level. In this instance, high MPOD may diminish visual discomfort but it will not increase stimulus visibility (Renzi et al., 2010a and Wenzel et al., 2006). Strictly speaking, MP filters the veiling luminance of the target at the retinal plane proportional to the MPOD for SW light.

Discomfort Glare

Discomfort glare has been characterized as exacerbation or generation of pain as a consequence of light exposure which does not necessarily impair object visibility. Digre and Brennan (2012) defined photophobia as 'a sensory state in which light causes discomfort in the eye or head possibly involving an avoidance reaction without overt pain'. The authors also drew a distinction with the term photo-oculodynia used to describe light-induced pain from a normally non-painful source such as ambient lighting. According to Lapid-Gortzak et al. (2011), clinical complaints of photophobia resulting from a small posterior capsulotomy following a cataract procedure were associated with increased straylight values. The authors concluded that, in some case, photophobia may be a result of increased intraocular scatter.

Stringham et al. (2003) and Stringham et al. (2004) evaluated the effects of MP

on glare discomfort. Together these two studies showed the degree of visual

discomfort was significantly higher if the glare source contained SW light

compared to mid and long wavelength visible light. Their results further identified

that in subjects with higher levels of MPOD, a greater intensity of SW light was

required to produce an avoidance response. In retinal eccentricities greater than

10^0 where MP levels are non-significant, significantly less intensity of SW light

was required to elicit the same avoidance response.

Dazzling Glare

Dazzling glare is a form of discomfort glare associated with disability glare.

Sheehy (1989) reported the loss in visual performance resulting from

wavelengths within the visible spectrum and detailed the characteristics of eye

protection necessary based on visual performance. It is commonly encountered

as high retinal illuminance across the visual field in scenarios such as expanses

of snow or water and facing the sun when it is low in the horizon (Vos 2003).

Dazzling glare typically results in a light avoidance behavior and is related to

photostress (high retinal illuminance leading to bleaching of photopigments,

afterimages and temporary, reduced retinal sensitivity) and scotomatic glare

(transient visual disturbances usually associated with minimal discomfort).

The Glare hypothesis is derived from the selective filtering properties of MP on

short wavelength light (Stringham et al., 2007). SW light as a significant

contributor to the ocular discomfort and disability related to exposure from a glare

source has been identified in the literature (Stringham et al., 2003 and Mainster

et al. 2012). A 2007 study by Stringham et al. defined the origins of disability

glare as the 'forward scattering of light resulting from illumination at the retina

that directly reduces image contrast '. Their results supported a significant

dependence of disability glare on the overall luminance created by a glare

source. Stringham et al. inferred that the global effects produced by MP optical

filtration are greater under broadband, achromatic light sources in contrast to

narrow-band SW light sources. Importantly, Stringham et al. (2007) recognized

that MP effects on glare disability result from the spectral characteristics of the

light source. Their technique involved the use of a 1^0 grating with a spatial

frequency of 5cpd at 100% contrast as a central stimulus. A xenon arc annulus

with an inner diameter of 11° was adjusted by the subject and the radiance of the

glare source was recorded when the subject reported that the grating was no

longer visible. Their findings demonstrated significance at 440nm (r = 0.36, p =

0.032) and 460nm (r = 0.34, p = 0.039) but non-significance at 550nm and

580nm. Overall, the authors were able to explain 58% of the variance of target

visibility through subject differences in MPOD. MP will not decrease glare

disability if the source does not contain a substantial amount of SW visible light

(Stringham et al., 2007).

These studies support the idea that MPOD plays a role in visual discomfort due

to glare reduction but do not address whether improvements in visual

performance occurs. Stringham and Hammond et al. (2007) performed an empiric study of both photostress and glare disability as they relate to MPOD. Their results revealed a significant correlation of visual thresholds under glare conditions with MP density (r = 0.76, p<0.0001) and photostress recovery time, after exposure to xenon-white light, was significantly lessened for subjects with higher MP levels (r = -0.79, p<0.0001). Results of the study also found that MP displayed a stronger correlation coefficient to both glare disability and photostress recovery in the broadband white testing conditions compared to narrow-band short-wavelength light.

iii. Visibility Hypothesis

The Visibility Hypothesis has its origins from Luria (1972) who demonstrated that resolution threshold for a yellow stimulus on a blue surround is improved when observed through SW-selective filters. The result was later confirmed by Wolffsohn et al. (2000) using contrast sensitivity measurements. A SW specific filter reduces the luminance of blue backgrounds resulting in increased visibility of the yellow stimulus.

The basic theory of the visibility hypothesis was summarized by McCartney (1976). At every point along a line of sight to a point on a distant object, light reflected from the object will interact with particles within the atmosphere and consequently increase light scatter towards the observer. Husar et al. (2000) suggested that, separate from the optical and neurological status of the subject,

scatter due to atmospheric composition is the primary determinant of visual discrimination and range at large distances.

Visibility was defined by Wooten et al. (2002) as the clearness with which objects in the atmosphere stand out from their surroundings. It is the atmospheric composition that guides the visibility hypothesis when considering the physics of light scatter. Light scattering results from particle interactions that occur along an electromagnetic wave path that simultaneously removes energy from the incident wave and emits that energy at a solid angle from the particle. Scattering only occurs when the particle's refractive index differs from the surrounding medium (e.g. smog, haze, and vapor). The amount of scatter depends on the particle type and concentration within the atmosphere. This particle-dependent scatter largely dictates the quality of vision in an outdoor environment. Rayleigh (elastic / small particle) and Mie (inelastic / large particle) scattering are essential theories for describing the effects SW light within the environment (Wooten et al., 2002).

If scatter within the eye is wavelength dependent as it is in the clear atmosphere, then MP may increase the resolution of the retinal image by selectively screening the highly scattered SW visible light. Straylight from the cornea and lens increases with decreasing wavelength showing a Rayleigh type of scattering (van den Berg, 1997) and straylight from fundus reflectance and transillumination decreases with decreasing wavelength (van den Berg et al., 1991). Coppen et al.

(2006) suggested the presence of significant forward scatter of SW light and relatively less backward scatter of SW light to be absorbed by MP.

The Visibility Hypothesis posits that the resolution of a distant object is affected in primarily two ways: 1) Light reflected from an object demonstrates increased scatter along the sight path and 2) Background light energy is scattered into the eye, not directly reflected from the target. Considering the object's visibility against the horizon, an underlying theory of the Visibility Hypothesis suggests that atmospheric scattering reduces the relative contrast of objects (Wooten et al., 2002). Wavelength dependence of object background and wavelength dependence of object are critical components of determining MP influences on the scatter resulting from atmospheric particle interactions referred to as the atmospheric haze coefficient by Wooten and Hammond.

Wooten et al. (2002) summarize the mathematical derivation of the atmospheric haze coefficient by integrating the CIE photopic luminosity function and the spectral energy of the natural illuminant. They proposed that the non-image forming portion of atmospheric light acts as a veiling luminance with respect to the targets seen through it. In addition, Rayleigh scattering influences the atmospheric background wavelength causing SW light to become the dominant wavelength as the viewing distance increases. MP absorbs wavelengths primarily in the 410-520nm range and will have a quantitatively different effect on the SW dominant background versus object wavelength (Snodderly et al., 1984).

The increased retina image resolution described by the Visibility Hypothesis may have its origins in the dichroic properties of MP due to its fundamental anatomic orientation features. Linear dichroism is defined as a difference in absorption of light linearly polarized parallel and perpendicular to an orientation axis (Bengt, 1997). In a 1980 paper, Bone briefly reviewed existing experimental evidence that partial symmetry of L orientation within the retina was created dichroic properties. His work proposed a 'dichroic ratio' investigating the absorption of incident polarized light parallel and perpendicular to the molecule axis. The presence of linear dichroic properties exhibited by the MP supports that a portion of the L orientation must be arranged tangential with respect to the fovea (Mission, 1993). Bone et al. (1985) speculated that Haidinger's brush phenomena are a result of the dichroic properties of L and Z. These identified dichroic properties are likely derived from the perpendicular arrangement of Z and the non-orthogonal positioning of L within the lipid membrane layer referenced above (N'Soukpoe-Kossi et al., 1988). Work by Hemenger (1992) agreed that MP exhibits these dichroic properties and may reduce glare disability through selective absorption of polarized light. Sujak et al. (2000) provided further support that the cone axons projections from the central fovea to form the outer plexiform layer or Henle fiber layer causes both L and Z to display dichroic properties. The perpendicular membrane orientation of both L and Z within the radial projections of the Henle fiber layer may allow specific absorption of plane-polarized light.

3. Neural Hypothesis

L and Z have been studied extensively for their roles in singlet oxygen scavenging and ROI neutralization within retinal tissue (Krinsky et al., 1989 and Khachik et al., 1997 and Paiva et al., 1999). L and Z models have proposed anti-inflammatory properties through modulation of lipoxygenase activity and decrease oxidative stress in high metabolic environments including the RPE (Krinsky et al., 2005).

Anatomically, the retina is an extension of the brain consisting of axons which form the optic nerve and project to both cortical and subcortical locations. Like the CNS, the retina also displays physiologic and immune responses similar to those found within the brain. The brain, like the retina, is susceptible to lipid peroxidation, increased production of ROI and increased levels of oxidative stress as a result of a high metabolic rate. Craft et al. (2004) identified that approximately 66-77% of the total carotenoids found in the brain were L and Z. These concentrations of L and Z were highest within the pons and medulla and cortical structures such as the frontal and occipital lobe. The preferential accumulation of L and Z within CNS tissue supports a potential role in neural function.

Vishwanathan et al. (2012) assessed a primate model of the retinal L and Z levels compared to brain L and Z levels. Their findings showed retinal L was significantly associated with levels of L in the pons, cerebellum and occipital

cortex with marginal significance in the frontal cortex. Macular Z was significantly associated with levels of Z in the cerebellum and frontal cortex with marginal significance in the pons and occipital cortex. The authors suggested that an integrated measure of MPOD has the potential to serve as a biomarker for brain L and Z level.

Early investigation into L and Z by Bernstein et al. (1997) showed that, within neural tissue, L and Z accumulate at the location of the microtubules forming the cytoarchitecture of retinal axons. Crabtree et al. (2001) identified the role of tubulin as a potential binding protein that specifically accumulates L and Z within axon cell membranes. Stahl et al. (2002) recognized that, in addition to structural roles, microtubules can also influence gap junction communication and neural transmission. Gap junction transmission is an important mediator between glial cells and neuron within the retina propagating action potentials. Gap junction communication has also been connected to the transfer of metabolites and electrolytes within the sensory retina. Wieslaw et al. (2004) identified positive metabolic effects of L and Z on the structure and equilibrium of neural membranes through the protein lattice structures formed from tubulin. Hammond et al. (2008) proposed that the physiologic and structural elements of L and Z combined with their conspicuous positioning within the CNS may influence neural processes. Zimmer and Hammond (2007) identified data showing the inverse relationship between MP density and rod-mediated (scotopic) noise hypothesized to originate at the level of the retina.

Akbaraly et al. (2007) identified a link between serum levels of Z and cognitive functioning. Using a Mini-Mental State Examination, Akbaraly et al. showed that participants with cognitive functioning in the lowest quartile had a significant probability of having plasma Z levels in the lowest quartile (OR: 1.97, CI:1.21-3.20). Johnson et al. (2008) demonstrated a significant relationship between L and both verbal fluency and memory scores in women ages 60-80 years in a placebo-controlled trial. Johnson et al. (2013) recognized serum L and Z were related to cognitive function including memory, processing speed, attention, and executive function. In brain sample, L was related lower dementia severity ($p<0.05$). Feeny et al. (2013) identified lower foveal MPOD with reduced performance in individuals over 50 years of age on a range of cognitive tasks including the Montreal cognitive assessment ($p = 0.011$) and a mini mental state assessment ($p = 0.026$).

Decreased L and Z serum levels have also been associated with mild cognitive impairment (MCI) and Alzheimer's disease (AD). Rinaldi et al. (2003) identified decreased levels of serum L in MCI ($p<0.01$) and AD ($p<0.0001$) and decreased levels of Z in MCI ($p<0.01$) and AD (0.0001). Nakagawa et al. (2011) hypothesized that the xanthophyllic carotenoids, specifically L, may inhibit amyloid-β damage to red blood cells and decrease the oxidative injury caused to the brain.

C. Measurement Methods

Widely accepted as the "gold standard" of MP measurement, high performance liquid chromatography (HPLC) has been employed in spatial distribution and quantitative analysis studies (Gellerman, 2004; Brown, 1990). HPLC is used extensively within biochemistry and analytical chemistry to identify and quantify individual components of a substance (Brown, 1990). Unfortunately, the *ex vivo* nature of HPLC measurement prevents application of this technique to a clinical population.

At the very core of an *in vivo* MP measurement lies the matching of spectral absorption curves from L and Z to any method, objective or subjective. The difficulty of this proposition is replicating the *in vivo* environment in an accurate, quantifiable *ex vivo* situation. For example, L and Z show a change in spectral absorption when isolated within ethanol versus lipid-rich preparations (Bone, 1985; Handelman, 1991). The orientation of these molecules also differ in their proposed role in spectral filtration and antioxidant properties, underscoring the importance of understanding the *in vivo* versus *ex vivo* data (Sujak, 1999).

The more recent development of *in vivo* techniques of MPOD measurement has shown great promise using both objective and subjective methods. Objective methods include fundus reflectometry, fundus autofluorescence, resonance Raman spectroscopy, and visually evoked potentials (Howells, 2011). Each of these techniques share the common advantage that all objective measurements

share: Objective results that require minimal patient participation. However, the previously listed objective measurement devices also share significant disadvantages such as minimum required pupil diameter, media opacity considerations (lens clarity), imaging artifacts, need for retinal bleaching to limit photopigment absorption, significant expense and, in the case of resonance Raman spectroscopy, no comparative data (Hammond, 2005).

Subjective methods of *in vivo* MPOD measurement are also commercially available. These include threshold spectral sensitivity, color matching, dichroism-based measurements, minimum motion photometry, apparent motion photometry, and heterochromatic flicker photometry (HFP) (Hammond, 2005). Threshold spectral sensitivity targets the difference spectrum of MP by comparing the spectral sensitivity of the M cone mechanism in the foveal and parafoveal region by isolating a single photoreceptor sensitivity range (Pease et al., 1983). Color matching techniques involves two separate color matches: one performed at the fovea and another performed at 5° of eccentricity. The reference stimulus contains 490nm wavelength desaturated by 650nm wavelength. The reference stimulus is then matched by combining spectral primaries of 460nm, 530nm and 650nm wavelengths. The ratio of the $0^0{:}5^o$ eccentricity color match determines the MPOD (Davies et al., 2002). Dichroism measurements rely on the partial plane polarization effects created by the shared distribution of L and Z orientations within the retinal layers. Dichroic measurements compare the foveal and parafoveal sensitivity against a

dichroism-based spectrum and difference measurements reflect the level of MP (Bone et al., 1992). Minimum motion photometry and apparent motion photometry share underlying perceptual principles: Moving square wave gratings are creating using alternating wavelengths with one wavelength strongly absorbed by MP and the other minimally absorbed by MP. The radiance of the longer wavelength is adjusted by the subject until the motion appears to slow (minimum motion photometry) or reverse (apparent motion photometry). The square wave target is presented at foveal and parafoveal locations and a log ratio of these values determine MPOD (Moreland, 2004).

HFP is the most common and widely studied method of measuring MP (Hammond, 2005). Within existing literature, over 50 publications utilized HFP in their studies of MPOD. This large collection of peer-reviewed work allows for the scrutiny of existing assumptions and further experimental evaluation. For these reasons, effort and resources were focused on HFP.

1. Heterochromatic Flicker Photometry

The ideal method of measuring MPOD depends on the specific application and a consideration of the limitations and assumptions underlying the use of each method. Preferably, the method employed should be capable of generating a spectral curve that can be compared with *ex vivo* template data. Provided below is a macular pigment spectral curve created from data by Wyszecki and Stiles

(1982) Bone et al. (1992), Ruddock (1963), and Pease et al. (1967) identifying

optical density as a function of wavelength
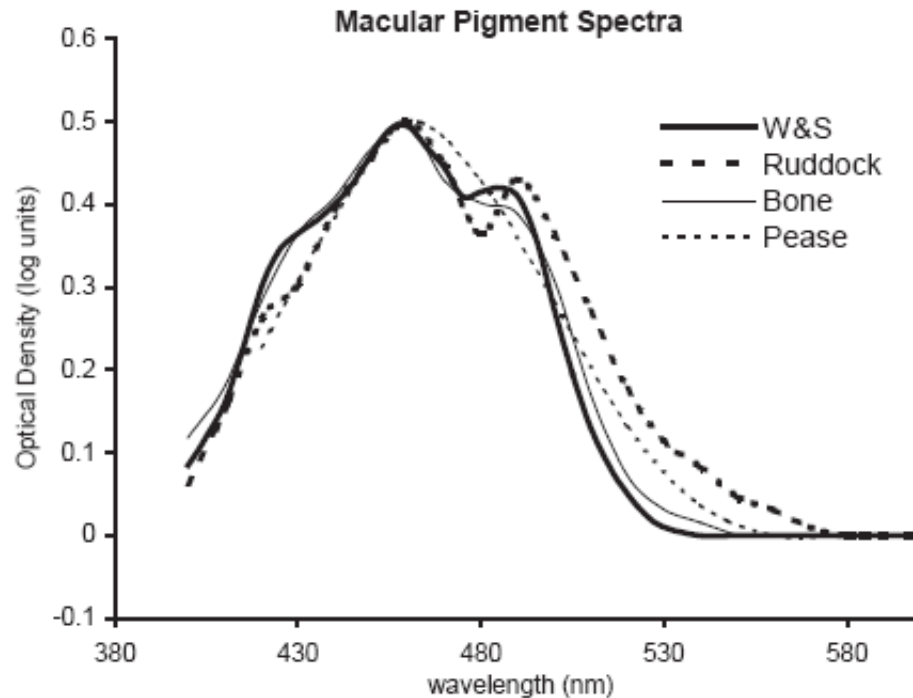
Figure 1
A fitted macular pigment spectral curve created from data by Wyszecki and Stiles (1982) Bone et al. (1992), Ruddock (1963), and Pease et al. (1967) identifying optical density as a function of wavelength.

Like many of the techniques described above, HFP utilizes the known spectral

absorption properties of L and Z in combination with the presumed anatomic

location of MP. HFP determines MPOD by presenting a stimulus of two

alternating narrowband wavelengths at the fovea and a parafoveal location. The

peak wavelengths are selected specifically to maximize macular pigment

absorption (458-476nm) and to minimize macular pigment absorption (530-

575nm). When the two alternating colors are presented at a proper frequency, a

dissimilar luminance of the two wavelengths will be perceived as a flickering light

with a mixture of the two source wavelengths. The radiance of the blue

wavelength is increased by the observer until the flicker is minimized and equiluminance of the blue and green wavelengths is achieved. This procedure is presented at the foveal location then a parafoveal reference location to measure a maximum of MP absorption and a minimum of MP absorption. The tenet of HFP is dependent upon the retinal location and absorption spectra of macular pigment. MP has peak absorption at 460nm and demonstrates its highest density at the fovea diminishing with eccentricity at ~7° where negligible MP is identified through HPLC. Using this approach, a greater intensity of blue light will be required at the fovea where MP is the highest relative to a parafoveal location. The log ratio of blue light radiance at the fovea compared to parafoveal location is the measured MPOD.

One type of HFP device utilizes a Maxwellian optical system with a bite bar for head stabilization. These complex designs require considerable training to operate and require considerable training associated with their set-up. Free-viewing devices have offered an alternative to the more complex Maxwellian system. Several studies has established the strong correlation between device results and determined that accuracy is not compromised (Wooten, 1999 and Beatty et al., 2000).

Of critical importance to measurement procedures are size of the testing fields, flicker rates of stimulus, and background luminance. First, the testing field is viewed a near-working distance using a 1° central stimulus. Exceptions to these

parameters exist but all fall within a similar range. The stimulus wavelength is determined to maximize MP absorption centered at 460nm and deviation from this peak must be corrected for during final determination of MPOD. Bandwidth of stimulus source may also be adjusted recognizing that the more narrow the bandwidth, the more accurate the MPOD measurement but at the cost of luminance. In the first HFP device described by Wooten et al. (1999), the LED source with peak energy at 458nm had a half-bandwidth of 20nm. As a result, the measured MPOD was corrected by a 15% constant. Parafoveal reference locations used by HFP devices range from 4° (Hammond, 200) to 12° (Werner, 2000) eccentric from the fovea. As alluded to above, the parafoveal reference locations are used under the assumption that no MP exists at these points. Accurate selection of the parafoveal retinal locus is critical for accurate MPOD measurement. Negligible MP has been identified at outside 7° of eccentricity by HPLC (Bone, 1992). Incorrect assumption of absent MP will lead to significant underestimation of true optical density.

Secondly, the selected flicker rates for alternating blue/green wavelength stimulus rely on individual subject's flicker sensitivity. If flicker rate is set too low, the subject will have trouble correctly identifying a point of null flicker. If the flicker rate is set too high, the subject will show a large range of null point variability creating variations in measurements. Ideally, the approach is to create a repeatable, customized flicker rate for each subject at both the foveal and

parafoveal locations. Parafoveal reference locations employ the same flicker stimulus with a properly calibrated flicker rate for a non-foveal point.

Finally, the background field that the stimulus is presented upon must both suppress the S-cone contribution and provide photopic conditions in order to suppress rod pathway interaction. Previous designs have utilized either a blue wavelength background or high luminance white background. The size of the background field that the stimulus is presented upon has also been reported in the literature from 4° to 30°. Small background fields of 4° present difficulty when parafoveal reference points require at least 7° of eccentricity to ensure absent macular pigment. Large fields of 30° however, present their own challenges with subject accuracy and sensitivity to a 1° stimulus within a high luminance field.

Interference of MPOD measurement from ocular media absorption or scattering is controlled in HFP by using the parafoveal reference location. For example, crystalline lens brunescence would influence MPOD values but is controlled for by using the equally-affected measure outside the fovea during calculations. Unequal intrasubject retinal distribution of L and M photoreceptors and their differing spectral sensitivities are also controlled for through an invariant background field with a superimposed stimulus measured at a foveal and parafoveal location.

II. Visual Performance

A. Spatial

Measurement of spatial visual acuity can be accomplished in several different ways. The more conventional measurements include a confirmation of the presence of an object (minimum visible), or the distinction between two point sources (minimum resolvable), or the detection of the minimum offset of position (hyperacuity) (Wyszecki and Stiles, 1982). In the case of all three measurements of acuity, both physical and physiological factors determine visual performance. These physical and physiological factors include the optics of the eye, the quality of the retinal image, the structure and function of the retina, and the capacity of the neural stages of transmission of visual information (Westheimer, 1964).

Resolution acuity (RA) is defined as the minimum perceivable angular distance subtended by the centers of two point sources that can reliably identified as two points as opposed to one (Westheimer, 2001 and 2003a). This threshold is determined by at least two of the above mentioned factors: 1) Ganglion cell packing density and receptive field convergence of the photoreceptor input and 2) the quality of the image dictated by the optical constituents of the eye.

Building on the established principle of cone receptor density and ganglion cell convergence, Virsu and Rovamo (1979) proposed the *invariance principle.* They suggested an equivalent resolution of visual stimuli existing at any point within the visual field if the stimuli are compared in terms of cortical projection or M-

scaled. The cortical magnification scaling, suggested by Virsu and Rovamo (1979), is designed to balance the area of V1 neurons stimulated so that cortical projection becomes independent of retinal location within a receptive field. The values of calculated cortical projection used in their scaling were directly related to the square root of retinal ganglion cell receptive field density. The orderly composition of V1 (Hubel and Weisel, 1977) allows M-scaling to keep the number of stimulated cortical neurons constant. Using equivalent quantities of stimulated retinal ganglion cells and cortical cells, Virsu and Rovamo (1979) further suggested that it was possible to generalize to other points within the visual pathway.

The spatial modulation transfer function (SMTF) is a measure of the object:image contrast ratio as a function of spatial frequency (Van Nes et al., 1967). Their work determined that when longitudinal chromatic aberration effects are controlled for, photopic contrast sensitivity function is equivalent across the visible spectrum. Van Nes et al also reported that low retinal illuminance followed the de Vries-Rose Law: under dim illumination, variations inherent in a background source largely determine threshold. At higher retinal illuminance, threshold modulation followed the Weber-Fechner Law: As the background illumination is increased, the intensity of the stimulus must also be increased so that the ratio of stimulus:background remains constant.

The SMTF describes the quality of an optical image produced by an optical system. The determination of the visual system SMTF utilizes a spatial grating

pattern of a known contrast to serve as the object. As the light from the object passes through the optical system, some degradation of the image occurs. The contrast of the resulting image is measured and the ratio of object:image contrast can be calculated. By performing this technique to a range of low to high spatial frequencies, a SMTF is produced and is commonly referred to as the contrast sensitivity function (CSF). Loughman et al. (2010b) reported a theoretical improvement of resolution acuity up to 0.1 log units by correction for chromatic aberration due to the characteristic short wavelength absorption. This theoretical refinement is in line with earlier published work involving the limiting effects of chromatic aberration on the SMTF (Thibos et al., 1991).

Thibos (1990) stated that an image-forming optical system exhibits chromatic aberration if its focal length is not independent of wavelength. Although differences in focal length among different wavelengths define chromatic aberration, SW light appears to be the principle contributor to reduced image quality when regarding the composition of the visible spectrum. The level of defocus due to chromatic aberration in addition to the typical diffraction pattern would operate in concert to widen Airy's disc. According to the hypothesis originally proposed by Schultze (Magnussen et al., 2001), the filtering effect MP on SW light would sacrifice a small amount of retinal illumination for a more narrow diffraction pattern resulting in increased contrast and potentially improved resolution acuity.

Engles et al. (2005a/b) used bandpass filters that provided a comparable spectral absorption profile of the human lens and macular pigment equivalent to 0.7 log optical density unit. Engles et al. demonstrated an improvement in visual acuity as measured by Landolt C (2005a) and contrast sensitivity (2005b) using the simulated SW filter under broadband illumination. Engles et al. (2007) later performed an empiric study of the Acuity Hypothesis involving human subjects. Using MP as a study variable and resolution and vernier acuity as visual performance measure, their group was unable to correlate MPOD with either resolution acuity or hyperacuity drawing the predictions of the Acuity Hypothesis into question.

Wooten and Hammond (2002) proposed that optical mechanisms separate from chromatic aberration may hypothetically improve visual performance under the type of conditions where most yellow filters show enhancement. The authors termed this improvement the Visibility Hypothesis of macular pigment proposing the idea that macular pigment may improve vision by reducing the forward scatter caused by short wavelength dominant light and reducing veiling luminance through selective absorption. Thibos et al. (1991) determined that the influences from chromatic aberration on the SMTF were relatively small, estimated at approximately 0.15D of defocus. Effects of chromatic aberration are most likely encountered at the upper resolution limits of visual acuity although the luminous efficiency curve predicts that wavelengths near the edges of the $V(\lambda)$ curve will have less effect on human visual sensitivity (Thibos et al., 1991).

B. Temporal

Neural transmission efficiency within the visual system, like other neural structures, is limited by a number of conditions including processing speed and conduction rate (Vaney et al., 1998). A review by Hammond (2005) outlined a method of determining variations the speed of temporal processing by calculating the temporal modulation transfer function (TMTF). Spatial visual function can be described by the contrast sensitivity function, or SMTF, (sensitivity versus spatial frequency) just as temporal vision can be described by the TMTF (sensitivity versus temporal frequency) (Regan, 1982). Several studies have explored the high frequency portion of the TMTF (Rovamo et al., 1984, Mayer et al. 1988 and Hammond et al., 2005). One of the methods available involves a counter-phased square wave and is known as the critical flicker fusion (CFF) threshold. Mayer et al. (1988) found significant differences in the TMTF thresholds related to age supporting a decline in temporal sensitivity with increasing age. Hammond et al. (2005) found a positive relationship between MP and CFF and identified that this association was independent of age. The authors suggested that L and Z could theoretically improve neural signaling efficiency throughout the visual system. Renzi and Hammond (2010) measured a comprehensive temporal contrast sensitivity function (TCSF) using a 1° circular stimulus at the fovea and a 7° parafoveal location. MPOD was measured using HFP and a 1° circular stimulus and found a significant relationship between MP and the full TCSF at the foveal location (p<0.01) but not the parafoveal location (p=0.07). Their results also

identified a significant, positive correlation between foveal MPOD and foveal CFF

(r = 0.21, p<0.001).

Renzi et al. (2010) summarize results from a number of sources including Curran

et al. (1990) and Parrot (2008) which indicate that CFF is likely determined post-

receptorally and CNS function has a direct influence on CFF thresholds. Hawken

et al. (1996) reviewed the temporal response characteristics between LGN

neurons, which receive direct input from the retinal ganglion cells, and V1

neurons. Their work showed V1 response characteristics with reduced sensitivity

to CFF rates indicating a possible loss of temporal information within the LGN.

Hawken et al. concluded that intracortical mechanisms likely influence V1

temporal response dynamics because their temporal properties are not derived

from the LGN and significant variability in temporal tuning exists. As described

above in the Neural Hypothesis, L and Z have been shown to improve gap

junction transmission efficiency and improvements in signal transduction velocity

(Stahl et al., 2002) both of which may improve temporal processing speed within

the visual system.

C. Differences across the Visual Field

Robson and Graham (1979) described a probability summation hypothesis which

involved 2 underlying assumptions: a target will be detected by a subject when

any one receptive field is activated by the target within the visual field and that

receptive field activation is independent of the likelihood that any other receptive

field will also be activated. They further hypothesized that the relationship between contrast sensitivity and spatial frequency can be explained by the probability summation across the stimulated area if variation in sensitivity across the visual field is accounted for.

Virsu and Rovamo (1979) described the effects of target area and spatial frequency on contrast sensitivity depends on a central integrator which sums the activity of a receptive field over large cortical areas. They determined that CS may be a result of extensive summation across a number of spatial frequency channels that have differing levels of sensitivity and specificity. Further, targets presented at different positions across the visual field will have equal sensitivity responses if they share equivalent cortical projections: contrast sensitivity is direct function of the number of stimulated receptive fields.

Pointer et al. (1989) measured differences in contrast sensitivity along each of the four principle meridians using horizontal grating targets. They determined that contrast sensitivity is highest for all spatial targets of 0.5-24cpd and parafoveal reduction in sensitivity can be conveyed as a linear function is contrast sensitivity is expressed in relative units such as periods of the target.

Previous psychophysical studies have explored the theoretical link between visual performance and underlying retinal ganglion cell density (Thibos et al., 1987, Anderson et al., 1991 and Thibos et al., 1996). Thibos et al. (1987)

provided findings that grating resolution in the peripheral retina is defined by the ganglion cell density. The authors referred to the underlying neural performance limitation as sample-limiting performance and further defined the resolution limit and its relation to aliasing. Further work by Anderson et al. (1991) concluded that for achromatic targets, peripheral spatial resolution is limited by both an underlying ganglion cell density and a post-receptoral mechanism.

Thibos et al. (1996) provided a brief review of two separate measures of visual performance across the visual field described as resolution thresholds and detection thresholds. Resolution thresholds are referred to as the highest spatial frequency at which orientation can be recognized and signifies the spacing of the retinal ganglion cells and the resulting Nyquist limit. Detection threshold is the highest spatial frequency at which contrast can be recognized and is determined primarily by the optics of the eye. Thibos et al. (1996) reported that the shape of the SMTF, or contrast sensitivity function, can be determined by whether a resolution threshold or detection threshold was used offering further support that resolution thresholds are restricted by the underlying retinal density of the ganglion cell receptive fields.

D. Interaction of Visual Performance Measures

A decrease in visual performance may be caused by the loss of retinal image contrast due to surface reflections or bright luminance sources creating increased forward scatter of light within the eye (De Waard et al., 1992).

Intraocular scatter has an inverse relationship to the glare angle squared. Vos (1984) suggested that visual effects experienced in disability glare, as defined by the CIE, are similar to visual effects experienced in intraocular scatter. The resulting disability glare can decrease visual performance by two primary means, direct reduction in the contrast of the retinal image and a veiling luminance at the retinal plane caused by peripheral intraocular scattering. According to a review by Vos (2003), at smaller angles of incidence, inhibitory neural interactions at the retinal level can add to disability glare.

Franssen et al. (2006) discussed intraocular scatter as a measure of the effects caused by the inhomogeneities of the eye's optical elements on incident light arriving at the cornea. Backward light scatter will primarily reduce the amount of light reaching the retina while forward scatter will reduce contrast (both chromatic and achromatic) at the retina by increasing the spread of light. This forward scattering may cause a veiling luminance across the retina leading to a decline of resulting image contrast (van den Berg, 1995). Puell et al. (2008) found that inter-subject differences in foveal MPOD showed a significant correlation with intraocular scatter in healthy, non-cataractous eyes. It has been identified by both Stringham et al. (2011) and Hammond et al. (2012) that MPOD has a positive effect on disability glare which suggests that MPOD may also have a role in the reduction of intraocular straylight.

Reading and Weale (1974) first introduced the role of MP on longitudinal

chromatic aberration and Thibos (1987) found that, in reference to lateral

chromatic aberration, selective filtering by MP increased target contrast by a level

that increases with spatial frequency to a factor of ~1.5 at the spatial resolution

limit. Hemenger (1992) introduced the proposed role the MP's preferential

absorption of plane polarized light may be related to lower root-mean-square

aberrations. The dichroic nature of MP (Bone et al., 1992), with its major axis of

absorption oriented tangential to a circle centered on the fovea support a

potential absorption property of plane polarized light.

III. Existing Evidence of Macular Pigment Role in Visual Performance

One of the first experiments to evaluate the association between MPOD and

visual performance under glare conditions was published by Stringham and

Hammond (2007). Thirty-six (36) subjects (age range: 18 to 41), using HFP with

a free-view macular densitometer, developed individual spatial distribution

profiles of MPOD. Photostress recovery times and grating target visibility under

glare conditions were measured in a Maxwellian-view optical system. For glare

disability assessments, subjects fixated a 1° target utilizing a 100% contrast

grating target. The radiometric power of an annulus (which served as the glare

source) with an 11°/12° inner/outer diameter was adjusted until the grating target

was no longer visible. Thresholds under glare conditions revealed significant

correlation coefficients related to MPOD (p< 0.001) when using a broadband

xenon light source. The authors concluded that an increase in MPOD is related

to decreases in glare disability and photostress recovery times consistent with known established spectral absorption characteristics and spatial distribution profile of MPOD.

The Stringham and Hammond investigation (2008) assessed the relationship of MP to improvements in glare disability and photostress recovery time after supplementation with lutein and zeaxanthin for 6 months. Forty (40) subjects (mean age 23.9) were evaluated by HFP to create spatial MPOD profiles at baseline, 1, 2, 4, and 6 months. Both disability glare and photostress recovery were assessed with a Maxwellian-view optical system. For assessments of disability glare, a 100% contrast, 1°grating stimulus of 5cpd was used and the intensity of an 11 °inner/12 °outer annular xenon-white source was adjusted until the grating stimulus could no longer be resolved. Photostress recovery employed the same target using a 5° central disc delivering 5.5 log Trolands of retinal illuminance for a 5 second duration. At baseline, visual performance as assessed by glare disability and photostress recovery showed high correlation with MPOD. After 6 months of L and Z supplementation, mean central MPOD increased nearly 40% and glare disability ($r = 0.59$, $p < 0.0001$) and photostress recovery ($r = -0.66$, $p < 0.0001$) were found to be significantly related to increases in MPOD.

Loughman et al. (2010) evaluated the association between MPOD and visual performance. One hundred forty-two (142) subjects (mean age: 41 with SD of +/- 6) were assessed to determine the spatial profile of their MPOD through HFP.

Visual performance measurements included best corrected visual acuity, contrast sensitivity, glare disability, and photostress recovery time. Glare disability was measured under medium and high glare conditions assessed at 42 lux and 84 lux, respectively. Psychophysical measurements of best corrected visual acuity and central contrast sensitivity showed a positive correlation ($p < 0.05$) with MPOD. Photostress recovery time and glare disability showed no significant correlation to MPOD ($p > 0.05$). Important to note, the glare source output utilized by Loughman et al. did not contain a significant amount of SW light. The source utilized for the glare disability and photostress recovery were tungsten-based sources. These sources provide substantially more spectral irradiance between 520-750nm than between 410-520nm where the spectral absorbance of MP is greatest.

Nolan et al. (2011) evaluated the augmentation effects of macular pigment (MP) and potential resulting enhancement of visual performance measured by best corrected visual acuity, contrast sensitivity, glare disability, photostress recovery time, and subjective questionnaire related to visual function. One hundred twenty-one (121) subjects were randomly divided into active (12mg L and 1mg Z oral supplement) and non-active (placebo oral supplement) group. Subjects were evaluated at baseline, 3, 6, and 12 months through HFP determination of their MPOD spatial profile and psychophysical measurements of visual performance. At 12 months, a statistically significant rise in MPOD was measured in the active group but this increase in MPOD was not linked with a corresponding

improvement in visual performance measures. Nolan et al. (2011) did report statistically significant differences in mesopic contrast sensitivity at high spatial frequencies and in mesopic contrast sensitivity at low spatial frequencies under high glare conditions. Important to note, the glare source output utilized by Nolan et al. was identical to the 2010 Loughman et al. study. The spectral output of the tungsten-based source created markedly greater LW visible light (520-750nm) than SW visible light (410-520nm). The lack of a SW light component within the glare source accompanied by the absence a significant correlation between MPOD and both glare disability and photostress recovery may offer further support of the wavelength dependence of MP-related improvements on visual function.

Stringham et al. (2011) evaluated 3 types of visual performance under glare conditions: photostress recovery time, disability glare, and discomfort glare. Twenty-six (26) subjects were measured to determine the spatial profile of their MPOD through HFP. Visual performance measurements for the photostress recovery and glare disability were determined through correct orientation identification of a Gabor patch. Discomfort glare was assessed during glare testing with a visual discomfort scale. Glare was produced using high intensity white LEDs. MP was shown to be significantly ($p<0.05$) associated with all 3 measures of visual performance. Importantly, this study utilized natural viewing that involved the effects of pupil diameter allowing a greater generalization to typical, environmental viewing.

Hammond et al. (2012) performed the first direct test of the Visibility Hypothesis originally proposed by Wooten and Hammond (2002). Five (5) young, healthy subjects experienced with psychophysical testing procedures were evaluated. MPOD was assessed with HFP and visibility was evaluated by measuring contrast sensitivity at 8cpd using a xenon source optical system which created a sine wave grating target. Natural sunlight and atmospheric haze was simulated using a broad-spectrum filter and alterations to MPOD were replicated by a variable path length filter that represented the absorption spectrum of MP. Results showed that a simulated increase in MPOD of 0.25 density units lowered the average contrast sensitivity threshold approximately 25% and an additional 0.25 density units lowered the threshold an additional 10% with an effect plateau at 0.50 density units. Their results suggested that the greatest improvements in CS are associated with modest increases in MPOD.

A 2013 study by Hammond et al. investigated the relationship of serum lutein and zeaxanthin with MPOD, glare disability, photostress recovery, and chromatic contrast. One hundred fifty (150) healthy subjects were assessed using cHFP to measure MPOD and a Maxwellian-view broadband light source to measure visual performance. Glare disability was evaluated by increasing the radiometric power of an annulus until it caused a loss of resolution for a 4cpd grating central target. Photostress recovery was recorded as the time elapsed before the subject was able to recognize a foveal target following a 5 second exposure to a glare source. Chromatic contrast was measured as the intensity of a 460nm

background which resulted in a loss of visibility of a 4cpd grating central target with a wavelength of 600nm. Their results showed a significant relationship between MPOD and glare disability (r = 0.24, p < 0.01), photostress recovery (r = 0.18, p = 0.01) and chromatic contrast sensitivity (r = 0.46, p < 0.001). MPOD was also found to be significantly related to combined serum L/Z (r = 0.31, p < 0.01).

To date, a majority of previous studies have focused on the establishment of central visual function with foveal MPOD measurement. A number of investigations have demonstrated the distribution profile of MP within the sensory retina (Loughman et al., 2010 and Nolan et al., 2011 and Stringham et al., 2011) and all used measures of central visual performance. Where the deficits can be found in the literature is in defining the role of parafoveal MPOD and its relation to visual performance. Also important is the relationship between visual performance and foveal MPOD versus integrated MPOD. Robson et al. (2003) and Trieschmann et al. (2006) reported that foveal measures of MPOD show low correlations with total amount of MPOD measure across the spatial distribution. Wenzel et al. (2006) also hypothesized that an integrated measure of MPOD is potentially more important than a measure at a single eccentricity. This underscores the importance of determining the complete spatial distribution profile of MPOD: Certain spatial distributions may show significantly different foveal versus parafoveal measurements and quantification of foveal MPOD

levels in isolation may poorly reflect the potential role of MP in visual

performance.

IV. Hypotheses

Previous studies have examined the relationship between foveal MPOD

measurements with central visual function thus ignoring the spatial distribution.

The previously identified relationship between MPOD and the 3 components of

the Optical Hypothesis in the foveal region supports the investigation of

parafoveal relationships with MPOD. My hypotheses include:

1)   MPOD has an inverse relationship with glare disability and contrast

         sensitivity at foveal and parafoveal retinal loci.

2)   Integrated measures of MPOD across the diameter of the stimulus will

         better predict visual performance compared to discrete point

         measurements

3)   Integrated MPOD is inversely related to intraocular scatter

V. Methods

The current study included a total of 33 subjects. The n-value was derived from

an *a priori* power analysis using an 80% power estimate and a Cohen's effect

size of 0.5 expressed by the equation: $N = (2.8/0.5)^2 + 1$ (Howell, 2007). The total

subject sample number was divided into three equal cohorts of 11 subjects. Each

cohort performed all testing over a 12 week period to ensure each subject was

able to complete all testing within a single academic semester and that all subjects progressed through the testing at the same rate.

Study inclusion criteria required no evidence of ocular pathology and best corrected visual acuity of 20/25 in the right eye and age less than 35 in order to avoid any presbyopic effects. Volunteer subjects were recruited from current optometry students enrolled at UMSL College of Optometry. All subjects were current optometry students familiar with the devices and techniques presented during testing. The study sample included 11 males and 22 females with a mean age of 24.2 years ($\sigma = 2.7$). All procedures were approved by the UMSL Institutional Review Board.

MPOD Spatial Distribution Measurements

The study utilized a novel device based on Wooten et al. (1999) (Figure xx) that used customized heterochromatic flicker photometry (cHFP) to measure the nasal, temporal, superior, and inferior MPOD at 0°, 2°, 4°, 6° and 8^0 eccentricity. This radial pattern was used to generate a spatial profile of an individual subject's MPOD that was then compared to a spatial distribution of contrast sensitivity and glare sensitivity at the corresponding degrees of eccentricity.
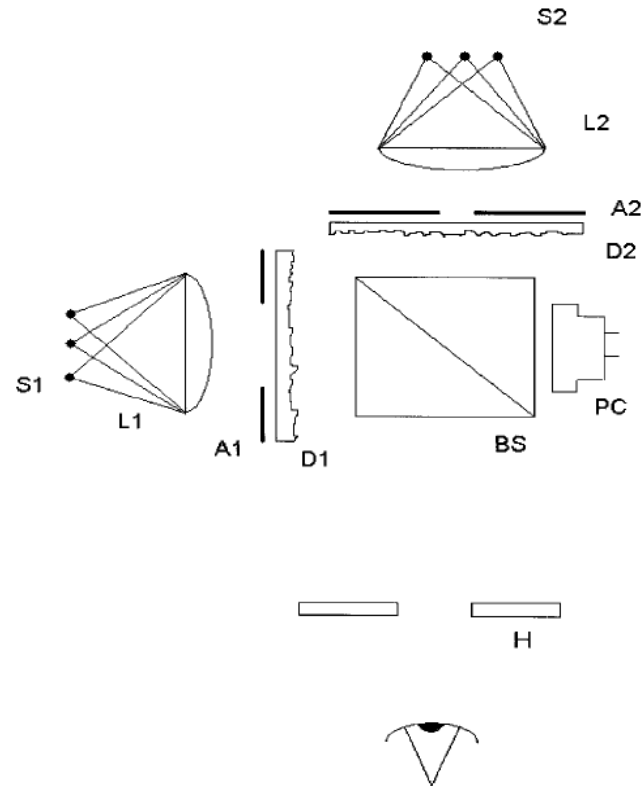
Figure 2
A diagram of the free-view optical system used to measure MPOD. (A1 and A2) Apertures 1 and 2; (BS) beam splitter; (L1 and L2) convex achromatic lenses; (PC) photocell; (S1 and S2) LED sources; (D1 and D2) optical diffusers (Wooten et al., 1999)

The cHFP device is a free-view device requiring no head stabilization (Fig xx) with a fixed 40cm distance consisting of a 10° background field generated by a LED (472nm peak) and a holographic diffuser (85% transmission with 20° viewing angle) measuring 2.75 cd/m^2. A 1° stimulus is superimposed on the background field using a beamsplitter and a triad LED arrangement consisting of two 460nm and one 564nm LED (half-bandwidth of 10nm). The measured peak output of the superimposed stimulus was 5.20cd/m^2 for the 564nm LED and 21.2cd/m^2 for the 460nm LEDs. The LED triad utilized a pulse-width modulation (PWM) frequency control. PWM was chosen to regulate frequency which allows use of contact current control of the LED input. Constant current LED input

allowed strict control of spectral output. The triad array created a peak

wavelength of 460nm and 564nm LEDs to flicker in counterphase to one another

and an inverse yoked luminance control set at 0.10 cd/m^2 for each detent of the

subject control knob. A 5 arcmin fixation dot was printed on a transparent thin

film and controlled by a step-motor which allowed precise positioning at

eccentricities relative to the center of the 1° stimulus target.

Figure 3
The cHFP device designed and built for use during this project used to measure MPOD along 8 meridians at 0°, 2°, 4° and 6° eccentricities.

Each MPOD assessment session lasted for approximately 45-50 minutes but

never exceeded 1 hour to control for fatigue and compliance. Three sessions

were scheduled for each subject and a fourth was optional if the subject required

additional familiarization with the technique to reach repeatability during the initial

training. Each session used 5 repeated measures of their individual critical

flicker fusion (CFF) threshold before any assessment of their MPOD was

performed.

In order to optimize the accuracy of the MPOD measurements, each subject was required to identify their central CFF that determined all stimulus flicker rates at each retinal location. To begin each trial, the subject was adapted in a dark room for 5 minutes prior to beginning the testing. The subject then placed an eye patch over their left eye and chin in the fixed chin rest. A 40cm distance check was performed to ensure proper alignment and distance. Subjects were instructed to maintain stable head posture during testing and to close and cover their patched left eye. Once the device and subject were comfortably aligned, the subject would then grasp the adjustment knob prior to flicker threshold testing. The CFF was determined by isolating the 564nm LED as the flickering stimulus superimposed on the 472nm background. The stimulus frequency was set at values well below expected CFF thresholds and the subject was asked about the perception of flicker. If no flicker was perceived, the frequency of the 564nm stimulus was decreased until a prominent flicker was achieved. If prominent flicker was recognized by the subject, they were then instructed to turn the adjustment dial to the right 1 click at a time at a rate approximate to 1-2 seconds per click. The subject was asked to maintain strict fixation on the black dot in the center of the stimulus and assess the entire stimulus for flicker. The subjects were instructed to blink enough to allow for comfort but to assess for presence of flicker only when holding eye open without blinking. When the subject reached a point that a null flicker was reported, they were asked to stop, blink several times, and refixate the stimulus center. If null flicker was still reported, the frequency value was recorded and the examiner reset the flicker frequency to a value well

below threshold. If minimal flicker was still perceived by the subject, they were instructed to add only 1 additional click to the right to eliminate the flicker. If null flicker was achieved, this flicker frequency was recorded. If minimal flicker was still reported, the flicker value was reset and the CFF procedure was performed from the beginning. Five consecutive measures were taken and all values were within 1 Hz of one another or the testing was stopped, the subject was allowed to rest, and the CFF procedure was started from the beginning. A mean value of the 5 repeated CFF measures were used to calculate the customized central flicker rate for each subject. Consistent with Snodderly et al. (2004) and Hammond et al. (2005) and Stringham et al. (2008), the subject's central CFF was applied to an algorithm lookup table within the device programming to determine the fixed stimulus flicker rate at foveal, 2°, 4°, 6^0 and 8° eccentricities.

Once the repeated measure CFF had been determined, the device was set to "LOCK" which then allowed the stimulus target to display the counter-phased 460nm/564nm stimulus. Foveal measurements of MPOD was assessed by maintaining the black fixation dot at the stimulus center and the examiner set the displayed relative units of the 460nm LED to values well-below equiluminance thresholds. The subject was then asked to assess the entire 1° stimulus for flicker. If flicker was perceived, the 460nm luminance was decreased by the examiner and the subject was reassessed. If flicker was still perceptible by the subject, the CFF testing was repeated to maximize subject familiarity with flicker perception and improve the accuracy of the subject's central CFF. If null flicker

P a g e | 83

was perceived, the subject was instructed to turn the adjustment dial to the right 1 click at a time at a rate approximate to 1-2 seconds per click. The subject was asked to maintain strict fixation on the black dot in the center of the stimulus and assess the entire stimulus for flicker. The subjects were instructed to blink enough to allow for comfort but to assess for presence of flicker only when holding eye open without blinking and follow a method of limits paradigm identical to the described CFF threshold measurement.

Each session included five 0° and 8^0 eccentricity measurement values. The first session assessed the 2° eccentricity, the second session assessed the 4° eccentricity, and the third session included the 6° eccentricity. These eccentricities were assessed using the same procedure as the foveal measurement with the exception of the point of fixation. The examiner set the fixation dot to the corresponding eccentricity relative to the stimulus center. Each subject began with a different meridian to control for order effects. For example, Subject 1 began with temporal measurements, Subject 2 began with superior measurements, Subject 3 began with nasal measurements, and Subject 4 began with inferior measurements. This pattern was followed for all subjects in the same eccentricity. During the second session for all subjects, each began with a different meridian than assigned during their first session (i.e. Subject 1: begins with Session #1 at temporal location, Session #2 at superior location, and Session #3 at nasal location). Subjects were instructed to occasionally move their eyes to the midpoint of black fixation dot and stimulus and then immediately

back to fixation to overcome stimulus fading effects. The subjects were also instructed to blink several times and refixate the black dot before assess presence of stimulus target flicker. When parafoveal stimulus flicker was first perceived, the subjects followed the same protocol for determining foveal flicker: When the subject reached a point that a first, perceptible flicker was reported, they were asked to stop, blink several times, and refixate the stimulus center. If no perceptible flicker was reported after the refixation, the subject was instructed to continue with the testing. If perceptible flicker was still reported after refixation, the subject was asked to add only 1 additional click to the right. If the subject reported more pronounced flicker, the examiner would record the 460nm radiance value was recorded. If no additional flicker prominence was still perceived by the subject, they were instructed to remove the extra click by turning the adjustment dial to the left. This technique was performed for 5 repeated measurements and a mean value was recorded for the foveal 460nm radiance value.

The cHFP device was used to create the spatial map of MPOD for each subject by assessing optical density of the macular pigment using a 1° stimulus at 2°, 4°, 6° eccentricity along four principle meridians: horizontal (0° / 180°) and vertical (90° / 270°) resulting in 13 discrete values (Figure 4). These values were recorded to produce a spatial map of MPOD.
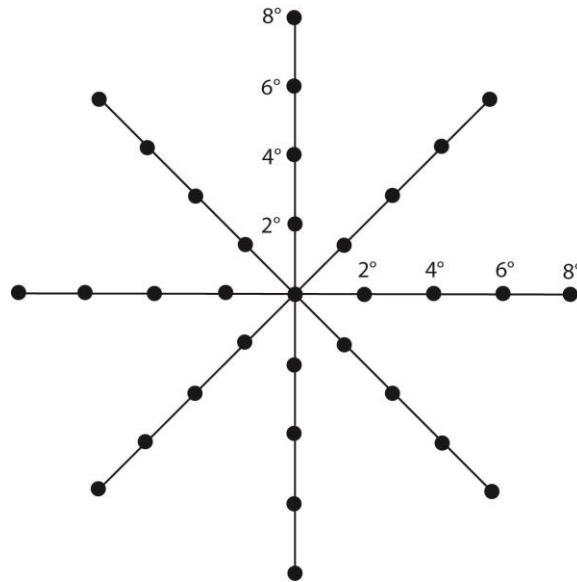
Figure 4
Example of a radial pattern depicting the 8 principle meridians. MPOD was measured at 0°, 2°, 4°, and 6° locations along the inferior, nasal and temporal meridians. Contrast sensitivity was determined at 3, 6, and 9cpd at the corresponding retinal locations.

Two methods of calculating the MPOD spatial distribution across the macula for each subject were employed. The first method calculated the kurtosis values for each spatial distribution. Kurtosis an indicator of normality and measures the peak of the distribution. The greater the kurtosis value the more peaked the distribution relative to a normal distribution and is typically referred to as leptokurtic. The lesser the kurtosis value the flatter the distribution relative to a normal distribution and is typically referred to as platykutic. The second method calculated the area under the curve (AUC) value. MPOD values from each measured loci were plotted using Cartesian coordinates on an x,y graph. OriginPro9 software (OriginPro Corp, Northampton, MA) was utilized to best-fit the spatial distribution across the entire 16° macula and calculate integrated values for the 1° stimulus diameter at each loci and the 16° distribution.

Contrast Sensitivity and Glare Disability Measurements

Stimuli for the CS and GD stimuli were generated with the Psykinematics program (Kybervision, Montreal, Canada) to create a vertical sinusoidal spatial grating pattern with a Gaussian envelope as a stimulus. These stimuli were presented on a 19"-CRT monitor using gamma correction of existing non-linearity. Display calibration of the CRT monitor was assessed using a Spyder 3 (Datacolor, Lawrenceville, NJ) device recognized and incorporated into the Psykinematics program. Non-linearity was measured regularly throughout the project. The range of gamma reported by the Spyder3 device was 1.91 to 1.98.The stimuli were presented on a background with a luminance controlled at 20cd/m^2. The psychophysical technique method of limits with an adaptive staircase (described below) was utilized to determine sensitivity threshold values. A mean value calculated from 6 reversals was recorded as a contrast sensitivity threshold estimation. The vertical sinusoidal spatial grating pattern was displayed with a 200 millisecond duration in order to control for fixation loss during stimulus presentation.

The Michelson contrast value for each retinal location began at suprathreshold levels (as determined from 10 subject pilot study) and decreased in a relative step size at 15% before 1st reversal and increase in a relative step size at 15% until second reversal. This relative change in contrast continued until 6 reversals were recorded and the mean of the 6 reversals was recorded as the threshold contrast sensitivity threshold.

Contrast sensitivity functions utilized luminance modulated sinusoidal gratings with a vertical orientation. The stimulus subtended a visual angle of 1° with a spatial Gaussian envelope. Measurements were taken under mesopic ($3cd/m^2$) conditions using a method of limits described above with respect to a central fixation cross. Values were recorded for 3 spatial frequencies (3 / 6 / 9cpd) at each eccentric point along the above listed meridians.

GD was determined as the difference in contrast sensitivity between glare conditions and no glare conditions ($CS_{No\ Glare} - CS_{Glare}$) at each retinal loci. Glare condition measurements were also taken at 2°, 4°, 6° of eccentricity along each of the above listed principle meridians. The glare apparatus utilized two 5° glare sources produced by two achromatic LEDs (Luxeon model LXHL LW6C, Luxeon Corp., Randoph, VT) located in 1" diameter optical tubes. Each LED is attached to the base of a 6" tube in conjunction with 3 other optical system elements: 1) a 10° holographic diffuser (used to make the glare image uniform, 2) an adjustable circular iris (used to define the glare circle size of 5°), and 3) a convex lens (used to focus the glare source at the distance of the CRT monitor). The two tubes were positioned below the subject's line of sight, directed vertically and reflected from a beam splitter oriented at 45° into the subject's line of sight. Based on the optical system, each glare source created a luminance of 1500 cd/m2 with a color temperature of 6500K. Measurement of the glare sources was taken with a spectrophotometer (model 650; Photo Research Inc., Chatsworth, CA). Strict control of the luminance output was achieved using software-controlled PWM

and luminance output was well within accepted safety values not to produce

visible light-induced ocular damage.

Figure 5
The novel glare device designed and built for use during this project used to produce flanking glare sources to surround
the 1° grating stimulus at each retinal loci along the four cardinal meridians at 0°, 2°, 4° and 6° eccentricities.

The two glare sources were aligned horizontally and each was centered 5° from

the midpoint of the 1° sinusoidal grating pattern. The inner boundaries of the

glare source and the center of the grating pattern are separated by 3° of visual

angle. The subject's view of the glare source is two circles of light spaced

laterally (inner edge to inner edge) by 5° of visual angle. Infra-red camera focus

and subject feedback were employed through a precise alignment protocol

ensuring that the glare circles were accurately positioned the correct distance

from the midpoint of the grating pattern. Subjects were presented the same

stimuli as used during the contrast sensitivity function testing described above. Subjects viewed the grating targets through a beam splitter that reflected the superimposed glare sources on the CRT background.

Subjects were adapted at mesopic ($<3cd/m^2$) conditions for 5 minutes preceding each session. Five (5) measurements were conducted in total in order to maximize validity and repeatability. Sequential presentation of the stimuli for each subject was uniquely determined by a random sequence generator to control for order effects. Single sessions included: 1) foveal threshold determinations for all 3 spatial frequencies and 2) All eccentricity measurements at each meridian (0°, 90°, 180°, 270°) for each spatial frequency. Each session was performed under no glare and glare conditions. This resulted in a total of 8 contrast sensitivity threshold sessions for each subject. Initial starting spatial frequency was randomized to control for order effects. CS threshold under no glare conditions was always performed first to allow familiarization of the task and, when possible, no more than 1 day would elapse between no glare and glare conditions.

An infrared camera was used to monitor the eye during stimulus presentation to ensure proper fixation within 0.5^o or less. A transparency overlay with concentric rings corresponding to 0.5^o of visual angle was applied to the video monitor. Subjects were encouraged throughout to blink frequently to minimize the Troxler effect and to regain fixation on central cross before button response to ensure

proper alignment of eye prior to stimulus presentation. Optional breaks were given at subjects request and mandatory breaks of 5 minutes were given at the completion of each eccentricity. Typical duration of contrast sensitivity testing was approximately 45 to 50 minutes per session.

MPOD was measured at four eccentricities (0°, 2°, 4° and 6°) and resulting values at each retinal eccentricity are a mean of five consecutive trials. With the exception of the foveal measurements, the MPOD at the remaining three retinal eccentricities were calculated as a mean of five consecutive superior inferior, nasal and temporal measurements at that eccentricity for a total of 20 measurements per mean eccentricity value.

MPOD mean values for each retinal loci (0°, 2°, 4° and 6°) were fit to a Lorentzian distribution for both stimulus center and stimulus point of highest retinal sensitivity using OriginPro9 software (Figure 6). For the resulting two distributions, MPOD values at each retinal loci were determined by three separate methods: [1] Stimulus discrete value, [2] stimulus integrated across 1° and [3] area under the curve (AUC) calculations integrated across 16°. Each distribution would have 4 discrete MPOD values and 5 integrated MPOD values from -0.5^o to 0.5^o, 1.5^o to 2.5^o, 3.5^o to 4.5^o, 5.5^o to 6.5^o and -8° to 8°. Peak foveal measures of MPOD will have only a single discrete measure due to the shared retinal point of stimulus center and stimulus point of highest retinal sensitivity.
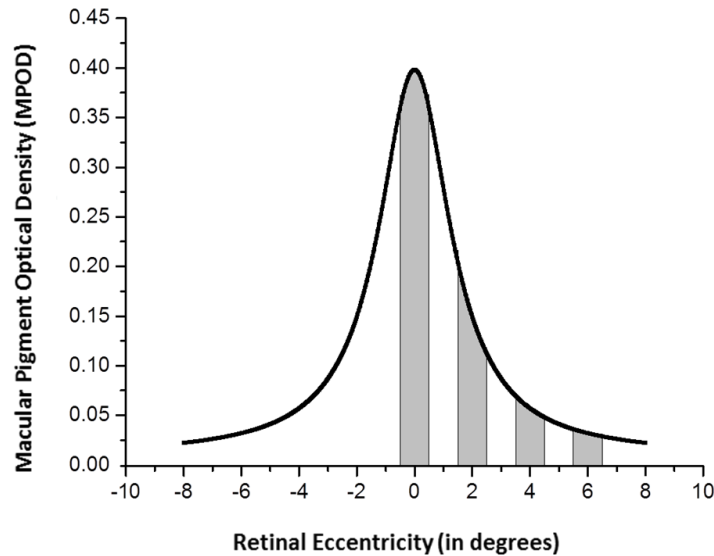
Figure 6

Hypothetical spatial distribution of MPOD fit to a Lorentzian function. The grey shaded area represents a 1^0 area from -0.5^0 to 0.5^0. Origin Pro9 software was used to calculate integration values of a 1^0 area at all measured eccentricities including the area under the curve from -8^0 to 8^0.

Contrast Sensitivity, Glare Disability and Relative Glare Disability Correlations

with MPOD

CS differences between horizontal and vertical meridians were expected and well-documented (Westheimer, 1982 and Pointer et al., 1989). Therefore, correlations between CS and calculated MPOD for 0°, 2°, 4° and 6° eccentricities were evaluated as separate analyses: a horizontal meridian mean CS, a vertical meridian mean CS and a mean CS including all four meridians. Glare disability (GD) was measured as a difference in CS between no glare conditions and glare conditions of the same visual stimuli. Resulting GD values were determined as absolute GD and relative GD. Absolute GD was calculated as: $CS_{No\ Glare} - CS_{Glare}$ and is referred to as GD. Relative GD was calculated as : $(CS_{No\ Glare} - CS_{Glare}) / CS_{No\ Glare}$ and is referred to as RGD.

Correlations of discrete MPOD values along with the two integrated values across the 1° stimulus for each Lorentzian distribution with CS, GD and RGD of the 1° grating target corresponding to the same retinal loci at 3 separate spatial frequencies: 3cpd, 6cpd and 9cpd were calculated. At all 3 spatial frequencies, MPOD correlations with GD and RGD were evaluated in two ways. First, existing literature exploring MPOD and potential effects on CS and GD have utilized foveal MPOD measurement in their analysis (Hammond et al., 2013 and Stringham et al., 2011). In an effort to build upon existing research, foveal measurements of MPOD were correlated with GD and RGD at each eccentricity $(0^o, 2^o, 4^o,$ and $6^o)$. Second, previous studies exploring MPOD and potential effects on CS and GD have not evaluated the relationship of parafoveal MPOD values with parafoveal visual performance. In an effort to expand existing research, correlations of corresponding eccentricities of MPOD and GD and RGD were also performed (i.e. 2^0 MPOD with 2^0 GD and RGD, 4^0 MPOD with 4° GD and RGD and 6^0 MPOD with 6° GD and RGD). The sample n-value was derived from an *a priori* estimate using 80% power and a Cohen's effect size of 0.5 and all correlational analyses were designed prior to data collection. Due to the *a prior* nature of the experimental design, Bonferroni corrections were not utilized in an effort to reduce the risk of false negatives and the consequent decrease in statistical power.

Independent sample t-tests were incorporated to evaluate differences in GD and RGD between the highest and lowest quartiles of foveal MPOD. A Levene's

Tests for Equality of Variances was also performed for each independent sample t-test. If a significant Levene's test was identified, the highest and lowest quartiles of foveal MPOD are assumed to have unequal variances. In such cases, a non-parametric Mann-Whitney test for significance was performed. Effect sizes for independent t-test results were also calculated.

Scatterplots were also performed across all 3 spatial frequencies and were evaluated using GD and RGD. First, foveal measurements of MPOD were correlated with GD at each eccentricity (0°, 2°, 4°, and 6°) as three different calculations (i.e. [1] foveal discrete value vs. 0° eccentricity, [2] foveal MPOD integrated across 1° assuming stimulus center vs. 0° eccentricity and [3] foveal MPOD integrated across 1° assuming stimulus point at highest retinal sensitivity vs. 0° eccentricity). Second, the same three foveal measurements of MPOD were plotted against RGD at each eccentricity. Covariance values and regression relationships between foveal MPOD and GD and RGD for each scatterplot were evaluated.

Intraocular Scatter Correlations with MPOD

Intraocular forward scatter was assessed through a direct compensation comparison method using the C-Quant device (Oculus, USA). The C-Quant device is a commercially-available clinical device able to measure forward scattered intraocular light through a direct comparison method. The device uses hemifield comparison of flicker, similar to the flicker perception utilized for the

cHFP device. The flicker compensation comparison is calculated using a 3.3^o diameter target along with a glare source annulus with an inner diameter of 10° and an outer diameter of 20° with a background luminance of $25cd/m^2$. A 2AFC method is employed using a fixed temporal rate of 8Hz randomly given to one side of the hemifield. The subject was instructed to indicate the lateral side of the target in which flicker is perceived. A complete description of the psychophysical technique is provided by van den Berg et al. (2011). The validity and reliability algorithms are incorporated within the C-Quant device and all assessments of intraocular scatter will follow the established guidelines of the commercial device. A mean intraocular scatter value was determined using the first 5 valid, repeatable measures as determined by the commercial device and represented as ESD (estimated standard deviation) and Q (reliability) parameters.

MPOD influences on intraocular scatter were evaluated by four different values: foveal stimulus discrete value, foveal stimulus integrated across 1°, AUC calculations integrated across 16° assuming stimulus center and AUC integrated across 16° assuming stimulus point of highest sensitivity were evaluated as Pearson correlation coefficients with measures of intraocular scatter.

Scatterplots were also performed and evaluated in four ways: foveal stimulus discrete value, foveal stimulus integrated across 1° and AUC calculations integrated across 16° for each distribution were plotted against the mean intraocular scatter value for each subject.

VI. Results

A. Macular Pigment Spatial Distribution

The MPOD spatial distribution results for the 33 subject sample was fit to a 1st-order exponential decay curve to assess the variability in the data described by the r^2 value in two different methods:

1) Center point of 1° stimulus at each foveal eccentricity

2) Point of highest sensitivity within the 1° stimulus at each foveal eccentricity

The resulting MPOD values at each foveal eccentricity are a mean of the superior inferior, nasal and temporal measurements from all 33 subjects. Resulting MPOD spatial distribution profiles were also fit to a Lorentzian curve and integrated values across the 1° stimulus at each retinal loci and across the 16° of central retina were calculated from both measurements. Individual Lorentzian distribution curves were also fit for each of the 33 subjects. The cHFP device identified reliable MPOD spatial distribution maps and showed a 1st order exponential decay function with eccentricity across the 33 subject study sample. Standard error of the mean measured for 0° eccentricity was less than 0.01 log unit, 2° eccentricity was 0.01, 4° eccentricity was 0.01 and 6^0 eccentricity was 0.02 log unit.

Correlations of MPOD at each eccentricity were performed among the superior, inferior, temporal, and nasal locations. Correlation values among the four measured meridians at 2° eccentricity range between 0.955 and 0.968 providing support of a high level of symmetry among measured meridians when MPOD is

fit to a 1st order exponential function at each of the measured meridians (Table 1). Correlations among the four measured meridians at 4° eccentricity range between 0.928 and 0.947 providing additional support of MPOD symmetry among the measured meridians when the spatial distribution is measured as a 1st order exponential function at each of the meridians (Table 2). Correlations among the four measured meridians at 6° eccentricity range between 0.875 and 0.929 supporting the symmetry of MPOD spatial distribution among the four measured meridians along with increased variability in MPOD assessment with increasing eccentricity (Table 3). MPOD spatial distribution of the subject sample fit to stimulus center showed an r^2 = 0.885 with a y-intercept of 0.426 corresponding to peak foveal density (Figure 7). The same MPOD values fit to the stimulus point at highest retinal sensitivity showed an r^2 = 0.907 with a y-intercept of 0.387 corresponding to peak foveal density (Figure 8).
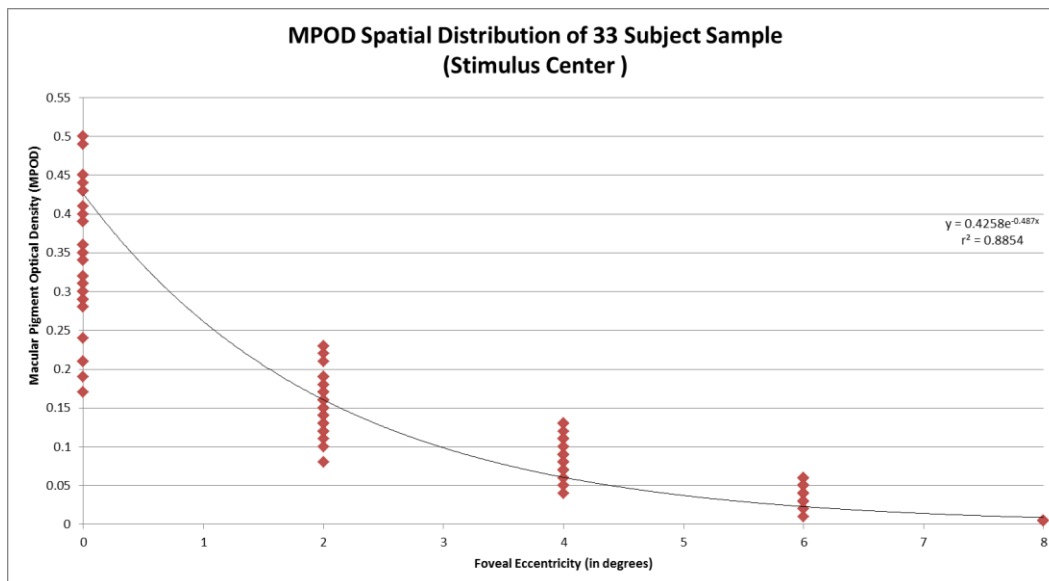
Figure 7
Graphical depiction of 1st-order exponential decay function demonstrated by MPOD spatial distribution in the 33 subject sample assuming a stimulus center measurement.
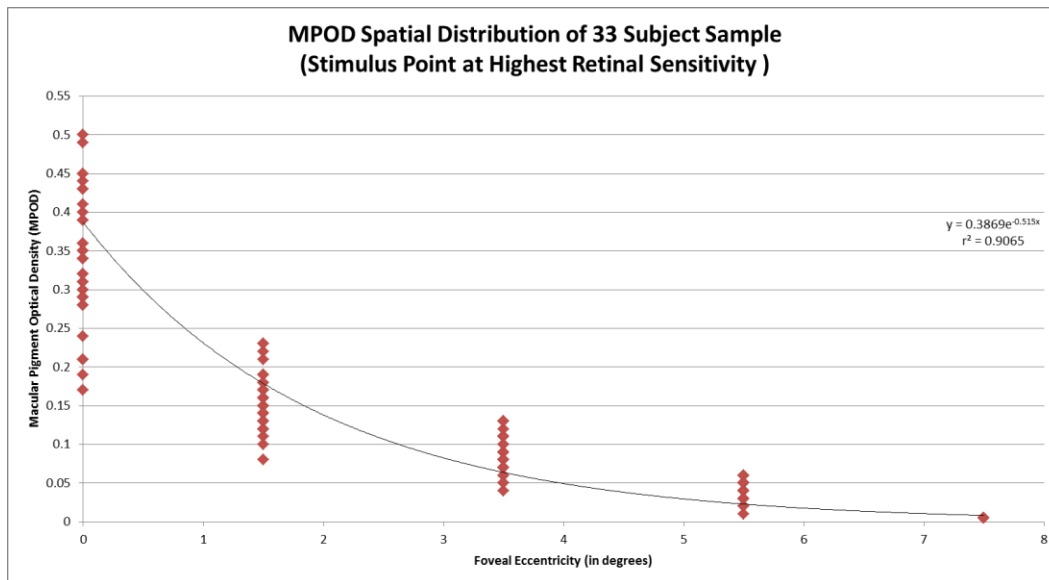
Figure 8
Graphical depiction of 1st-order exponential decay function demonstrated by MPOD spatial distribution in the 33 subject sample assuming a highest retinal sensitivity stimuli measurement.

The cHFP device used to assess MPOD was designed with 1° stimuli set to equal center-to-center stimuli spacing of 2° across the macula. When MPOD spatial distribution is fit to the center of the stimulus, the 2° stimulus spacing remains constant. When the spatial distribution is fit to the inner edge, the foveal measurement edge lies at 0.5^o and the stimulus inner edge at 2° lies at 1.5^o of foveal eccentricity. MPOD spatial distribution was also fit to a 1st order exponential curve excluding the central measurement value. This approach allowed a fixed 2° separation for the center of the stimulus fit (e.g. 2°, 4°, 6°) and the inner edge of the stimulus fit (e.g. 1.5^o, 3.5^o, 5.5^o). The stimuli center fit (Figure 9) and the stimuli point at highest retinal sensitivity fit (Figure 10) revealed similar covariance measures of $r^2 = 0.877$ and $r^2 = 0.876$, respectively.
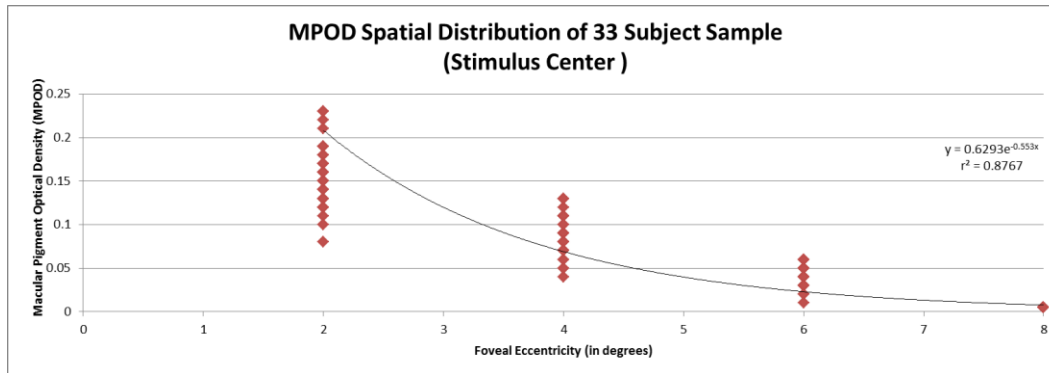
Figure 9
Graphical depiction of 1st-order exponential decay function demonstrated by MPOD spatial distribution in the subject sample assuming a stimuli center measurement excluding foveal measurement.
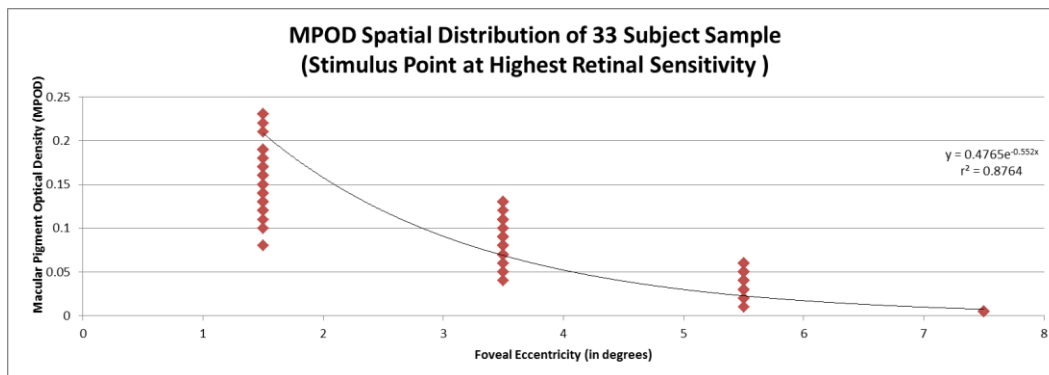
Figure 10
Graphical depiction of 1st-order exponential decay function demonstrated by MPOD spatial distribution in the subject sample assuming stimulus point at highest retinal sensitivity measurement excluding foveal measurement.

The center stimuli fit exhibited a y-intercept of 0.629 while the inner edge of the stimuli, analogous to the point of highest retinal sensitivity, fit exhibited a y-intercept of 0.474. The inner stimuli edge fit agrees more closely with the peak foveal density of both the central (y-intercept = 0.426) and point of highest retinal sensitivity (y-intercept = 0.387) stimuli fit when the foveal measurement value is included in the 1st order exponential fit.

Results from the kurtosis calculations for the 33 subject sample revealed a mean value of 2.78 (σ=1.81). The positive mean value with a relatively large variance

indicate a leptokurtic distribution that shows a sharp, central peak compared to a Gaussian distribution and substantial variability in spatial distribution across the sample. Examples of the variability in kurtosis values are displayed as Lorentzian curves fit for the subject with the highest kurtosis value (Figure 11) and the subject with the lowest kurtosis value (Figure 12). The Lorentzian curves for each subject are fit assuming stimulus center and assuming stimulus point at highest retinal sensitivity.
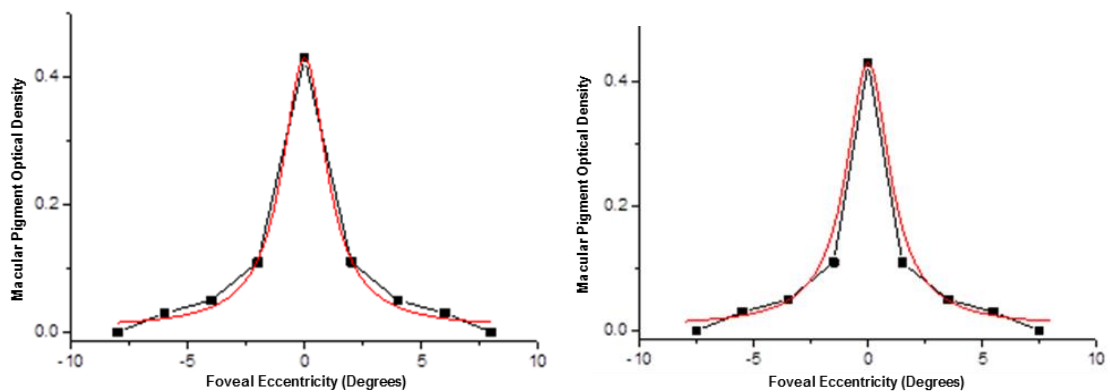
Figure 11
Lorentzian fit to stimulus center (left) and stimulus point of highest retinal sensitivity (right) for subject with highest kurtosis value.
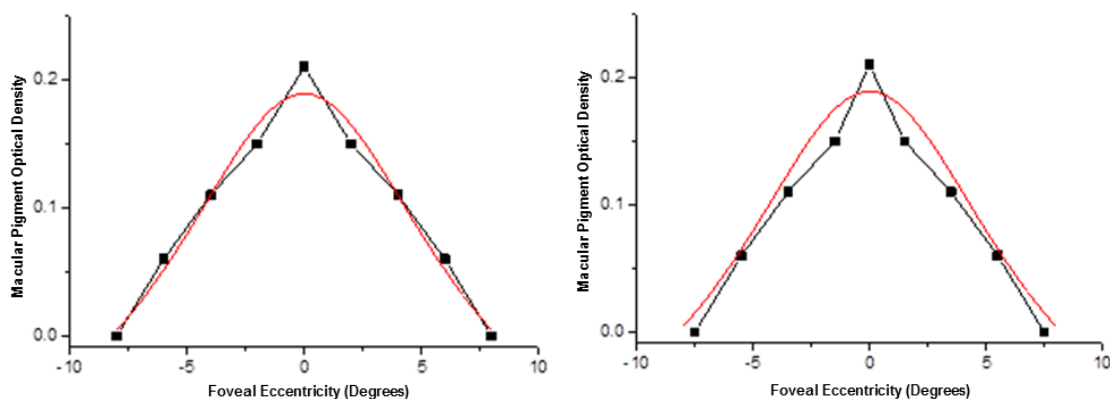
Figure 12
Lorentzian fit to stimulus center (left) and stimulus point of highest retinal sensitivity (right) for subject with highest kurtosis value.

AUC calculations showed differences in mean integrated values when spatial distributions were fit to the center of the stimuli [mean of 1.778 (0.393)] versus the stimuli position at highest retinal sensitivity [mean of 1.489 (0.331)] (Table 4). The AUC calculations were highly correlated with one another (r = 0.997, p<0.001) and showed a non-significant relationship with kurtosis values (AUC center stimuli r = -0.004, p=0.984 and AUC highest sensitivity stimuli position r = -0.062, p=0.733).

B. Contrast Sensitivity and Glare Disability across the Macula

Across all three spatial frequency stimuli, a decrease in CS was displayed with increasing retinal eccentricity. Targets with the lowest spatial frequency (3cpd) resulted in the highest mean CS at all retinal loci measured and targets with the highest spatial frequency (9cpd) resulted in the lowest mean CS. Variability within the 33 subject sample also showed a consistent trend: targets with a lowest spatial frequency (3cpd) demonstrated the lowest variability and targets with the highest spatial frequency (9cpd) demonstrated the highest variability. Variability also increases as a function of retinal eccentricity with the highest variability at the greatest eccentricity. This relationship was consistent across all subjects.

CS showed differences along the horizontal meridians as compared to the vertical meridians. The vertical meridians demonstrated a greater decrease in CS as a function of eccentricity than the horizontal meridians. The differences in

CS along the horizontal versus vertical meridians also demonstrated a dependence on spatial frequency. All three spatial frequencies (3,6,9cpd) demonstrated a significant difference in measured CS between horizontal and vertical meridians at 2°, 4° and 6° of eccentricity (Table 4, Table 5 and Table 6).

Independent Samples t-test		
2° Eccentricity		
	t-value	**Sig.**
3cpd stimuli CS	4.761**	<0.001
6cpd stimuli CS	2.617**	0.01
9cpd stimuli CS	2.374*	0.019

Table 5

Independent samples t-test for horizontal versus vertical meridians at 2° for 3, 6 and 9cpd grating targets Levene's Test for Equal Variances was non-significant so equal variances were assumed (* $p \leq 0.05$ and** $p \leq 0.01$)

Independent Samples t-test		
4° Eccentricity		
	t-value	**Sig.**
3cpd stimuli CS	5.268**	<0.001
6cpd stimuli CS	3.638**	<0.001
9cpd stimuli CS	3.162**	0.002

Table 6

Independent samples t-test for horizontal versus vertical meridians at 4° for 3, 6 and 9cpd grating targets Levene's Test for Equal Variances was non-significant so equal variances were assumed (* $p \leq 0.05$ and** $p \leq 0.01$)

Independent Samples t-test		
6° Eccentricity		
	t-value	**Sig.**
3cpd stimuli CS	4.242**	<0.001
6cpd stimuli CS	4.881**	<0.001
9cpd stimuli CS	8.002**	<0.001

Table 7

Independent samples t-test for horizontal versus vertical meridians at 6° for 3, 6 and 9cpd grating targets Levene's Test for Equal Variances was significant so equal variances were not assumed (* $p \leq 0.05$ and** $p \leq 0.01$)

The highest spatial frequencies (3cpd) showed the least differences in CS between the horizontal and vertical meridians (Figure 15 and Figure 16) when compared to the 6cpd targets (Figure 17 and Figure 18) and the 9cpd targets (Figure 19 and Figure 20). A complete picture of mean CS under no glare conditions and glare conditions at 0°, 2°, 4° and 6° as a function of eccentricity for 3, 6 and 9cpd stimuli is included in Appendix 2 (Figure 21). The plotted mean values show a substantial loss of CS with increasing eccentricity using 9cpd stimuli relative to 3cpd stimuli with greater loss of CS under glare conditions for 9cpd stimuli relative to 3cpd stimuli. Error bars indicate a 95% confidence interval.

At 3cpd, 21 of 33 subjects showed increased GD with increased foveal eccentricity. However, 24 of 33 subjects showed increased RGD with increasing foveal eccentricity. Overall, both GD and RGD were slightly higher at the fovea where peak MPOD is located relative to GD at 2^0 where MPOD is measured lower.

At 6cpd, 24 of 33 subjects showed increased GD with increased foveal eccentricity. However, 26 of 33 subjects showed increased RGD with increased foveal eccentricity. Overall, GD was slightly higher at the fovea where peak MPOD is located relative to GD at 2^0 where MPOD is measured lower while RGD tended to be lower at the fovea where peak MPOD is relatively higher.

At 9cpd, 25 of 33 subjects showed increased GD with increased foveal eccentricity. However, 28 of 33 subjects showed increased RGD with increased foveal eccentricity. Overall, GD was slightly higher at the fovea where peak MPOD is located relative to GD at 2^0 where MPOD is measured lower while RGD tended to be lower at the fovea where peak MPOD is relatively higher.

Across all three spatial frequency stimuli, a general trend of increased GD and RGD with increasing retinal eccentricity was seen, although a number of subjects showed violations of this trend. More direct relationships between RGD and eccentricity (i.e. increased RGD with increased eccentricity) were identified than between GD and eccentricity. Both GD and RGD exhibited a spatial frequency influence: Higher spatial frequencies showed less inverse relationships. Increasing retinal eccentricity resulting in increased GD and RGD was identified more often for 9cpd targets than for 3cpd targets.

GD and RGD also showed less differences along the horizontal meridians versus the vertical meridians as compared CS. The measured GD and RGD between the horizontal and vertical meridians showed similar values supporting a comparable function of MP along all meridians. The effects of MP GD radiate outward from the fovea where MPOD is the highest to the 6^0 eccentricity where MPOD greatly reduced.

C. Relationship between MPOD, Contrast Sensitivity, Glare Disability, Relative Glare Disability and Intraocular Scatter

MPOD results at each eccentricity were fit to a Lorentzian distribution for both stimulus center and stimulus point of highest sensitivity. For the resulting two distributions, MPOD values were determined by three separate methods: [1] Stimulus discrete value, [2] Stimulus integrated across 1° and [3] AUC calculations integrated across 16°. Each eccentricity (0°, 2°, 4°, 6°) had three resulting measures correlated with corresponding eccentricities of CS, GD and RGD. Foveal MPOD measures were correlated with all measured eccentricities (0°, 2°, 4°, 6°) of CS, GD and RGD. Foveal discrete values, foveal stimulus center integrated across 1^0, AUC calculations integrated across 16° assuming stimulus center and AUC integrated across 16° assuming stimulus point of highest sensitivity were evaluated as Pearson correlation coefficients with measures of intraocular scatter.

Independent sample t-testing of differences in CS between the highest and lowest quartiles of foveal MPOD required ranking of foveal MPOD values. In all cases, the top and bottom quartiles followed the same ordering when ranked as foveal MPOD measured as a discrete point, foveal MPOD measured as a 1^0 integrated area assuming stimulus center measure or foveal MPOD measured as a 1^0 integrated area assuming a stimulus point at highest retinal sensitivity. Therefore, independent samples t-testing will refer to MPOD quartiles as 'foveal MPOD'. In general, correlation coefficients of foveal MPOD measured as a 1^0

integrated area assuming a stimulus point at highest retinal sensitivity and RGD tended to show the highest values. Therefore, scatterplot analysis will refer to foveal MPOD measured as a 1^0 integrated area assuming a stimulus point at highest retinal sensitivity as the abscissa value 'MPOD' and RGD as the ordinate value for all figures.

Contrast Sensitivity correlations with MPOD

Overall, no significant correlation between CS and MPOD was demonstrated within the 33 subject sample. At all 3 spatial frequencies, MPOD associations with CS were evaluated in 2 ways. First, foveal measurements of MPOD were correlated with both horizontal meridian CS and vertical meridian CS separately then as a mean CS incorporating all four meridians at all eccentricities (i.e. Foveal MPOD vs. foveal CS, foveal MPOD vs. 2° CS, foveal MPOD vs. 4° CS and foveal MPOD vs. 6° CS). Second, correlations of corresponding eccentricities of MPOD and both horizontal meridian CS and vertical meridian CS then as a mean CS incorporating all four meridians were performed (i.e. 2° MPOD vs. 2° CS, 4° MPOD vs. 4° CS and 6° MPOD vs. 6° CS).

3cpd CS correlations with MPOD

At 3cpd, horizontal meridian CS, vertical meridian CS and mean CS correlations at all eccentricities (0°, 2°, 4° and 6°) with foveal MPOD measured as a discrete point, foveal MPOD measured as a 1° integrated area assuming stimulus center measure and foveal MPOD measured as a 1° integrated area assuming a

stimulus point at highest retinal sensitivity were non-significant (Table 8, Table 9, Table 10).

At 3cpd, 2° horizontal meridian CS, 2° vertical meridian CS and mean 2° CS correlations with 2^0 MPOD measured as a discrete point, 2° MPOD measured as a 1^0 integrated area assuming stimulus center point measure and 2° MPOD measured as a 1° integrated area assuming a stimulus point at highest retinal sensitivity were non-significant (Table 11, Table 12, Table 13). Horizontal meridian 4° CS, vertical meridian 4° CS and mean 4° CS correlations with all three measures of MPOD at 4° eccentricity were non-significant (Table 14, Table 15, Table 16). Horizontal meridian 6° CS, vertical meridian 6° CS and mean 6° CS correlations with all three measures of MPOD at 6° eccentricity were also non-significant (Table 17, Table 18, Table 19).

An independent sample t-test of CS differences at 0°, 2°, 4° and 6° eccentricities between the highest and lowest quartiles of foveal MPOD as a 1° integrated area assuming a stimulus point at highest retinal sensitivity was also performed using an independent sample t-test. Results for Levene's Test for Equal Variances were non-significant so equal variances were assumed. At 3cpd, no significant differences in CS between top and bottom quartiles of foveal MPOD were identified (Table 20).

6cpd CS correlations with MPOD

At 6cpd, horizontal meridian CS, vertical meridian CS and mean CS correlations at all eccentricities (0°, 2°, 4° and 6°) with foveal MPOD measured as a discrete point, foveal MPOD measured as a 1° integrated area assuming stimulus center measure and foveal MPOD measured as a 1° integrated area assuming a stimulus point at highest retinal sensitivity were non-significant (Table 21, Table 22, Table 23).

At 6cpd, 2° horizontal meridian CS, 2° vertical meridian CS and mean 2° CS correlations with 2^0 MPOD measured as a discrete point, 2° MPOD measured as a 1^0 integrated area assuming stimulus center point measure and 2° MPOD measured as a 1^0 integrated area assuming a stimulus point at highest retinal sensitivity were non-significant (Table 24, Table 25, Table 26). Horizontal meridian 4° CS, vertical meridian 4° CS and mean 4° CS correlations with all three measures of MPOD at 4° eccentricity were non-significant (Table 27, Table 28, Table 29). Horizontal meridian 6° CS, vertical meridian 6° CS and mean 6° CS correlations with all three measures of MPOD at 6° eccentricity were also non-significant (Table 30, Table 31, Table 32).

An independent sample t-test of CS differences at 0°, 2°, 4° and 6° eccentricities between the highest and lowest quartiles of foveal MPOD as a 1° integrated area assuming a stimulus point at highest retinal sensitivity was also performed using an independent sample t-test. Results for Levene's Test for Equal Variances were

non-significant so equal variances were assumed. At 6cpd, no significant differences in CS between top and bottom quartiles of foveal MPOD were identified (Table 33).

9cpd CS correlations with MPOD

At 6cpd, horizontal meridian CS, vertical meridian CS and mean CS correlations at all eccentricities (0°, 2°, 4° and 6°) with foveal MPOD measured as a discrete point, foveal MPOD measured as a 1° integrated area assuming stimulus center measure and foveal MPOD measured as a 1° integrated area assuming a stimulus point at highest retinal sensitivity were non-significant (Table 34, Table 35, Table 36).

At 9cpd, 2° horizontal meridian CS, 2° vertical meridian CS and mean 2° CS correlations with 2° MPOD measured as a discrete point, 2° MPOD measured as a 1° integrated area assuming stimulus center point measure and 2° MPOD measured as a 1° integrated area assuming a stimulus point at highest retinal sensitivity were non-significant (Table 37, Table 38, Table 39). Horizontal meridian 4° CS, vertical meridian 4° CS and mean 4° CS correlations with all three measures of MPOD at 4° eccentricity were non-significant (Table 40, Table 41, Table 42). Horizontal meridian 6° CS, vertical meridian 6° CS and mean 6° CS correlations with all three measures of MPOD at 6° eccentricity were also non-significant (Table 43, Table 44, Table 45).

An independent sample t-test of CS differences at 0°, 2°, 4° and 6° eccentricities between the highest and lowest quartiles of foveal MPOD as a 1° integrated area assuming a stimulus point at highest retinal sensitivity was also performed using an independent sample t-test. Results for Levene's Test for Equal Variances were non-significant so equal variances were assumed. At 9cpd, no significant differences in CS between top and bottom quartiles of foveal MPOD were identified (Table 46).

Glare Disability and Relative Glare Disability correlations with MPOD
Non-significant correlations between both horizontal and vertical meridian CS with MPOD allowed the use of a mean GD value and RGD value incorporating all four meridians. GD and RGD are measurements of the SW attenuation property exhibited by MP. This attenuation should be exhibited in the same symmetric pattern as MPOD spatial distribution indicated by the highly correlated MPOD values among the four meridians at each eccentricity.

At 3cpd, both foveal GD and RGD correlations with foveal MPOD measured as a discrete point, foveal MPOD as a 1° integrated area assuming stimulus center measure and foveal MPOD as a 1° integrated area assuming a stimulus point at highest retinal sensitivity were non-significant. Two degree GD correlations with foveal MPOD measured as a discrete point (GD: r = -0.327, p = 0.063), foveal MPOD as a 1° integrated area assuming stimulus center measure (GD: r = -0.333, p = 0.058) and foveal MPOD as a 1° integrated area assuming a stimulus

point at highest retinal sensitivity (GD: r = -0.331, p = 0.060) were near

significant. Two degree RGD correlations with foveal MPOD measured as a

discrete point (RGD: r = -0.335, p = 0.058), foveal MPOD as a 1° integrated area

assuming stimulus center measure (RGD: r = -0.342, p = 0.056) and foveal

MPOD as a 1° integrated area assuming a stimulus point at highest retinal

sensitivity (RGD: r = -0.341, p = 0.055) were also near significant. Four degree

GD and RGD correlations with all three foveal MPOD measurements were non-

significant. Six degree GD and RGD correlations with all three foveal MPOD

measurements were also non-significant (Table 47).

At 3cpd, 2° GD and RGD correlations with 2° MPOD measured as a discrete

point, 2° MPOD measured as a 1° integrated area assuming stimulus center

measure and 2° MPOD measured as a 1° integrated area assuming a stimulus

point at highest retinal sensitivity were non-significant (Table 48). Four degree

GD and RGD correlations with all three measures of MPOD at 4^oeccentricity

were non-significant (Table 49). Six degree GD and RGD correlations with all

three measures of MPOD at 6^oeccentricity were also non-significant (Table 50).

An independent sample t-test analysis of GD and RGD differences at 0°, 2°, 4°

and 6° eccentricities between the highest and lowest quartiles of foveal MPOD as

a 1° integrated area assuming a stimulus point at highest retinal sensitivity was

also performed. At 3cpd, GD differences at all retinal eccentricities were non-

significant between top and bottom quartiles of foveal MPOD. However,

significant RGD differences were identified at 2°, 4° and 6° eccentricity. An effect size correlation between t-test values and degrees of freedom for GD and RGD at each eccentricity was also calculated (Table 51).

Independent Samples t-test			
3cpd			
	t-value	**Sig.**	**Effect Size (r)**
GD_0^o	-0.522	0.609	0.129
RGD_0^o	-1.040	0.314	0.252
GD_2^o	-1.798	0.102	0.410
RGD_2^o	-2.210*	0.048	0.484
GD_4^o	-1.741	0.116	0.399
RGD_4^o	-2.356*	0.043	0.580
GD_6^o	-1.216	0.246	0.291
RGD_6^o	-2.287*	0.045	0.496

Table 51

Independent samples t-test for glare disability and relative glare disability at 0°, 2°, 4° and 6° for 3cpd grating targets between the highest and lowest foveal MPOD as a 1° integrated area assuming a stimulus point at highest retinal sensitivity quartiles. Effect size correlations were calculated using degrees of freedom = 16. Levene's Test for Equal Variances was significant so equal variances were not assumed (* $p \leq 0.05$ and**$p \leq 0.01$)

A Levene's Test for Equality of Variances between the highest and lowest quartile were significant at 2° RGD, 4° RGD and 6° RGD. A non-parametric Mann-Whitney U test between the highest and lowest foveal MPOD quartiles for RGD at 4° and 6° resulted in a significant difference at 4° and a non-significant difference at 6° (Table 52).

Mann-Whitney U Test		
Null Hypothesis of Equal Means Between Quartiles:	**Significance**	**Decision**
GD_0°	0.489	Retain Null Hypothesis
RGD_0°	0.436	Retain Null Hypothesis
GD_2°	0.113	Retain Null Hypothesis
RGD_2°	0.040*	Reject Null Hypothesis
GD_4°	0.136	Retain Null Hypothesis
RGD_4°	0.024*	Reject Null Hypothesis
GD_6°	0.387	Retain Null Hypothesis
RGD_6°	0.094	Retain Null Hypothesis

Table 52

A non-parametric independent samples Mann-Whitney U test for glare disability and relative glare disability at $0°$, $2°$, $4°$ and $6°$ for 3cpd grating targets between the highest and lowest foveal MPOD as a $1°$ integrated area assuming a stimulus point at highest retinal sensitivity quartiles (* $p ≤ 0.05$ and **$p ≤ 0.01$)

The range of calculated values for RGD using 3cpd stimuli at each eccentricity was 0.37 at $0°$, 0.36 at $2°$, 0.35 at $4°$ and 0.36 at $6°$. The similar range at each retinal eccentricity indicates no trend of increasing GD with increasing eccentricity and concurrent decreasing MPOD. Scatterplots of all 3 foveal measures of MPOD against RGD revealed that in all cases, a positive relationship was seen at all eccentricities. Scatterplots using RGD and foveal MPOD measured as a $1°$ integrated area assuming a stimulus point at highest retinal sensitivity explained low amounts of variance at all eccentricities ($0°$ r^2 = 0.052 [Figure 20], $2°$ r^2 = 0.116 [Figure 21], $4°$ r^2 = 0.069 [Figure 22] and $6°$ r^2 = 0.062 [Figure 23]). Significance for the regression scatterplots was calculated for foveal MPOD as a $1°$ integrated area assuming a stimulus point at highest retinal sensitivity and RGD at $0°$, $2°$, $4°$ and $6°$ for 3cpd stimuli. Non-significant F scores were found between integrated foveal MPOD and RGD at all eccentricities for 3cpd stimuli (Table 53). A multiple regression using foveal MPOD as a $1°$ integrated area assuming a stimulus point at highest retinal sensitivity and

corresponding kurtosis value as predictors for resulting RGD at all eccentricities was also performed. Non-significant F scores were identified at all eccentricities (0°, 2°, 4° and 6°) (Table 54).
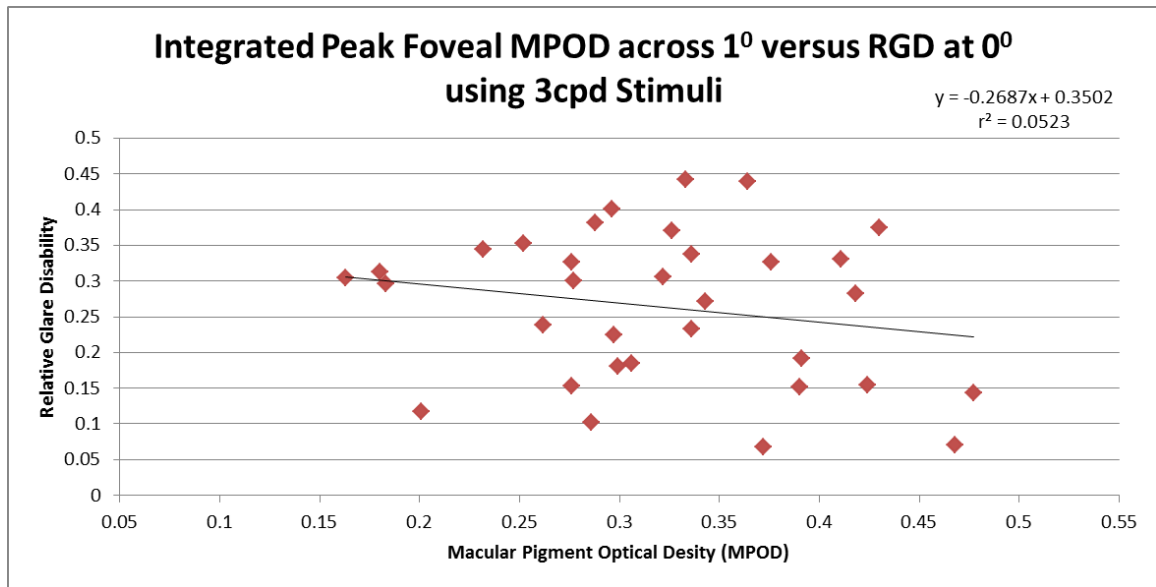
Figure 20
Scatterplot of integrated foveal MPOD at highest retinal sensitivity across 1^0 stimuli versus RGD at 0^0 eccentricity at 3cpd.
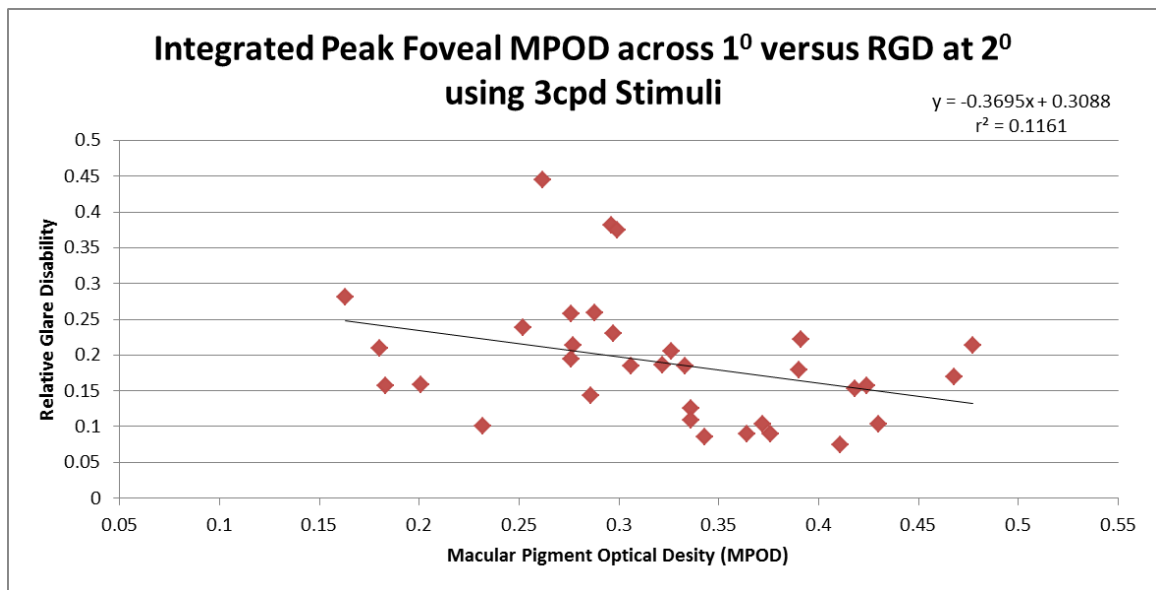
Figure 21
Scatterplot of integrated foveal MPOD at highest retinal sensitivity across 1^0 stimuli versus RGD at 2^0 eccentricity at 3cpd.
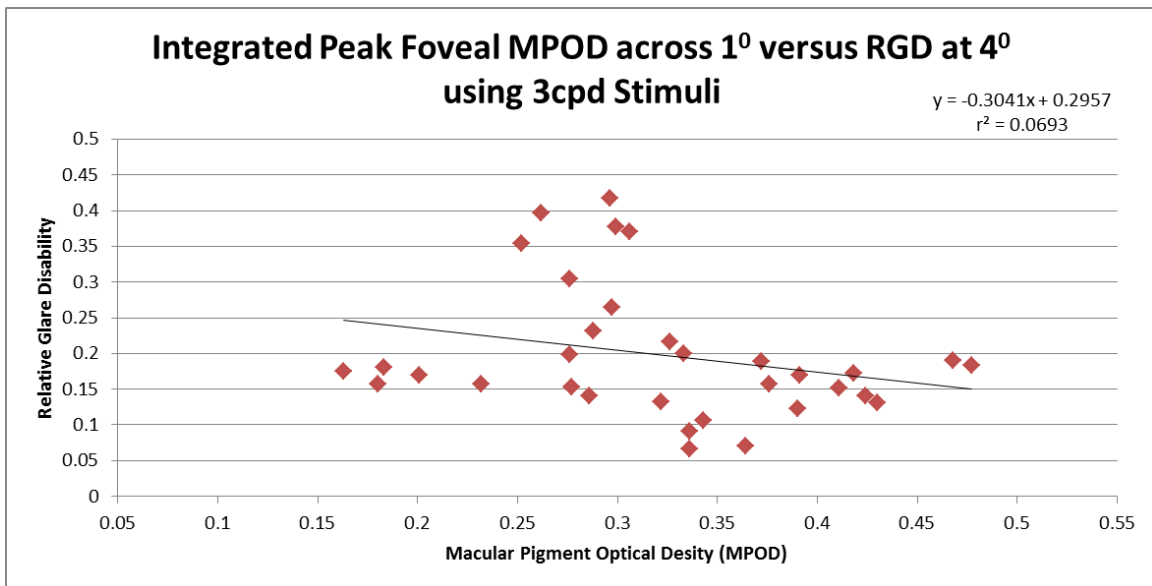
Figure 22
Scatterplot of integrated foveal MPOD at highest retinal sensitivity across 1° stimuli versus RGD at 4⁰ eccentricity at 3cpd.
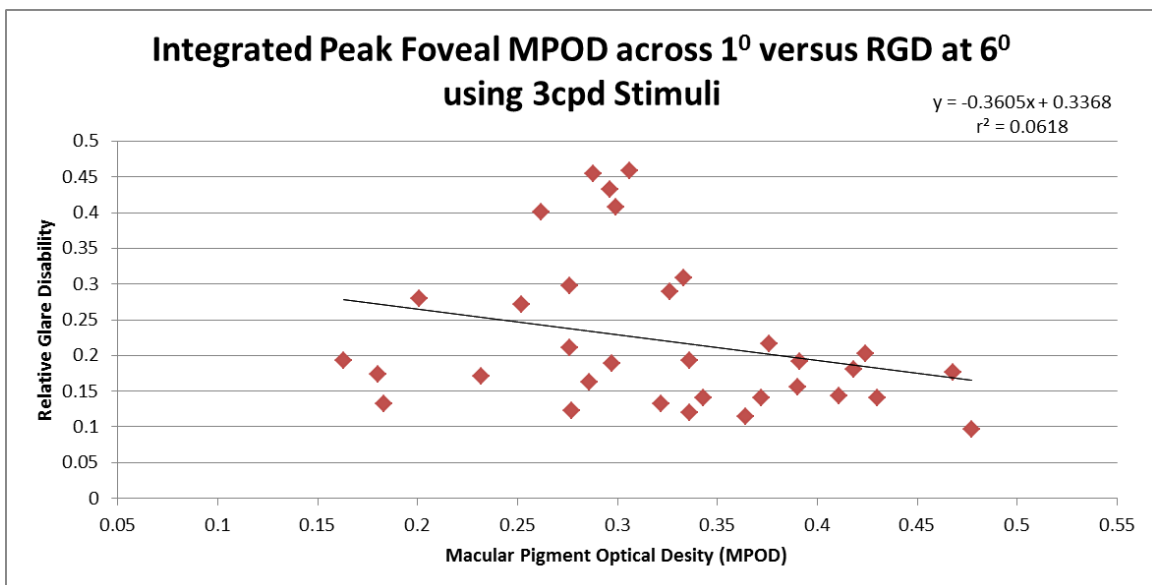
Figure 23
Scatterplot of integrated foveal MPOD at highest retinal sensitivity across 1° stimuli versus RGD at 6⁰ eccentricity at 3cpd.

Although the independent sample t-test revealed significant differences in RGD between the highest and lowest quartiles of foveal MPOD at 2° and 4° eccentricity, scatterplot results demonstrated relatively low amount of variance

explained at 0° eccentricity ($r^2 = 0.052$) and the 2° eccentricity ($r^2 = 0.116$) and nearly equivalent covariance measures between 4° ($r^2 = 0.069$) and 6° ($r^2 = 0.062$) eccentricity.

6cpd Glare Disability and Relative Glare Disability correlations with MPOD

At 6cpd, foveal GD correlations with foveal MPOD measured as a discrete point, foveal MPOD as a 1° integrated area assuming stimulus center measure and foveal MPOD as a 1° integrated area assuming stimulus point at highest retinal sensitivity were all non-significant. However, RGD correlations with foveal MPOD measured as a discrete point (RGD: r = -0.401, p = 0.023), foveal MPOD measured as a 1° integrated area assuming stimulus center (RGD: r = -0.412, p = 0.017) and foveal MPOD measured as a 1° integrated area assuming a stimulus point at highest retinal sensitivity (RGD: r = -0.418, p = 0.015) were significant (Table 55).

6cpd		GD_0^o	RGD_0^o	GD_2^o	RGD_2^o	GD_4^o	RGD_4^o	GD_6^o	RGD_6^o
Foveal MPOD Discrete Point	Pearson Correlation	-0.240	-0.401*	-0.294	-0.355*	-0.164	-0.255	-0.044	-0.189
	Sig. (2-tailed)	0.178	0.023	0.097	0.041	0.362	0.151	0.807	0.293
Foveal MPOD Integrated Stimulus Center	Pearson Correlation	-0.255	-0.412*	-0.291	-0.352*	-0.159	-0.252	-0.034	-0.180
	Sig. (2-tailed)	0.152	0.017	0.100	0.044	0.378	0.158	0.850	0.317
Foveal MPOD Integrated Stimulus Highest Sensitivity	Pearson Correlation	-0.265	-0.418*	-0.292	-0.354*	-0.155	-0.248	-0.030	-0.173
	Sig. (2-tailed)	0.137	0.015	0.099	0.043	.390	0.163	0.870	0.335

Table 55

Correlation coefficients for MPOD at 0° and glare disability and relative glare disability at 0°, 2°, 4° and 6° for 6cpd grating targets. (* p ≤ 0.05 and **p ≤ 0.01)

Two degree GD correlations with foveal MPOD measured as a discrete point, foveal MPOD measured as a 1° integrated area assuming stimulus center measure and foveal MPOD measured as a 1° integrated area assuming a stimulus point at highest retinal sensitivity were non-significant. Two degree RGD correlations with foveal MPOD measured as a discrete point (RGD: r = -0.355, p= 0.041), foveal MPOD measured as a 1° integrated area assuming stimulus center measure (RGD: r = -0.352, p = 0.044) and foveal MPOD as a 1° integrated area assuming a stimulus point at highest retinal sensitivity (RGD: r = -0.354, p = 0.043) were significant. Four degree GD and RGD correlations with all three foveal MPOD measurements were non-significant. Six degree GD and RGD correlations with all three foveal MPOD measurements were non-significant (Table 55).

At 6cpd, 2° GD and RGD correlations with 2° MPOD measured as a discrete point, 2° MPOD measured as a 1° integrated area assuming stimulus center measure and 2° MPOD measured as a 1° integrated area assuming a stimulus point at highest retinal sensitivity were non-significant (Table 56). Four degree GD and RGD correlations with all three measures of MPOD at 4^oeccentricity were non-significant (Table 57). Six degree GD and RGD correlations with all three measures of MPOD at 6^oeccentricity were also non-significant (Table 58).

An independent sample t-test analysis of GD and RGD differences at 0°, 2°, 4° and 6° eccentricities between the highest and lowest quartiles of foveal MPOD

was performed. At 6cpd, non- significant GD differences were identified at 0°, 2°, 4°, and 6° eccentricities between top and bottom quartiles of foveal MPOD. However, significant RGD differences were identified at 0°, 2° and 4° eccentricity between top and bottom quartiles of foveal MPOD. An effect size correlation between t-test values and degrees of freedom for GD and RGD at each eccentricity was also calculated (Table 59). A Levene's Test for Equality of Variances between the highest and lowest quartile was significant at 6° RGD, however the non-significant t-value required no additional non-parametric testing.

Independent Samples t-test			
6cpd			
	t-value	**Sig.**	**Effect Size (r)**
GD_0^o	-1.203	0.246	0.288
RGD_0^o	-2.118*	0.049	0.468
GD_2^0	-1.919	0.073	0.433
RGD_2^0	-2.443*	0.027	0.521
GD_4^0	-1.143	0.207	0.274
RGD_4^0	-2.158*	0.046	0.475
GD_6^0	-0.205	0.840	0.051
RGD_6^0	-1.007	0.329	0.244

Table 59

Independent samples t-test for glare disability and relative glare disability at 0°, 2°, 4° and 6° eccentricity for 6cpd grating targets between the highest and lowest foveal MPOD as a 1° integrated area assuming a stimulus point at highest retinal sensitivity quartiles. Effect size correlations were calculated using degrees of freedom = 16. Levene's Test for Equal Variances was non-significant so equal variances were assumed. (* $p \leq 0.05$ and **$p \leq 0.01$)

The range of calculated values for RGD using 6cpd stimuli at each eccentricity was 0.21 at 0°, 0.34 at 2°, 0.45 at 4° and 0.59 at 6°. The trend of increasing GD was seen with increasing eccentricity and concurrent decreasing MPOD. Scatterplots of all three foveal measures of MPOD against RGD revealed that in all cases, a positive relationship was seen at all eccentricities. Scatterplots using RGD and foveal MPOD measured as a 1° integrated area assuming a stimulus

point at highest retinal sensitivity explained the greatest amount of variance at all eccentricities (0° r^2 = 0.175 [Figure 24], 2° r^2 = 0.126 [Figure 25], 4° r^2 = 0.062 [Figure 26] and 6° r^2 = 0.030 [Figure 27]).

Significance for the scatterplots was calculated for foveal MPOD as a 1^0 integrated area assuming a stimulus point at highest retinal sensitivity and RGD at 0°, 2°, 4° and 6° for 6cpd stimuli. A significant F value was found between foveal MPOD as a 1° integrated area assuming stimulus point at highest retinal sensitivity and 0° and non-significant F values were at 2°, 4° and 6° eccentricities for 6cpd stimuli (Table 60). A multiple regression using foveal MPOD as a 1° integrated area assuming a stimulus point at highest retinal sensitivity and corresponding kurtosis value as predictors for resulting RGD at all eccentricities was also performed. Non-significant F scores were identified at all eccentricities (0°, 2°, 4° and 6°) (Table 61).
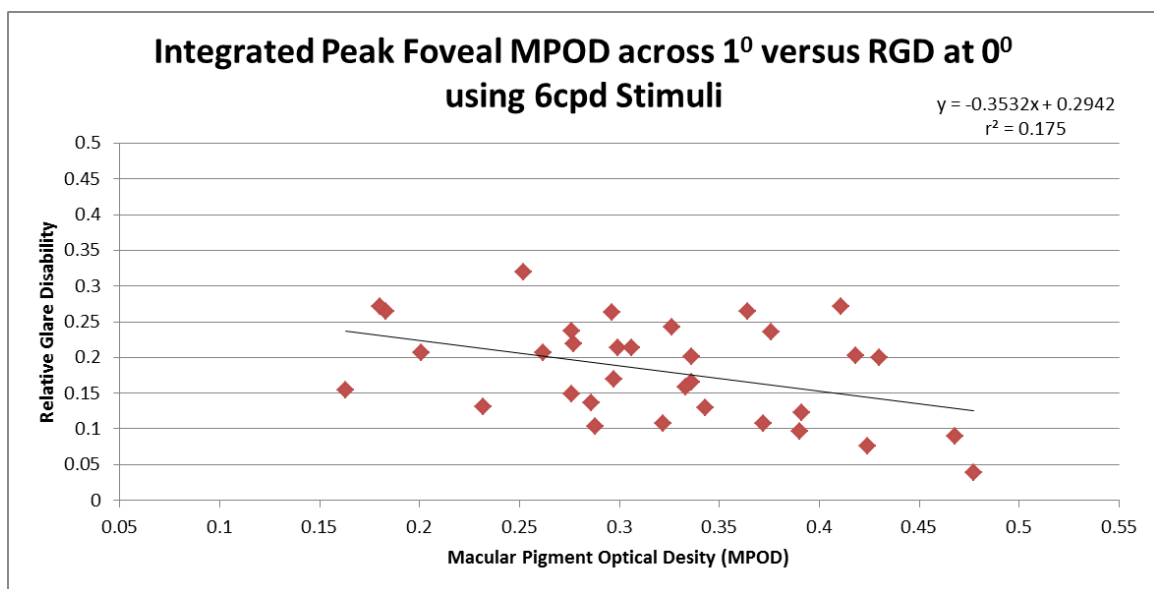
Figure 24
Scatterplot of integrated foveal MPOD at highest retinal sensitivity across 1° stimuli versus RGD at 0° eccentricity at 6cpd.
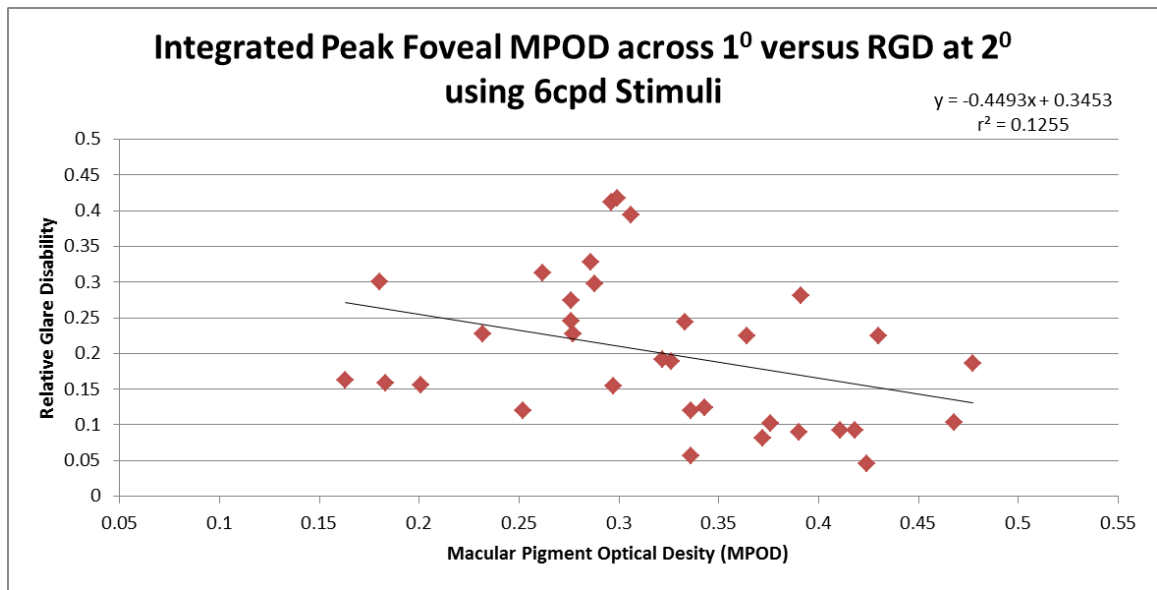
Figure 25
Scatterplot of integrated foveal MPOD at highest retinal sensitivity across 1° stimuli versus RGD at 2° eccentricity at 6cpd.
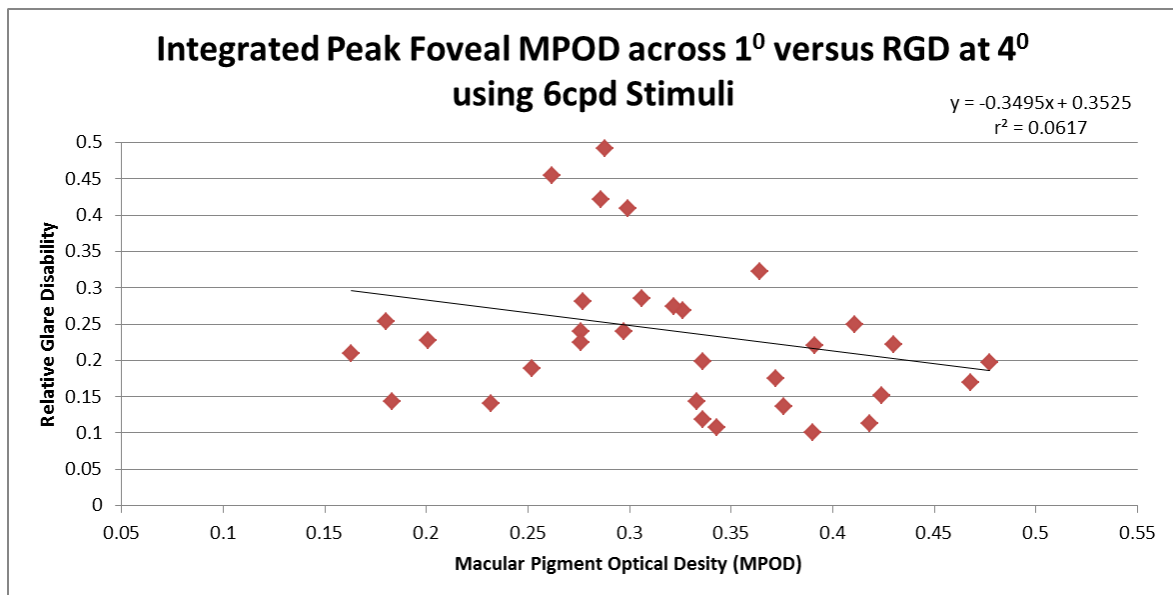
Figure 26
Scatterplot of integrated foveal MPOD at highest retinal sensitivity across 1° stimuli versus RGD at 4° eccentricity at 6cpd.
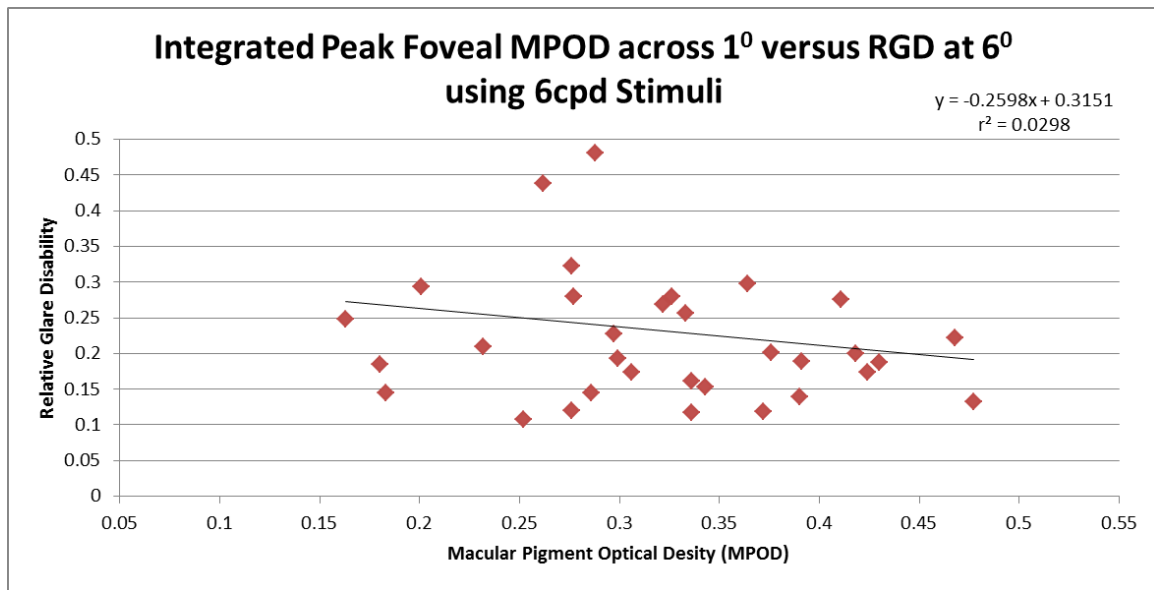
Figure 27
Scatterplot of integrated foveal MPOD at highest retinal sensitivity across 1° stimuli versus RGD at 6° eccentricity at 6cpd.

Regression Fit for 6cpd Stimuli		
Integrated Foveal MPOD	**F**	**Significance**
RGD_0°	6.575*	0.015
RGD_2°	4.449*	0.043
RGD_4°	2.039	0.163
RGD_6°	0.958	0.335

Table 60
Regression fit significance table for foveal MPOD as a 1° integrated area assuming stimulus point at highest retinal sensitivity and relative glare disability at 0°, 2°, 4° and 6° using 6cpd grating targets. (* $p \leq 0.05$ and **$p \leq 0.01$)

As the independent sample t-test revealed significant differences in RGD at 0°, 2° and 4° of eccentricity between the highest and lowest quartiles of foveal MPOD as a 1° integrated area assuming stimulus point at highest retinal sensitivity, scatterplot results demonstrated the greatest amount of variance explained at the 0° ($r^2 = 0.175$) followed by the 2° eccentricity ($r^2 = 0.1255$) and 4° eccentricity ($r^2 = 0.069$) and the least amount of variance explained at the 6° eccentricity ($r^2 = 0.030$).

9cpd Glare Disability and Relative Glare Disability correlations with MPOD

At 9cpd, both foveal GD and RGD with foveal MPOD measured as a discrete

point (GD: r = -0.395, p= 0.023 and RGD: r = -0.491, p = 0.004), foveal MPOD

measured as a 1° integrated area assuming stimulus center measure (GD: r = -

0.406, p = 0.019 and RGD: r = -0.501, p = 0.003) and foveal MPOD measured as

a 1^0 integrated area assuming a stimulus point at highest retinal sensitivity (GD: r

= -0.413, p = 0.017 and RGD: r = -0.505, p = 0.003) were significant. Two degree

GD and RGD correlations with foveal MPOD measured as a discrete point (GD: r

= -0.358, p = 0.043 and RGD: r = -0.401, p = 0.017), foveal MPOD measured as

a 1° integrated area assuming stimulus center measure (GD: r = -0.359, p =

0.043 and RGD: r = -0.407, p = 0.016) and foveal MPOD measured as a 1°

integrated area assuming a stimulus point at highest retinal sensitivity (GD: r = -

0.377, p = 0.032 and RGD: r = -0.421, p = 0.015) were significant (Table 62).

Four degree GD correlations with all three foveal MPOD measurements were

non-significant. However, four degree RGD correlations with foveal MPOD

measured as a discrete point (RGD: r = -0.372, p = 0.033), foveal MPOD

measured as a 1° integrated area assuming stimulus center measure (RGD: r = -

0.368, p = 0.035) and foveal MPOD measured as a 1° integrated area assuming

a stimulus point at highest retinal sensitivity (RGD: r = -0.373, p = 0.033) were

significant. Six degree GD and RGD correlations with all three measures of

foveal MPOD were non-significant (Table 62).

9cpd		GD_0°	RGD_0°	GD_2°	RGD_2°	GD_4°	RGD_4°	GD_6°	RGD_6°
Foveal MPOD Discrete Point	Pearson Correlation	-0.395*	-0.491**	-0.358*	-0.401*	-0.282	-0.372*	-0.051	-0.168
	Sig. (2-tailed)	0.023	0.004	0.043	0.017	0.112	0.033	0.777	0.351
Foveal MPOD Integrated Stimulus Center	Pearson Correlation	-0.406*	-0.501**	-0.359*	-0.407*	-0.270	-0.368*	-0.044	-0.162
	Sig. (2-tailed)	0.019	0.003	0.043	0.016	0.128	0.035	0.808	0.368
Foveal MPOD Integrated Stimulus Highest Sensitivity	Pearson Correlation	-0.413*	-0.505**	-0.377*	-0.421**	-0.274	-0.373*	-0.043	-0.162
	Sig. (2-tailed)	0.017	0.003	0.032	0.015	0.123	0.033	0.814	0.367

Table 62

Correlation coefficients for foveal MPOD as a 1° integrated area assuming stimulus point at highest retinal sensitivity at 0° and glare disability and relative glare disability at 0°, 2°, 4° and 6° for 9cpd grating targets. (* p ≤ 0.05 and **p ≤ 0.01)

At 9cpd, 2° GD and RGD correlations with 2° MPOD measured as a discrete point (GD: r = -0.421, p = 0.015 and RGD: r = -0.445, p = 0.009), 2° MPOD measured as a 1⁰ integrated area assuming stimulus center measure (GD: r = -0.434, p = 0.011 and RGD: r = -0.457, p = 0.008) and 2° MPOD measured as a 1° integrated area assuming a stimulus point at highest retinal sensitivity (GD: r = -0.399, p = 0.021 and RGD: r = -0.411, p = 0.018) were significant (Table 63).

9cpd		GD_2°	RGD_2°
2° MPOD Discrete Point	Pearson Correlation	-0.421*	-0.445**
	Sig. (2-tailed)	0.015	0.009
2° MPOD Integrated Stimulus Center	Pearson Correlation	-0.434**	-0.457**
	Sig. (2-tailed)	0.011	0.008
2° MPOD Integrated Stimulus Highest Sensitivity	Pearson Correlation	-0.399*	-0.411*
	Sig. (2-tailed)	0.021	0.018

Table 63

Correlation coefficients for MPOD at 2° and glare disability and relative glare disability at 2° for 9cpd grating targets. (* p ≤ 0.05 and **p ≤ 0.01)

Four degree GD correlations with 4° MPOD measured as a 1° integrated area assuming stimulus center measure (GD: r = -0.353, p = 0.044) was significant. Four degree RGD correlations with 4° MPOD measured as a 1° integrated area assuming stimulus center measure (RGD: r= -0.381, p = 0.029) and MPOD measured as a 1° integrated area assuming a stimulus point at highest retinal sensitivity (RGD: r = -0.359, p = 0.040) were significant (Table 64). Six degree GD and RGD correlations with all three measures of MPOD at 6° eccentricity were non-significant (Table 65).

9cpd		GD_4^o	RGD_4^o
4° MPOD Discrete Point	Pearson Correlation	-0.332	-0.341
	Sig. (2-tailed)	0.059	0.052
4° MPOD Integrated Stimulus Center	Pearson Correlation	-0.353*	-0.381*
	Sig. (2-tailed)	0.044	0.029
4° MPOD Integrated Stimulus Highest Sensitivity	Pearson Correlation	-0.339	-0.359*
	Sig. (2-tailed)	0.054	0.040

Table 64
Correlation coefficients for MPOD at 4° and glare disability and relative glare disability at 4° for 9cpd grating targets. (*p ≤ 0.05 and **p ≤ 0.01)

An independent sample t-test analysis of GD and RGD differences at 0°, 2°, 4° and 6° eccentricities between the highest and lowest quartiles of foveal MPOD as a 1° integrated area assuming stimulus point at highest retinal sensitivity was also performed. At 9cpd, significant GD and RGD differences were demonstrated at 0° and 2° with non-significant differences at 4° and 6° eccentricity between top and bottom quartiles of foveal MPOD (Table 66).

Independent Samples t-test			
9cpd			
	t-value	**Sig.**	**Effect Size (r)**
GD_0^o	-2.184*	0.049	0.479
RGD_0^o	-2.867*	0.015	0.583
GD_2^o	-2.527*	0.022	0.534
RGD_2^o	-2.811*	0.016	0.575
GD_4^o	-2.215*	0.042	0.484
RGD_4^o	-2.452*	0.026	0.523
GD_6^o	-0.055	0.957	0.014
RGD_6^o	-0.808	0.431	0.198

Table 66

Independent samples t-test for glare disability and relative glare disability at 0°, 2°, 4° and 6° for 9cpd grating targets between the highest and lowest foveal MPOD as a 1° integrated area assuming stimulus point at highest retinal sensitivity quartiles. Effect size correlations were calculated using degrees of freedom = 16. Levene's Test for Equal Variances was significant so equal variances were not assumed. (* p ≤ 0.05 and **p ≤ 0.01)

Levene's Test for Equality of Variances between the highest and lowest quartiles of foveal MPOD as a 1° integrated area assuming stimulus point at highest retinal sensitivity was significant at 0° RGD, 2° RGD and 4° GD indicating a non-normal distribution. A non-parametric Mann-Whitney U test between the highest and lowest foveal MPOD quartiles resulted in a significant difference at both 0° and 2° RGD and non-significance at 4° GD (Table 67).

Mann-Whitney U test		
Null Hypothesis of Equal Means Between Quartiles:	**Significance**	**Decision**
GD_0^o	0.031*	Reject Null Hypothesis
RGD_0^o	0.024*	Reject Null Hypothesis
GD_2^o	0.019*	Reject Null Hypothesis
RGD_2^o	0.031*	Reject Null Hypothesis
GD_4^o	0.063	Retain Null Hypothesis
RGD_4^o	0.016*	Reject Null Hypothesis
GD_6^o	0.605	Retain Null Hypothesis
RGD_6^o	0.387	Retain Null Hypothesis

Table 67

A non-parametric independent samples Mann-Whitney U test for glare disability and relative glare disability at 0°, 2°, 4° and 6° for 9cpd grating targets between the highest and lowest quartiles of foveal MPOD as a 1° integrated area assuming stimulus point at highest retinal sensitivity (*p ≤ 0.05 and **p ≤ 0.01)

The range of calculated values for RGD using 9cpd stimuli at each eccentricity was 0.27 at 0°, 0.35 at 2°, 0.43 at 4° and 0.46 at 6°. The trend of increasing GD was seen with increasing eccentricity and concurrent decreasing MPOD. Scatterplots of all three foveal measures of MPOD with RGD revealed that in all cases, a positive regression relationship was seen at all eccentricities. Scatterplots using RGD explained a moderate to high amount of variance in the data at 0°, 2° and 4° eccentricities (0° r^2 = 0.255 [Figure 28], 2° r^2 = 0.177 [Figure 29], 4° r^2 = 0.139 [Figure 30]) and a low amount of variance at 6° (r^2 = 0.026) [Figure 31].

Significance for the scatterplots was calculated for foveal MPOD as a 1° integrated area assuming a stimulus point at highest retinal sensitivity and RGD at 0°, 2°, 4° and 6° for 6cpd stimuli. A significant F value was found between foveal MPOD as a 1° integrated area assuming stimulus point at highest retinal sensitivity and RGD at 0°, 2° and 4° and non-significance at 6° (Table 68). A multiple regression using foveal MPOD as a 1° integrated area assuming a stimulus point at highest retinal sensitivity and corresponding kurtosis value as predictors for resulting RGD at all eccentricities was also performed. Significant F scores were identified at 0°, 2° and 4° eccentricities with non-significance at 6° (Table 69).
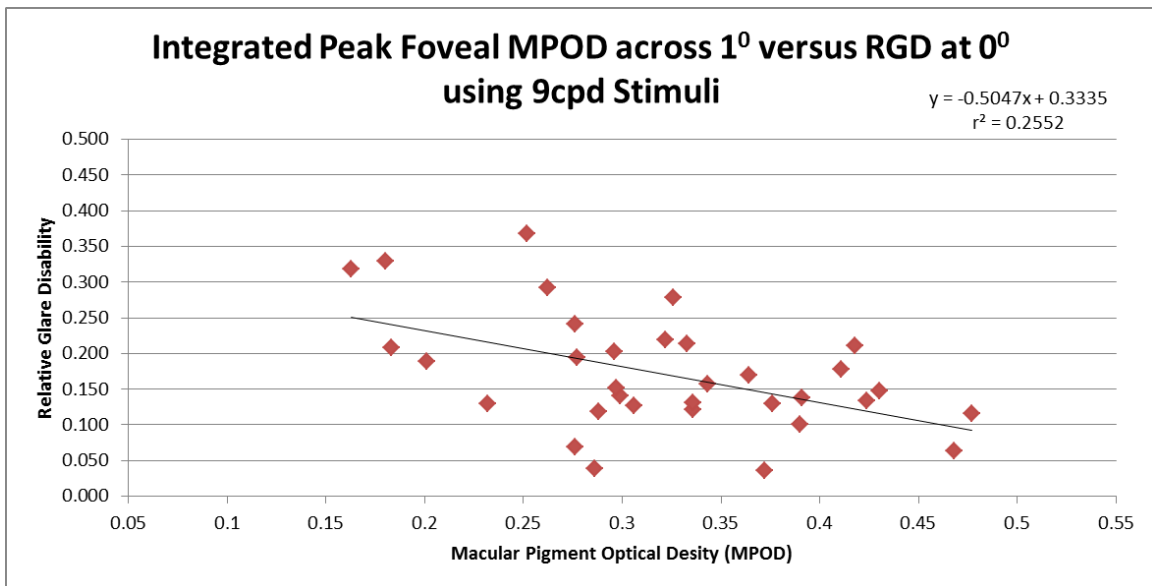
Figure 28
Scatterplot of integrated foveal MPOD at highest retinal sensitivity across 1° stimuli versus RGD at 0° eccentricity at 9cpd.
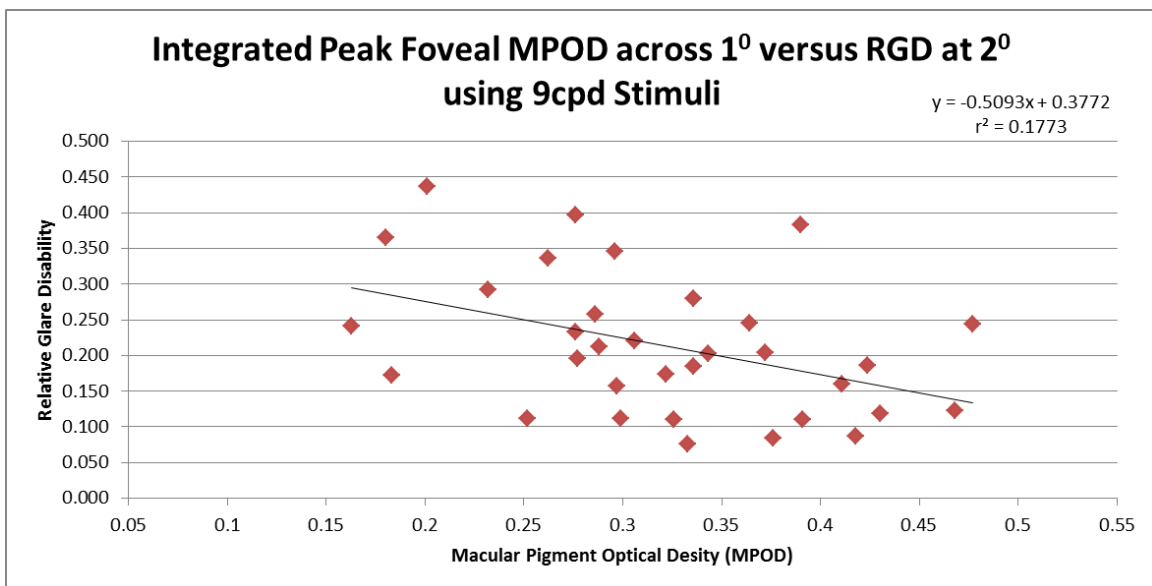
Figure 29
Scatterplot of integrated foveal MPOD at highest retinal sensitivity across 1° stimuli versus RGD at 2° eccentricity at 9cpd.
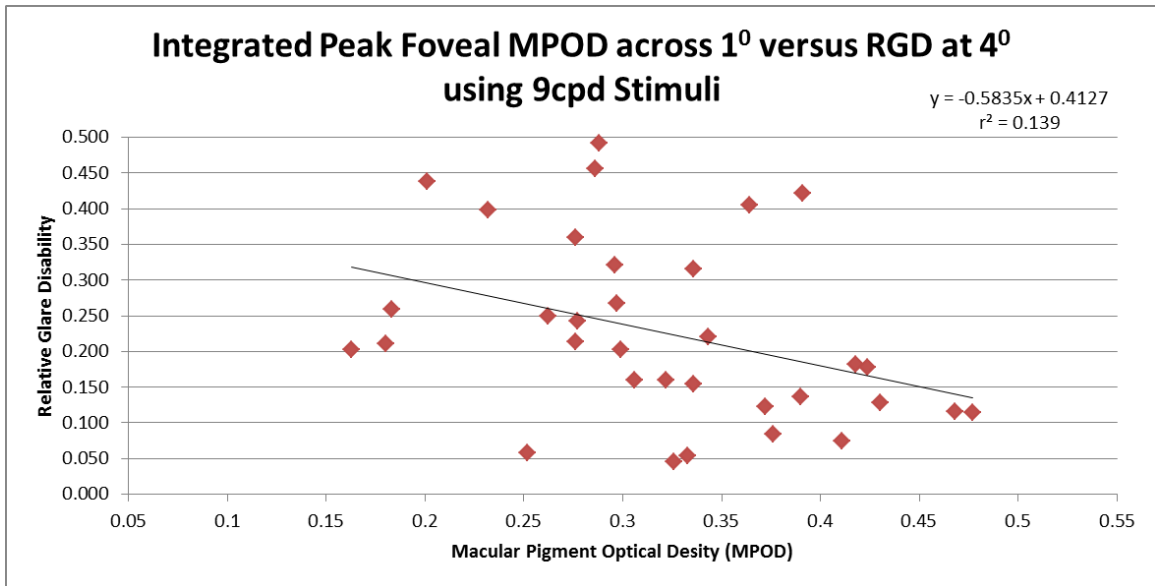
Figure 30
Scatterplot of integrated foveal MPOD at highest retinal sensitivity across 1° stimuli versus RGD at 4° eccentricity at 9cpd.
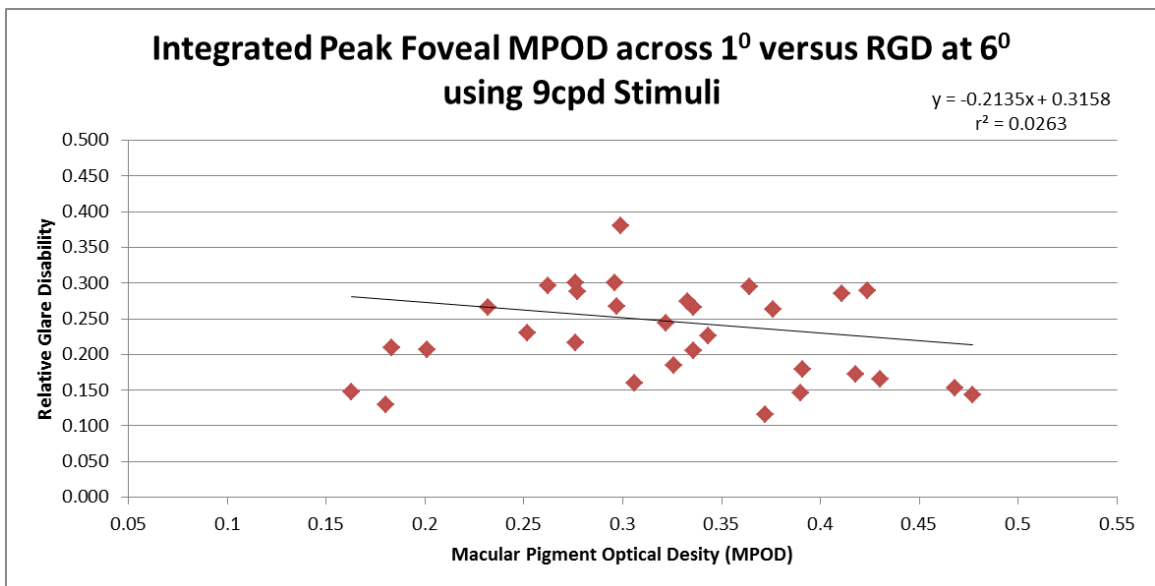
Figure 31
Scatterplot of integrated foveal MPOD at highest retinal sensitivity across 1° stimuli versus RGD at 6° eccentricity at 9cpd.

Regression Fit for 9cpd Stimuli		
Integrated Foveal MPOD	F	Significance
RGD_0^o	10.614 **	0.003
RGD_2^o	6.681 *	0.015
RGD_4^o	5.007 *	0.033
RGD_6^o	0.834	0.369

Table 68
Regression fit significance table for foveal MPOD integrated across 1^0 assuming stimulus point at highest retinal sensitivity and relative glare disability at 0°, 2°, 4° and 6° using 9cpd grating targets. (*p ≤ 0.05 and **p ≤ 0.01)

Multiple Regression Fit for 9cpd Stimuli		
Integrated Foveal MPOD and Kurtosis as Predictors	F	Significance
RGD_0^o	5.174*	0.012
RGD_2^o	3.610*	0.039
RGD_4^o	3.397*	0.047
RGD_6^o	0.414	0.665

Table 69
Multiple regression fit significance table for foveal MPOD integrated across 1° assuming stimulus point at highest retinal sensitivity and kurtosis values as predictors for relative glare disability at 0°, 2°, 4° and 6° using 9cpd grating targets. (*p ≤ 0.05 and **p ≤ 0.01)

As the independent sample t-test revealed significant differences between RGD at 0°, 2° and 4° of eccentricity, scatterplot results demonstrated the greatest amount of variance explained at the 0° (r^2 = 0.255) followed by the 2° eccentricity (r^2 = 0.177) then 4° eccentricity (r^2 = 0.139) and the least amount of variance explained at the 6° eccentricity (r^2 = 0.026).

Below shows a radial summary plot of correlation values between MPOD calculated as a discrete value with GD and RGD (Figure 32). The plots show the differences in correlation results among meridians as well as decreasing correlation between MPOD and glare attenuation with increasing eccentricity. A similar radial summary plot of correlation values between MPOD calculated as a

1° integrated area assuming stimulus point at highest retinal sensitivity with GD and RGD. Similar differences in correlation results among meridians as well as decreasing correlation between MPOD and glare attenuation with increasing eccentricity are seen (Figure 33).
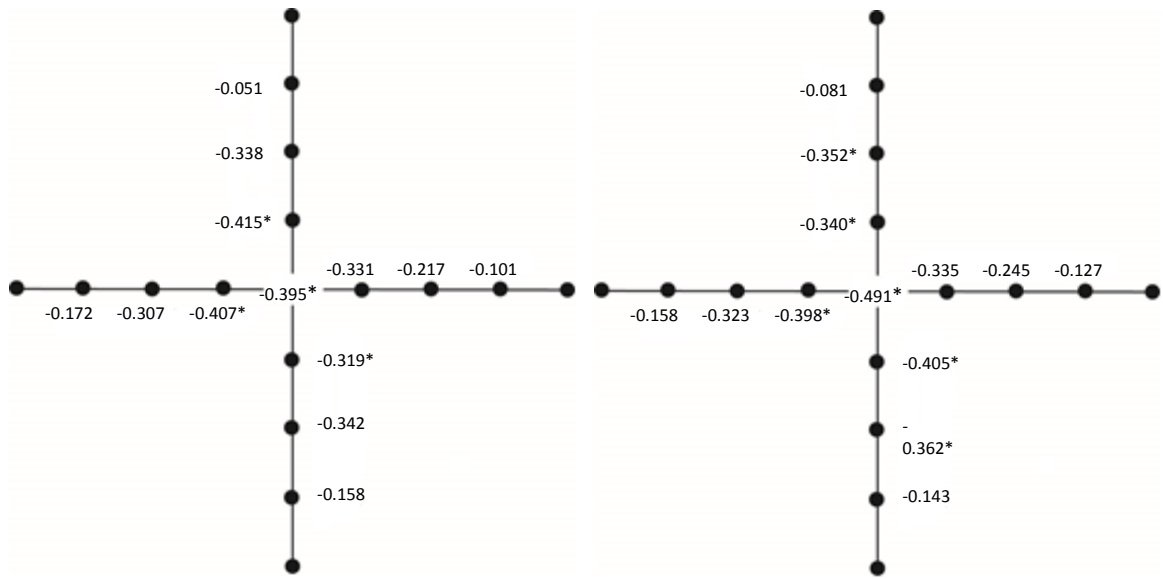
Figure 32
Summary plots indicating correlation and significance values for corresponding locations of MPOD measured as a discrete value and both GD (left) and RGD (right) using 9cpd stimuli . (*p ≤ 0.05 and **p ≤ 0.01)
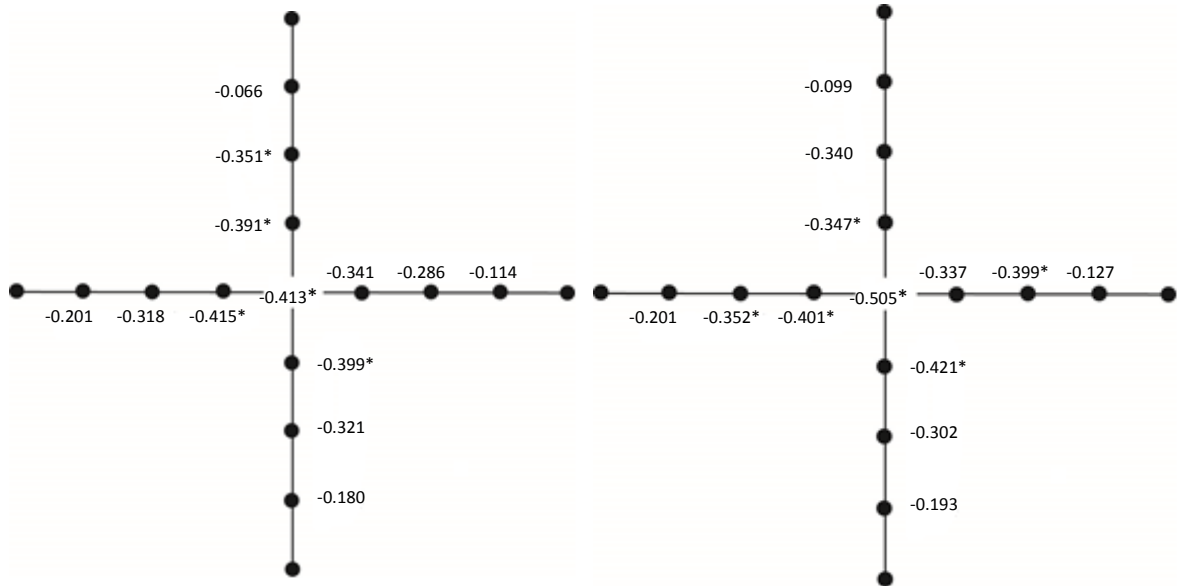
Figure 33
Summary plots indicating correlation and significance values for corresponding locations of MPOD as a 1° integrated area assuming stimulus point at highest retinal sensitivity and GD (left) and RGD (right) using 9cpd stimuli. (*p ≤ 0.05 and **p ≤ 0.01)

Intraocular Scatter Correlations with MPOD

Intraocular scatter was evaluated as four separate correlation coefficients: [1] foveal MPOD discrete value, [2] foveal MPOD integrated across 1°, [3] AUC integrated across 16° assuming stimulus center and [4] AUC integrated across 16° assuming stimulus point of highest sensitivity

Intraocular scatter correlations with foveal MPOD discrete value ($r = -0.348$, $p = 0.078$), foveal MPOD integrated across 1° ($r = -0.346$, $p = 0.080$), AUC integrated across 16° assuming stimulus center ($r = -0.261$, $p = 0.142$) and AUC integrated across 16° assuming stimulus point of highest sensitivity ($r = -0.253$, $p = 0.156$) were non-significant (Table 70).

		Foveal MPOD Discrete Point	Foveal MPOD Integrated Stimulus Highest Sensitivity	Integrated AUC MPOD across 16° Stimulus Center	Integrated AUC MPOD across 16° Stimulus Highest Sensitivity
Intraocular Scatter	Pearson Correlation	-0.348	-0.346	-0.261	-0.253
	Sig. (2-tailed)	0.078	0.080	0.142	0.156

Table 70
Correlation coefficients for intraocular scatter thresholds and MPOD measured at 0° integrated across the 1° stimulus and integrated across the 16° macula.

An independent sample t-test analysis of intraocular scatter differences between the highest and lowest quartiles of foveal MPOD revealed significant differences (Table 71).

Independent Samples t-test		
	t-value	Sig.
Intraocular Scatter	-2.715*	0.015

Table 71
Independent samples t-test for intraocular scatter between the highest and lowest foveal MPOD quartiles. Levene's Test for Equal Variances was non-significant so equal variances were assumed. (* $p \leq 0.05$ and **$p \leq 0.01$)

A scatterplot of foveal MPOD integrated across 1° with intraocular scatter values was performed resulting in a $r^2 = 0.117$. An inverse relationship was seen supporting the hypothesis that higher foveal MPOD levels are associated with decreased levels of intraocular scatter (Figure 34). Significance for the scatterplot was calculated for foveal MPOD as a 1° integrated area assuming a stimulus point at highest retinal sensitivity and intraocular scatter. A non- significant F value was found between foveal MPOD and intraocular scatter (Table 72).
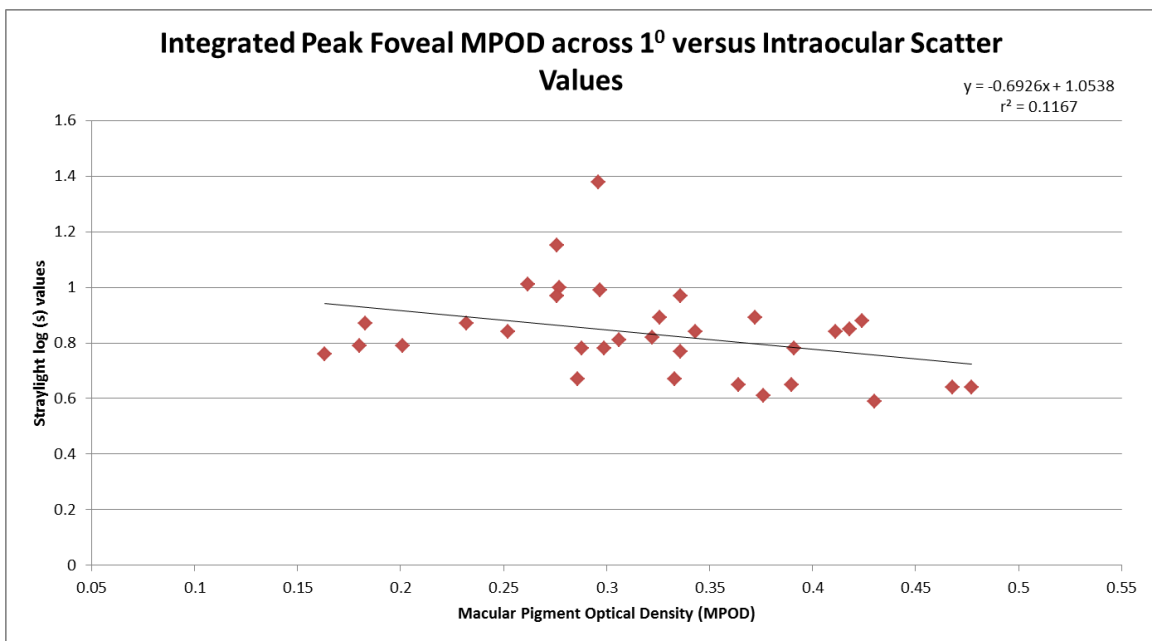
Figure 34
Scatterplot of integrated foveal MPOD at highest retinal sensitivity across 1° stimuli versus intraocular scatter.

Regression Fit for Intraocular Scatter		
Integrated Foveal MPOD	**F**	**Significance**
Intraocular Scatter	3.179	0.084

Table 72
Regression fit significance table for foveal MPOD integrated across 1° and intraocular scatter values

Three summary tables of correlations between foveal MPOD measured as a discrete point (Table 73), foveal MPOD measured as a 1° integrated area assuming stimulus center measure (Table 74) and foveal MPOD measured as a

1° integrated area assuming a stimulus point at highest retinal sensitivity (Table 75) with CS, GD and RGD at all measured retinal eccentricities (0°, 2°, 4° and 6°) at all measured spatial frequencies (3, 6, 9cpd) are provided below.

Foveal MPOD Measured as a Discrete Point								
Contrast Sensitivity			**Glare Disability**			**Relative Glare Disability**		
3cpd	*6cpd*	*9cpd*	*3cpd*	*6cpd*	*9cpd*	*3cpd*	*6cpd*	*9cpd*
0° NS	NS	NS	NS	NS	-0.392*	NS	-0.401*	-0.491**
2° NS	NS	NS	NS	NS	-0.358*	NS	-0.316*	-0.469**
4° NS	NS	NS	NS	NS	NS	NS	NS	-0.372**
6° NS	NS	NS	NS	NS	NS	NS	NS	NS

Table 73
Correlation coefficients for foveal MPOD as a discrete point measure and contrast sensitivity, glare disability and relative glare disability at 0°, 2°, 4° and 6° of eccentricity for 3, 6 and 9cpd grating targets. (* p ≤ 0.05 and **p ≤ 0.01)

Foveal MPOD as 1° Integrated Area Assuming Stimulus Center								
Contrast Sensitivity			**Glare Disability**			**Relative Glare Disability**		
3cpd	*6cpd*	*9cpd*	*3cpd*	*6cpd*	*9cpd*	*3cpd*	*6cpd*	*9cpd*
0° NS	NS	NS	NS	NS	-0.406*	NS	-0.412*	-0.501**
2° NS	NS	NS	NS	NS	-0.359*	NS	-0.316*	-0.475**
4° NS	NS	NS	NS	NS	NS	NS	NS	-0.368**
6° NS	NS	NS	NS	NS	NS	NS	NS	NS

Table 74
Correlation coefficients for foveal MPOD measured as a 1° integrated area assuming stimulus center measure and contrast sensitivity, glare disability and relative glare disability at 0°, 2°, 4° and 6° of eccentricity for 3, 6 and 9cpd grating targets. (* p ≤ 0.05 and **p ≤ 0.01)

Foveal MPOD as 1°Integrated Area Assuming Stimulus Point of Highest Retinal Sensitivity								
Contrast Sensitivity			**Glare Disability**			**Relative Glare Disability**		
3cpd	*6cpd*	*9cpd*	*3cpd*	*6cpd*	*9cpd*	*3cpd*	*6cpd*	*9cpd*
0° NS	NS	NS	NS	NS	-0.413*	NS	-0.418*	-0.505**
2° NS	NS	NS	NS	NS	-0.377*	NS	-0.315*	-0.489**
4° NS	NS	NS	NS	NS	NS	NS	NS	-0.373**
6° NS	NS	NS	NS	NS	NS	NS	NS	NS

Table 75
Correlation coefficients for foveal MPOD measured as a 1° integrated area assuming a stimulus point at highest retinal sensitivity and contrast sensitivity, glare disability and relative glare disability at 0°, 2°, 4° and 6° of eccentricity for 3, 6 and 9cpd grating targets. (* p ≤ 0.05 and **p ≤ 0.01)

VII. Discussion

A. Macular Pigment Spatial Distribution

The spatial distribution of MP in this sample as measured by cHFP was well-described by a first-order exponential function originating at the foveal center in agreement with *ex vivo* HPLC studies (Handelman et al., 1988) and a Lorentzian function across the macula (Stringham et al., 2003 and Wenzel et al., 2006). Spatial distribution results from this experiment show similar covariance values when MPOD measures at eccentricities across the macula assuming stimulus point at highest retinal sensitivity ($r^2 = 0.907$) versus stimulus center ($r^2 = 0.885$) are fit to a Lorentzian function. The similar covariance values support an adequate description of MPOD spatial distribution by assuming either stimulus center measurement or stimulus point at highest retinal sensitivity. Although the study sample distribution is best fit by a Lorentzian function across the macula, large individual differences in distribution shape are seen.

The study sample demonstrates a mean positive kurtosis (i.e. leptokurtic) value. This offers support of the Lorentzian fit to MPOD spatial distribution over a Gaussian fit due to the higher central peak of the Lorentzian function. The relatively large variance in the kurtosis values also supports the large variability in individual MPOD spatial distributions when fit to a Lorentzian function. The close agreement between the separate AUC measurements suggest that when considering the spatial distribution across the 16° macula, stimulus center and stimulus point at highest retinal sensitivity are comparable descriptors. Methods

of MPOD spatial distribution including kurtotic descriptions and integrated AUC

calculations show substantial variability among individuals and within the

substantial variability is where differences in visual performance measures may

lie.

In an effort to minimize receptive field interaction or underlying photoreceptor

response differences, the MPOD spatial distribution was also fit to a 1st order

exponential curve excluding the 0° measurement value. The relative agreement

of the y-intercept of the highest retinal sensitivity when the 0° measurement is

excluded (y-intercept = 0.477) versus stimulus center when 0° measurement is

excluded (y-intercept = 0.629) with both the stimulus point of highest retinal

sensitivity with 0° measurement (y-intercept = 0.387) and stimulus center with 0°

measurement (y-intercept = 0.426) may offer support that the point of highest

retinal sensitivity subtended by the stimuli is the measurement point of MPOD

using HFP techniques.

The overall distribution measure of MPOD shows an inverse association with

retinal eccentricity. The trend of decreasing MPOD as a function of eccentricity

has been documented by both *ex vivo* studies (Snodderly et al., 1984 and Bone

et al., 1985) and *in vivo* studies (Hammond et al., 1997 and Wooten et al., 2005)

of the MP spatial distribution. The results of this experiment support and confirm

the previously identified first order exponential decay curve exhibited by MP as a

function of retinal eccentricity. Several studies have described a secondary peak

or ring-like structure of MPOD that is found between approximately 0.50^0 and

0.85^0 eccentric to fovea in 10-20% of the general population (Berendschot et al.,

2006 and Dietzel et al., 2011). The cHFP device designed and built for this

project focused on the overall spatial distribution from 0° to 8° eccentricity

measured with a 1° stimulus at 2° intervals. Due to this device design,

measurement and verification of predicted ring-like MPOD findings is not within

the scope of the current project but design modifications to the existing cHFP

device would allow such a measurement.

Anatomic structure has also been demonstrated to influence MPOD spatial

profiles. Specifically, Nolan et al. (2008) found that foveal width was associated

with non-typical MP spatial distribution. Increased foveal width was significantly

related to MP spatial profiles due in part to increased length of the foveal cone

axons. The slope of the foveal depression was also shown to influence the slope

of the MPOD spatial distribution: Steep foveal depressions were significantly

related to steep MPOD spatial distributions.

Risk factors such as age and increased oxidative stress along with differences in

foveal anatomic architecture have been shown to create non-exponential

declines in MPOD spatial distribution with increasing eccentricity. Assessment of

MPOD spatial distribution for these individuals would likely be better expressed

as an integrated area under the curve. Results from the current experiment

across 33 subjects ages 22-34 supported a monotonic exponential decay curve

consistent with Kirby et al. (2010) which found that younger subjects tended to exhibit a typical exponential decay function with increasing eccentricity when measured by HFP. Kirby et al. also hypothesized that changes in the typical exponential function of MPOD distribution with age may be in part to cumulative SW absorption.

B. Contrast Sensitivity and Glare Disability Across the Macula

The overall distribution measures of CS and GD show an inverse association with retinal eccentricity. The decreasing CS with increasing retinal eccentricity demonstrated in this experiment is also supported in previous studies (Pointer et al., 1989). The inverse association of CS and retinal eccentricity is a consequence of the simultaneous decreasing cone density and increasing receptive field size that occurs with increasing retinal eccentricity (Virsu and Rovamo, 1979). The measure of GD was defined as a difference in CS under no glare and glare conditions. The subjects' underlying CS affects both measures and absolute GD reflected greater variability in sensitivity measures than relative GD. In order to parse out existing differences in GD specific to glare effects among individuals, a normalization of the absolute GD measure was determined through calculation of the RGD defined as $(CS_{No\ Glare} - CS_{Glare}) / CS_{No\ Glare}$.

Theoretically, as the MPOD decreases with increasing retinal eccentricity, the resulting GD should increase and sensitivity measures will decrease. GD was measured as a difference in CS and followed similar inverse associations with

retinal eccentricity. When GD was calculated, large variability at each retinal eccentricity within the sample was seen. The transformation of absolute GD into RGD allowed differences in sensitivity specific to glare to be identified and created less variability within the measures at each eccentricity. A greater number of RGD than GD results followed an expected trend of decreasing sensitivity with decreasing retinal eccentricity.

Stimuli were not scaled to account for receptive field changes with increasing sensitivity in order to compare equivalent integrated MPOD measures with grating targets areas. Increased parafoveal target sizes would require increased HFP stimuli to allow for equivalent integration comparisons. Due to the Lorentzian spatial distribution of MPOD across the macula, larger areas of integration would likely mask small differences between individual MPOD distributions.

Vertical grating orientations were utilized for CS and GD stimuli to allow for direct comparisons of results to the existing studies that also used vertical grating orientations (Loughman et al., 2010 and Nolan et al., 2011). The experimental design of this project utilized the same vertical grating targets for both glare and no glare conditions. Identical stimuli for both conditions allowed target resolution threshold by each subject to be identified in the same manner for both conditions helping to control for edge detection resulting from microsaccadic activity during fixation.

C. Relationship between MPOD, Contrast Sensitivity, Glare Disability and Intraocular Scatter

Hypothesis #1

MPOD has an inverse relationship with glare disability and contrast sensitivity at both foveal and parafoveal retinal loci.

Results from this study did not identify an association between MPOD and CS at foveal or parafoveal loci. Due the non-significant relationship between MPOD and CS and the calculation of GD as $CS_{No\ Glare}$ - CS_{Glare}, no significant correlations between MPOD and GD were found. However, when underlying CS results were controlled for by calculating RGD as ($CS_{No\ Glare}$ - CS_{Glare}) / $CS_{No\ Glare}$, study results supported a significant inverse relationship between foveal MPOD and RGD out to 4° eccentricity using 9cpd targets.

Hypothesis #2

Integrated measures of MPOD across the diameter of the stimulus will better predict visual performance compared to discrete point measurements.

MPOD was calculated as an integrated measure across the 1° stimulus assuming a central stimulus measure and across the 1° stimulus assuming a point of highest retinal sensitivity. Results from this study demonstrated similar significant correlations when MPOD measurements assumed either an integrated measure or a discrete measure. These similarities may be due to relatively small

differences in corresponding integrated and discrete MPOD measures within an individual subject. It is likely that both HFP and the adaptive staircase method of limits CS task involved the stimulus point which subtended the highest retinal sensitivity.

Hypothesis #3

Integrated MPOD is inversely related to intraocular scatter.

Intraocular scatter was assessed using a psychophysical central flicker comparison technique. Similar to the HFP device, the perception of subtle flicker differences were likely identified by the point of highest retinal sensitivity. The corresponding regions of subtle flicker comparison difference measurement and MPOD measurement may explain the higher correlation values between foveal MPOD and intraocular scatter rather than integrated MPOD across the 16° macula. Although correlations between foveal MPOD and intraocular scatter were non-significant, an inverse trend between was demonstrated.

Overall, results of this study demonstrated non-significant correlations between MPOD and CS at all retinal eccentricities at 3, 6 and 9cpd spatial frequencies. Only 1 previous non-supplementation study of MP has reported significant findings between MPOD and CS (Loughman et al., 2010). These differences in results may be due to differences in experimental design including stimuli configuration and psychophysical methods. The Loughman et al. (2010) study

utilized vertical Gabor patches with a spatial Gaussian envelope generated by a Metropsis Visual Stimulus Generation device (Cambridge Research Systems Ltd., Cambridge, UK) presented on a 19" CRT monitor which subtended 4.2^0 of visual angle. A four alternative forced choice test was used and targets were randomly presented at a 2^0 spatial offset from a central fixation cross. An adaptive staircase method was used to determine contrast threshold. The target visibility was started above expected subject threshold values (determined from previous pilot study) and decreased at 0.3 log unit steps until the first reversal then was presented at 0.15 log unit steps until 12 reversal were recorded. Threshold was identified at the midpoint of 12 reversal points for five different spatial frequencies: 1.0, 4.1, 7.5, 11.8 and 20.7cpd.

The hypothesized role of MP influences on CS has been attributed to SW attenuation effects of chromatic aberration and intraocular scatter leading to retinal image resolution increases through reduced lateral inhibition and enhanced receptive field responses (Loughman et al., 2010). Lack of correlation significance between MPOD and CS may also have been due to the spectral composition and the predominance of LW light contained within the stimuli and background. Spectral analysis of the CRT display used in stimuli generation was performed using the same spectrophotometer (model 650; Photo Research Inc., Chatsworth, CA) used in calibration of the LED glare sources.

P a g e | 141

Spectrophotometer results for the CRT used showed a luminance output of

20cd/m^2 with a peak wavelength of 624nm. The well-documented SW

attenuation property of MP underlies the Optical Hypothesis described earlier.

The absorption bandwidth of MP extends from approximately 400nm to 520nm

with a peak absorbance of 460nm. The peak spectral output of the stimuli and

background of produced by the CRT display used in the experiment is far outside

the absorption spectrum of MP providing a possible explanation for the non-

significant relationship between MPOD and CS.

3cpd Stimuli GD and RGD

Non-significant correlations of GD at 3cpd with both foveal and eccentric MPOD

measures are likely due to the influence of the underlying CS variability among

subjects. The method used to calculate GD was a difference in CS under no

glare and glare conditions. CS at the fovea and across the macula showed high

variability within the study sample and no significant relationship with MPOD

measures. The lack of significant correlation between foveal and eccentric

MPOD measures with CS likely influences the same lack of correlation between

foveal and eccentric MPOD measures with GD. A function of calculating relative

GD is a normalization of GD and an isolation of glare-dependent effects on CS

measures. Non-significant correlations of RGD at 3cpd with both foveal and

eccentric MPOD measures may be a result of the low spatial frequency stimuli

used. Roumes et al. (2001) and Aguirre et al. (2007) found that the effect of glare

is greatest within spatial frequencies with the highest CS and visual effects due

to glare conditions decreased CS primarily within the low spatial frequency range.

Although correlations were non-significant, a significant difference in RGD between the highest and lowest quartiles of foveal MPOD was identified at 2° and 4°. Theses significant differences between quartiles exist at low foveal eccentricities where MPOD is relatively higher than 6°. Additionally, the calculated effect sizes at 2° and 4° eccentricity were r = 0.484 and r = 0.508, respectively. Using Cohen's guidelines (Howell, 2007), correlational effect sizes greater than 0.4 are generally accepted as large providing that differences between the highest and lowest foveal MPOD quartiles are statistically significant and meaningful.

No significant difference in RGD was found at 6° where MPOD is relatively lower. This dependence on foveal eccentricity and relative MPOD may support a minimum value of MPOD may be necessary to confer RGD benefits to a subject. The lack of a significant difference in RGD at 0^0 eccentricity between the highest and lowest MPOD quartiles was unexpected. The non-significant difference may be a result of the high degree of variability within the RGD calculations at 0^0 among the subject sample for 3cpd stimuli compared to 6cpd and 9cpd stimuli.

6cpd Stimuli GD and RGD

Non-significant correlations between GD and foveal measures at 6cpd were identified. These non-significant correlations are likely a result of the underlying non-significant CS correlations with foveal MPOD or a lesser effect of MPOD glare attenuation on low to moderate spatial frequencies. Significant correlations of RGD with foveal MPOD measures were found at 0^0 and 2^0 and marginal significance of RGD with foveal MPOD measures at 4^0 foveal eccentricity. The findings of correlational significance with 6cpd stimuli and non-significance with 3cpd stimuli support a possible spatial frequency influence on RGD effects.

Significant differences in RGD between the highest and lowest quartiles of foveal MPOD were identified at 0°, 2° and 4° of foveal eccentricity with non-significant differences in GD at the same foveal eccentricities. These differences between GD and RGD support the importance of normalizing the effects of CS in order to evaluate distinct glare attenuation effects. Additionally, the calculated effect sizes for RGD at 0°, 2° and 4° eccentricity were r = 0.468, r = 0.521 and r = 0.475, respectively. The combination of statistical significance with a robust effect size suggests that differences between the highest and lowest foveal MPOD quartiles are meaningful.

The overall range of RGD for 6cpd stimuli at all eccentricities revealed a trend of increasing RGD with decreasing MPOD. Significant differences in RGD found at low foveal eccentricities with relatively greater MPOD in combination with non-

significant differences in RGD at high foveal eccentricities with relatively lower MPOD further supports a possible minimum value of MPOD necessary to confer RGD benefits.

9cpd Stimuli GD and RGD

Significant correlations of GD and RGD with foveal MPOD measures at 9cpd may indicate the influence of MPOD glare attenuation on moderate to high spatial frequencies. Significant correlations of GD with foveal MPOD is demonstrated at 0° and 2° foveal eccentricity while significant correlations of RGD with foveal MPOD are shown at 0°, 2° and 4° of foveal eccentricity. Significant correlations are also seen between GD and RGD with parafoveal MPOD measures at 2° and 4° not seen using the 3cpd and 6cpd stimuli. The overall range of RGD for 9cpd stimuli at all eccentricities revealed a trend of increasing RGD with decreasing MPOD. The trend of increasing RGD with decreasing MPOD is exhibited at 6cpd stimuli and 9cpd stimuli but not 3cpd stimuli, may also support a spatial frequency dependence of MPOD on glare attenuation. Additionally, the emergence of a significant relationship between corresponding parafoveal MPOD with both GD and RGD out to 4° eccentricity using 9cpd targets suggests a spatial frequency dependence on the glare attenuation afforded by MP.

The analysis of RGD between the highest and lowest quartiles of foveal MPOD shows the largest statistically significant effects. The combination of statistical

significance with a robust effect provides further support of a possible spatial frequency influence on the glare attenuation effects of MPOD.

The large variability of CS and overlapping 95% confidence intervals within the study sample at retinal eccentricities of 4° and 6° may explain the significance of RGD and MPOD and the non-significance of GD and MPOD. The GD value is an absolute difference between CS under glare conditions and CS with no glare conditions. This value will be greatly influenced by the underlying CS of the subject at a given retinal eccentricity. The RGD value is a relative difference between CS under glare conditions and CS with no glare conditions. Specifically, RGD is calculated as: RGD = ($CS_{No\ Glare}$ - CS_{Glare}) / (CS_{Glare}) and may better identify the glare attenuation effects separate from the underlying CS at a given retinal eccentricity.

Within our study sample, relatively similar significant correlation coefficients were found between both integrated and discrete measures of MPOD and RGD. These findings support the shared association between integrated and discrete MPOD measurements in regards to glare attenuation across the macula. Overall, foveal MPOD showed the most consistent associations with all 3 spatial frequency stimuli than parafoveal measures of MPOD. Only at the 9cpd stimuli did RGD show significant correlations with corresponding MPOD loci. Results from the data show a similar number of significant coefficients when either integrated MPOD or discrete is correlated with RGD.

At all three spatial frequencies, a multiple regression using integrated foveal MPOD and corresponding kurtosis values as predictors of resulting RGD for each subject was performed. In all cases, adding kurtosis as an additional predictor did not increase the variance explained within the regression model.

Intraocular Scatter

Intraocular correlations with foveal and AUC integrated MPOD measurements were non-significant. However, quartile analysis of the highest and lowest foveal MPOD found significant differences in intraocular scatter values. The intraocular scatter assessment required fixation of a central target and direct comparison of a flickering hemifield. The spectral composition of the glare annulus contained a large SW light component with a peak wavelength of 460nm closely matching the spectral absorption characteristics of MP. It is likely that peak MPOD is a greater contributor to SW light attenuation in regards to intraocular scatter than AUC integration MPOD values.

Future Directions

A potential follow-up study to the results of this project would be to evaluate the impact of scaled stimuli on relationship between glare disability and MPOD. The current results demonstrate decreasing correlation coefficients with increasing retinal eccentricity using 9cpd stimuli. It would be interesting to learn whether that decreased significance is a result of lower MPOD creating less glare attenuation and if the corresponding glare attenuation has a spatial frequency dependence.

The lack of significant correlations between MPOD and CS could also be explored further by utilizing chromatic stimuli rather than the achromatic stimuli reported here. The SW absorption properties of MP are well-documented and described in detail above. An evaluation of CS using a grating pattern generated on a SW-dominant background would theoretically be influenced by MPOD.

A number of studies have explored the relationship between CS and supplementation MP with mixed results. A few of the studies have identified a significant improvement in CS following supplementation (Richer et al., 1999 and Richer et al., 2004 and Olmedilla et al., 2003 and Kvansakul et al., 2006) and a few of the studies have failed to identify a significant association (Bartlett and Eperjesi, 2007 and Bartlett and Eperjest, 2008 and Nolan et al., 2011). It may be possible that differences in the findings may be a result of metabolic bioavailability of the L and Z from the supplement or possible differences in retinal transport and bindings among participants. In the absence of a SW component, any improvements in CS due to MP have a likely etiology in the Neural Hypothesis.

Future directions stemming directly from this project include the isolation of a neural component to the CS at different retinal loci at different spatial frequency. A current model of neural blur (η) incorporates 2 components, equivalent intrinsic blur (σ_{int}) assessed as visual acuity and optical blur (σ_{opt}) assessed as higher order aberrations. The model suggests the two components, intrinsic blur and

optical blur, are related to neural blur in the following equation: $\eta = 1 - (\sigma_{opt} / \sigma_{int})$. The resulting neural blur is the limiting component in visual function. An intriguing question lies in the role of MP on the resulting neural blur both from the baseline characteristics to results following supplementation.

Intraocular scatter is highly influenced by inhomogeneities within the ocular media, lenticular transmission being the primary source. The finding of correlation non-significance between foveal MPOD and intraocular scatter values is not surprising given the potential range of ocular transmission values. A potential supplementation study of the influences of L only, L+Z and L+Z+MZ oral formulations on resulting MPOD spatial distribution correlated with repeated intraocular scatter values at 3, 6 and 12 months in younger subjects without evidence of lenticular changes. This subject sample would likely exhibit the highest ocular media transmission and may help to identify any improvement in intraocular scatter correlated to MPOD, if any is to be found.

MPOD has been well-established in the literature in regard to the 3 components of the Optical Hypothesis when evaluated centrally. Due to the variable nature of MPOD spatial distribution within the population as a whole, the parafoveal relationship requires further detailed investigation. Integrated MPOD measurements demonstrated a significant relationship to relative glare disability and showed an increased association with higher spatial frequencies. This may influence how MPOD is currently assessed clinically and how supplementation

studies evaluating visual performance related to MPOD are performed. Foveal

MPOD measurements remained the strongest predictor of disability glare from 0^0

to 4^0 of retinal eccentricity and, although non-significant, showed an inverse

relationship with measured intraocular scatter values. The spatial distribution

profile likely remains a critical part of both the Neural and Protection Hypotheses.

REFERENCES

Aguirre R, Barraza J, Colombo E. (2007). The effect of glare on visibility depends on spatial frequency. *Journal Vision,* 7, 259-260

Akbaraly NT, Faure H, Gourlet V, Favier A, Berr C. (2007). Plasma carotenoid levels and cognitive performance in an elderly population: results of the EVA Study. *The Journals of Gerontology Series A: Biological Sciences and Medical Sciences*, 62(3), 308-316.

Anderson SJ, Mullen KT, Hess RF. (1991). Human peripheral spatial resolution for achromatic and chromatic stimuli: limits imposed by optical and retinal factors. *Journal of physiology*, *442*(1), 47-64.

Aslam TM, Haider D, Murray IJ. (2007). Principles of disability glare measurement: an ophthalmological perspective. *Acta Ophthalmologica Scandinavica, 8*5, 354-360

Bartlett H, Stainer L, Singh S, Eperjesi F, Howells O. (2010c). Clinical evaluation of the MPS 9000 Macular Pigment Screener. *British Journal Ophthamologyl, 94, 753-756*

Beatty S, Boulton M, Henson D, Koh HH, Murray IJ. (1999). Macular pigment and age-related macular degeneration. *British Journal Ophthamology,* 83(7), 867-877

Beatty S, Koh HH, Carden D, Murray IJ. (2000). Macular pigment optical density measurement: a novel compact instrument. *Ophthalmic and Physiological Optics*. 2000, 20(2), 105-111.

Bengt N. (1997). *Circular dichroism & linear dichroism* (Vol. 1). Oxford University Press.

Berendschot TT, van Norren D. (2006). Macular pigment shows ringlike structures. *Investigative ophthalmology visual science*, 47(2), 709-714.

Bernstein PS, Balashov NA, Tsong ED, Rando RR. (1997). Retinal tubulin binds macular carotenoids. *Investigative Ophthalmology Vis Science,* 38, 167-175.

Bernstein PS, Delori FC, Richer S, van Kuijk FJM, Wenzel AJ. (2010). The value of measurement of macular carotenoid pigment optical densities and distributions in age-related macular degeneration and other retinal disorders. *Vision Research,* 50, 716-728

Bhosale P, Larson AJ, Frederick JM, Southwick K, Thulin CD, Bernstein PS. (2004). Identification and characterization of a Pi isoform of glutathione S-transferase (GSTP1) as a zeaxanthin-binding protein in the macula of the human eye. *Journal of Biological Chemistry*. 279(47), 49447-49454.

Bhosale P, Zhao DY, Bernstein PS (2007). HPLC measurement of ocular carotenoid levels in human donor eyes in the lutein supplementation era*. Investigative Ophthalmology Vision Science.* 48, 543-549.

Bhosale P, Li B, Sharifzadeh M, Gellermann W, Frederick JM, Tsuchida K, Bernstein PS. (2009). Purification and partial characterization of a lutein-binding protein from human retina. *Biochemistry*, *48*(22), 4798-4807.

Bone RA, Landrum JT, Tarsis SL (1985). Preliminary identification of the human macular pigment*. Vision Res,* 25, 1531-1535.

Bone RA, Landrum JT, Fernandez L, Tarsis SL (1988). Analysis of the macular pigment by HPLC - retinal distribution and age study*. Investigative Ophthalmology Vision Science.* 29, 843-849.

Bone RA, Landrum JT, Cains A. (1992). Optical density spectra of the macular pigment in vivo and in vitro*. Vision research.* 1992, 32(1), 105-110.

Bone RA, Landrum JT, Hime GW, Cains A, Zamor J (1993). Stereochemistry of the human macular carotenoids*. Investigative Ophthalmology Vision Science,* 34, 2033-2040.

Bone RA, Landrum JT, Friedes LM, Gomez CM, Kilburn MD, Menendez E, Vidal I, Wang W (1997). Distribution of lutein and zeaxanthin stereoisomers in the human retina. *Experimental Eye Research,* 64, 211-218.

Bone RA, Landrum JT, Mayne ST, Gomez CM, Tibor SE, Twaroska EE. (2001). Macular pigment in donor eyes with and without AMD: a case-control study. *Investigative ophthalmology visual science*, 42(1), 235-240.

Bone RA, Landrum JT, Guerra LH, Ruiz CA. (2003). Lutein and zeaxanthin dietary supplements raise macular pigment density and serum concentrations of these carotenoids in humans. *Journal of nutrition*, 133(4), 992-998.

Bone RA, Landrum JT. (2004). Heterochromatic flicker photometry. *Archives of biochemistry and biophysics*. 430(2), 137-142.

Bone RA, Landrum JT, Cao Y, Howard AN, Alvarez-Calderon F. (2007). Macular pigment response to a supplement containing meso-zeaxanthin, lutein and zeaxanthin. *Nutritional Metabolism.* 4(12).

Brown PR. (1990). High-Performance Liquid Chromatography Past Developments, Present Status, and Future Trends. *Analytical Chemistry*, 62(19), 995A-1008A.

Campbell FW, Gubisch RW. (1966). Optical quality of the human eye. *Journal of Physiology*, *186*(3), 558-578.

Ciulla TA, Curran-Celantano J, Cooper DA, Hammond BR, Danis RP, Pratt LM, Filloon TG. (2001). Macular pigment optical density in a midwestern sample. *Ophthalmology*, 108(4), 730-737.

Coppens JE, Franssen L, van den Berg TJ. (2006). Wavelength dependence of intraocular straylight. *Experimental eye research*, 82(4), 688-692.

Crabtree DV, Ojima I, Geng X. (2001). Tubulins in the primate retina: Evidence that xanthophylls may be endogenous ligands for the paclitaxel-binding site. *Bioorganic and Medical Chemistry,* 9, 1967-1976.

Craft NE, Haitema HB, Garnett KM. (2004). Carotenoid, tocopherol and retinol concentrations in the elderly human brain. *Journal of Nutrition, Health and Aging,* 8, 156-162.

Curcio CA, Sloan KR, Kalina RE, Hendrickson AE. (1990). Human photoreceptor topography. *Journal of Comparative Neurology*, 292(4), 497-523.

Curran S, Hindmarch I, Wattis JP, Shillingford C. (1990). Critical flicker fusion in normal elderly subjects; a cross-sectional community study. *Current Psychology*, 9(1), 25-34.

Davies NP, Morland AB. (2002). Color matching in diabetes: optical density of the crystalline lens and macular pigments. *Investigative ophthalmology visual science*, *43*(1), 281-289.

De Waard PW, Ljspeert JK, van den Berg TJ, de Jong. (1992). Intraocular light scattering in age-related cataracts. *Investigative Ophalmology Vision Science*, 33(3), 618-625

Di Mascio P, Kaiser S, Sies H. (1989) Lycopene as the most efficient biological carotenoid singlet oxygen quencher. *Archives of biochemistry and biophysics*, 274(2), 532-538.

Dietzel M, Zeimer M, Heimes B, Pauleikhoff D, Hense HW. (2011). The ringlike structure of macular pigment in age-related maculopathy: results from the Muenster Aging and Retina Study (MARS). *Investigative ophthalmology visual science*, 52(11), 8016-8024.

Digre KB, Brennan KC. (2012). Shedding light on photophobia. *Journal of neuro-ophthalmology*, 32(1), 68.

Engles MP, Náñez JE, Sr., Elliott J, Holloway SR, Barrera A, Cheshire C, Cox M, Valderrama K, Kipena S. (2005). The effect of short-wave filters on standard acuity under broadband illumination. *Presented at the Rocky Mountain Psychological Association*, Phoenix, AZ.

Engles MP, Náñez JE, Holloway SR, Elliot J, Malcom M, Bautista R. (2005). The effect of short-wave filters on contrast sensitivity. *Presented at the Rocky Mountain Psychological Association*, Phoenix, AZ.

Engles M, Wooten B, Hammond B (2007). Macular pigment: a test of the acuity hypothesis*. Investigative ophthalmology visual science*, 48, 2922-2931

Eperjesi F, Fowler CW, Evans BJ. (2002). Do tinted lenses or filters improve visual performance in low vision? A review of the literature. *Ophthalmic and Physiological Optics*, 22(1), 68-77.

Feeny J, Finucane C, Savva GM, Cronin H, Beatty S, Nolan JM, Kenny RA. (2013). Low macular pigment optical density is associated with lower cognitive performance in a large population-based sample of older adults. *Neurobiology of Aging. 1-8*

Franssen L, Coppens JE, van den Berg JTP. (2006). Comparison method for assessment of retinal straylight. *Investigative ophthalmology visual science*, 47(2), 768-776

Gass JD. (1999). Muller cell cone, an overlooked part of the anatomy of the fovea centralis: hypotheses concerning its role in the pathogenesis of macular hole and foveomacualr retinoschisis. *Archives Ophthalmology,* 117(6), 821-823.

Gellermann W, Bernstein PS (2004). Noninvasive detection of macular pigments in the human eye*. Journal Biomedical Optics,* 9, 75-85.

Haegerstrom-Portnoy G. (1988). Short wavelength-sensitive-cone sensitivity loss with aging: a protective role for macular pigment. *Journal American Optical Society A*, 5(12), 2140-2144.

Ham WT, Mueller HA, Sliney DH (1976). Retinal sensitivity to damage from short wavelength light*. Nature,* 260, 153-155.

Ham, W. T., Mueller, H. A., Ruffolo, J. J., & Clarke, A. M. (1979). Sensitivity of the retina to radiation damage as a function of wavelength. *Photochemistry and photobiology*, 29(4), 735-743.

Ham WT, Mueller HA, Ruffolo JJ, Millen JE, Cleary SF, Guerry RK, Guerry D. (1984). Basic mechanisms underlying the production of photochemical lesions in the mammalian retina. *Current eye research*, *3*(1), 165-174.

Hammond BR, Curran-Celentano J, Judd S, Fuld K, Krinsky NI, Wooten BR, Snodderly DM (1996a). Sex differences in macular pigment optical density: relation to plasma carotenoid concentrations and dietary patterns. *Vision Research,* 36, 2001-2012.

Hammond BR, Fuld K, Snodderly DM (1996b). Iris color and macular pigment optical density. *Experimental Eye Research,* 62, 715-720.

Hammond BR, Johnson EJ, Russell RM, Krinsky NI, Yeum KJ, Edwards RB, Snodderly DM (1997a). Dietary modification of human macular pigment density*. Investigative Ophthalmology Vision Science,* 38, 1795-1801.

Hammond BR, Wooten BR, Snodderly DM (1997b). Density of the human crystalline lens is related to the macular pigment carotenoids, lutein and zeaxathin. *Optometry Vision Science,* 74, 499-504.

Hammond BR, Wooten BR, Snodderly DM (1997c). Individual variations in the spatial profile of human macular pigment. *Journal American Optical Society A Optics Image Science Vision,* 14, 1187-1196.

Hammond BR, Wooten BR, Snodderly DM. (1998). Preservation of visual sensitivity of older subjects: association with macular pigment density. *Investigative ophthalmology visual science*, 39(2), 397-406.

Hammond BR, Caruso-Avery M (2000). Macular pigment optical density in a southwestern sample*. Investigative ophthalmology visual science,* 41, 1492-1497.

Hammond BR, Wooten BR (2005). CFF thresholds: relation to macular pigment optical density*. Ophthalmic Physiological Optics,* 25, 315-319.

Hammond BR, Renzi L. (2008). The characteristics and function of lutein and zeaxanthin within the human retina. *Phytochemicals: aging and health*. *Boca Raton, Fla.: CRC Press.*

Hammond BR, Wooten BR, Engles M, Wong JC. (2012). The influence of filtering by the macular carotenoids on contrast sensitivity measured under simulated blue haze conditions. *Vision research*, 63, 58-62

Hammond BR, Fletcher LM, Elliott JG. (2013). Glare disability, photostress recovery, and chromatic contrast: relation to macular pigment and serum lutein and zeaxanthin. *Investigative ophthalmology visual science,* 54(1), 476-481.

Handelman GJ, Dratz EA, Reay CC, Vankuijk F (1988). Carotenoids in the human macula and whole retina*. Investigative ophthalmology visual science,* 29, 850-855.

Handelman GJ, Snodderly DM, Krinsky NI, Russett MD, Adler AJ (1991). Biological control of primate macular pigment - biochemical and densitometric studies*. Investigative ophthalmology visual science,* 32, 257-267.

Hawken MJ, Shapley RM, Grosof DH. (1996). Temporal-frequency selectivity in monkey visual cortex. *Visual neuroscience*, 13(3), 477-492.

Hemenger RP. (1992). Sources of intraocular light scatter from inversion of an empirical glare function. *Applied optics*, 31(19), 3687-3693.

Hollyfield JG, Bonilha VL, Rayborn ME, Yang X, Shadrach KG, Lu L, Perez VL. (2008) Oxidative damage–induced inflammation initiates age-related macular degeneration. *Nature medicine*, 14(2), 194-198.

Howarth PA, Bradley A. (1986). The longitudinal chromatic aberration of the human eye, and its correction. *Vision research*, 26(2), 361-366.

Howell DC. (2007). Statistical methods for psychology. Thomson Wadsworth: Belmont, CA.

Howells O, Eperjesi F, Bartlett H. (2011). Measuring macular pigment optical density in vivo: a review of techniques. *Graefe's archive for clinical and experimental ophthalmology*, 249(3), 315-347.

Hubel DH, Wiesel TN. (1977). Ferrier lecture: Functional architecture of macaque monkey visual cortex. *Proceedings of the Royal Society of London. Series B, Biological Sciences*, 1-59.

Husar RB, Husar JD, Martin L. (2000). Distribution of continental surface aerosol extinction based on visual range data. *Atmospheric Environment*, 34, 5067–5078.

Jaffe GJ, Irvine AR, Wood IS, Severinghaus JW, Pino GR, Haugen C. (1988). Retinal phototoxicity from the operating microscope: the role of inspired oxygen. *Ophthalmology*, 95(8), 1130-1141.

Johnson EJ, McDonald K, Caldarella SM, Chung HY, Troen AM, Snodderly DM. (2008). Cognitive findings of an exploratory trial of docosahexaenoic acid and lutein supplementation in older women. *Nutritional neuroscience*, 11(2), 75-83.

Johnson EJ. (2012). A possible role for lutein and zeaxanthin in cognitive function in the elderly. *American Journal Clinical Nutrition,* 96(5), 1161S-1165S

Johnson E J, Vishwanathan R, Johnson M A, Hausman DB, Davey A, Scott TM, Poon LW. (2013). Relationship between Serum and Brain Carotenoids,-Tocopherol, and Retinol Concentrations and Cognitive Performance in the Oldest Old from the Georgia Centenarian Study. *Journal of Aging Research*. 2013.

Junghans A, Sies H, Stahl W. (2001). Macular pigments lutein and zeaxanthin as blue light filters studied in liposomes. *Archives Biochemistry Biophysics,* 391, 160-164

Kaiser PK. (1988). Sensation luminance: a new name to distinguish CIE luminance from luminance dependent on an individual's spectral sensitivity. *Vision Research*, 28, 455–456.

Khachik F, Bernstein PS, Garland DL (1997a). Identification of lutein and zeaxanthin oxidation products in human and monkey retinas. *Investigative ophthalmology visual science,* 38, 1802-1811.

Kirby ML, Galea M, Loane E, Stack J, Beatty S, Nolan JM (2009). Foveal anatomic associations with the secondary peak and the slope of the macular pigment spatial profile. *Investigative ophthalmology visual science,* 50, 1383-1391.

Kirby ML, Beatty S, Loane E, Akkali MC, Connolly EE, Stack J, Nolan JM. (2010). A central dip in the macular pigment spatial profile is associated with age and smoking. *Investigative ophthalmology visual science*. 51(12), 6722-6728.

Krinsky NI. (1989). Antioxidant functions of carotenoids. *Free Radical Biology and Medicine*, *7*(6), 617-635.

Krinsky NI, Landrum JT, Bone RA. (2003). Biologic mechanisms of the protective role of lutein and zeaxanthin in the eye. *Annual review of nutrition*, *23*(1), 171-201.

Krinsky NI, Johnson EJ. (2005). Carotenoid actions and their relation to health and disease. *Molecular aspects of medicine*, 26(6), 459-516.

Kvansakul J, Rodriguez-Carmona M, Edgar DF, Barker FM, Kopcke W, Schalch W, Barbur JL (2006). Supplementation with the carotenoids lutein or zeaxanthin improves human visual performance. *Ophthalmic Physiological Optics,* 26, 362-371.

Krutmann J. (2000). Ultraviolet A radiation-induced biological effects in human skin: relevance for photoaging and photodermatosis. *Journal of dermatological science*, *23*, S22.

Lam RF, Rao SK, Fan DS, Lau FT, Lam DS. (2005). Macular pigment optical density in a Chinese sample. *Current eye research*, 30(9), 729-735.

Landrum JT, Bone RA, Joa H, Kilburn MD, Moore LL, Sprague KE (1997). A one year study of the macular pigment: the effect of 140 days of a lutein supplement. *Experimental Eye Research,* 65, 57-62.

Landrum JT, Bone RA (2001). Lutein, zeaxanthin, and the macular pigment. *Archives Biochemistry Biophysics,* 385, 28-40.

Landrum JT. (2013). Reactive Oxygen and Nitrogen Species in Biological Systems: Reactions and Regulation by Carotenoids. *Carotenoids and Human Health*. Humana Press.

Lapid-Gortzak R, van der Linden JW, van der Meulen I, Nieuwendaal C, van den Berg T. (2010). Straylight measurements in laser in situ keratomileusis and laser-assisted subepithelial keratectomy for myopia. *Journal of Cataract Refractive Surgery*, 36(3), 465-471.

Li B, Vachali P, Frederick JM, Bernstein PS. (2011). Identification of StARD3 as a lutein-binding protein in the macula of the primate retina. *Biochemistry,* 50, 2541–2549.

Lim BP, Nagao A, Terao J, Tanaka K, Suzuki T, Takama K. (1992). Antioxidant activity of xanthophylls on peroxyl radical-mediated phospholipid peroxidation. *Biochimica et Biophysica Acta-Lipids and Lipid Metabolism*, 1126(2),178-184.

Loughman J, Akkali MC, Beatty S, Scanlon G, Davison PA, O'Dwyer V, Cantwell T, Major P, Stack J, Nolan JM (2010a). The relationship between macular pigment and visual performance. *Vision Research,* 50, 1249-1256.

Loughman J, Davison PA, Nolan JM, Akkali MC, Beatty S (2010b). Macular pigment and its contribution to visual performance and experience. *Journal Optometry,* 3, 74-90.

Loughman J, Nolan JM, Howard AN, Connolly E, Meagher K, Beatty S. (2012). The impact of macular pigment augmentation on visual performance using different carotenoid formulations. *Investigative ophthalmology visual science, 53*(12), 7871-7880.

Luria S. (1972). Vision with chromatic filters. *American journal of optometry and archives of American Academy of Optometry*, *49*(10), 818.

Magnussen S, Spillmann L, Stürzel F, Werner JS. (2001) Filling-in of the foveal blue scotoma. *Vision research*. 41(23), 2961-2967.

Mainster MA, Turner PL. (2012). Glare's causes, consequences, and clinical challenges after a century of ophthalmic study. *American Journal Ophthalmology,* 153, 587-593.

Mayer MJ, Kim CB, Svingos A, Glucs A. (1988). Foveal flicker sensitivity in healthy aging eyes. I. Compensating for pupil variation. *Journal American Optical Society A*, 5(12), 2201-2209.

McCartney EJ. (1976). Optics of the Atmosphere: Scattering by molecules and particles. *New York, John Wiley and Sons, Inc., 1976. 421 p.*, *1.*

Mellerio J, Ahmadi-Lari S, Van Kuijk FJGM, Pauleikhoff D, Bird AC, Marshall J. (2002). A portable instrument for measuring macular pigment with central fixation. *Current eye research*, 25(1), 37-47.

Michels M, Lewis H, Abrams GW, Han DP, Mieler WF, Neitz J. (1992). Macular phototoxicity caused by fiberoptic endoillumination during pars plana vitrectomy. *American Journal Ophthalmology,*114, 287-296.

Misson GP. Form and behaviour of Haidinger's brushes. (1993). *Ophthalmic Physiological Optics,* 13, 392-396.

Moreland JD. (2004). Macular pigment assessment by motion photometry. *Archives of biochemistry and biophysics*, 430(2), 143-148.

Nakagawa K, Kiko T, Miyazawa T, Sookwong P, Tsuduki T, Satoh A, Miyazawa, T. (2011). Amyloid β-induced erythrocytic damage and its attenuation by carotenoids. *FEBS letters*, 585(8), 1249-1254.

N'soukpoé-Kossi CN, Sielewiesiuk J, Leblanc RM, Bone RA, Landrum JT. Linear dichroism and orientational studies of carotenoid Langmuir-Blodgett films. (1988). *Biochimica et Biophysica Acta-Biomembranes*, 940(2), 255-265.

Noell WK. (1980). Possible mechanisms of photoreceptor damage by light in mammalian eyes. *Vision research*, 20(12), 1163-1171.

Nolan JM, Stack J, O'Connell E, Beatty S. (2007). The relationships between macular pigment optical density and its constituent carotenoids in diet and serum. *Investigative ophthalmology visual science*, 48(2), 571-582.

Nolan JM, Stringham JM, Beatty S, Snodderly DM (2008). Spatial profile of macular pigment and its relationship to foveal architecture. *Investigative Ophthalmology Vision Science,* 49, 2134-2142.

Nolan JM, Kenny R, O'Regan C, Cronin H, Loughman J, Connolly EE, Beatty S. (2010). Macular pigment optical density in an ageing Irish population: The Irish Longitudinal Study on Ageing. *Ophthalmic research*, 44(2), 131-139.

Nolan JM, Loughman J, Akkali MC, Stack J, Scanlon G, Davison P, Beatty S (2011). The impact of macular pigment augmentation on visual performance in normal subjects: COMPASS. *Vision Research,* 51, 459-469.

Nouritt V, Kelly JMF. (2009). Intraocular scatter and visual performances. *Optometry in Practice.* 10, 117-128

Nussbaum JJ, Pruett RC, Delori FC (1981). Historic perspectives. Macular yellow pigment. The first 200 years. *Retina,* 1, 296-310.

O'Connell E, Neelam k, Nolan J, AuEong KG. (2006). Macular carotenoids and agre-related maculopathy. *Annals Academy Medicine Singapore,* 35, 821-830.

Osterberg G. (1935) Topography of the layer of rods and cones in the human retina, *Acta Ophthalmol*ogy. Supplement. 6: 1.

Paiva SA, Russell RM. (1999). β-carotene and other carotenoids as antioxidants. *Journal of the American College of Nutrition*, 18(5), 426-433.

Parrott AC. (2008). Critical flicker fusion thresholds and their relationship to other measures of alertness. *Pharmacopsychiatry*, 15, 39-43.

Pease PL, Adams AJ. (1983). Macular pigment difference spectrum from sensitivity measures of a single cone mechanism. *American Journal of optometry and physiological optics*, 60(8), 667-672.

Perry A, Rasmussen H, Johnson EJ. (2009). Xanthophyll (lutein, zeaxanthin) content in fruits, vegetables and corn and egg products. *Journal of food composition and analysis*, 22(1), 9-15.

Pointer JS, Hess RF. (1989). The contrast sensitivity gradient across the human visual field: With emphasis on the low spatial frequency range. *Vision research*, 29(9), 1133-1151.

Pokorny J, Lutze M, Cao D, Zele AJ. (2006). The color of night: Surface color perception under dim illuminations. *Visual neuroscience*, 23(3/4), 525.

Polidori MC, Stahl W, Eichler O, Niestroj I, Sies H. (2001). Profiles of antioxidants in human plasma. *Free Radical Biology and Medicine*, *30*(5), 456-462.

Puell M, Perez-Carrasco MJ, Barrio A, Palomo-Alvarez C, Sanchez R. (2008). Relationship between macular pigment and straylight on the retina. *Acta Ophthalmologica*, 86, 243.

Rapp LM, Maple SS, Choi JH. (2000). Lutein and zeaxanthin concentrations in rod outer segment membranes from perifoveal and peripheral human retina. *Investigative Ophthalmology Visual Science*, 41(5), 1200-1209.

Reading VM, Weale RA. (1974). Macular pigment and chromatic aberration. *Journal Optical Society America*, 64(2), 231-234

Regan D. (1982). Visual information channeling in normal and disordered vision. *Psychological Review*, 89(4), 407.

Reichenbach A, Bringmann A. (2013) New functions of Muller cells. *Glia,* 61(5), 651-678.

Renzi LM, Hammond BR (2010a). The effect of macular pigment on heterochromatic luminance contrast. *Experimental Eye Research,* 91, 896-900.

Renzi LM, Hammond BR (2010b). The relation between the macular carotenoids, lutein and zeaxanthin, and temporal vision. *Ophthalmic Physiological Optics,* 30, 351-357.

Richer S, Stiles W, Statkute L, Pulido J, Frankowski J, Rudy D, Nyland J. (2004). Double-masked, placebo-controlled, randomized trial of lutein and antioxidant supplementation in the intervention of atrophic age-related macular degeneration: the Veterans LAST study (Lutein Antioxidant Supplementation Trial). *Optometry,* 75(4), 216-229.

Richer SP, Stiles W, Graham-Hoffman K, Levin M, Ruskin D, Wrobel J, Thomas C. (2011). Randomized, double-blind, placebo-controlled study of zeaxanthin and visual function in patients with atrophic age-related macular degeneration: the Zeaxanthin and Visual Function Study (ZVF). *Optometry,* 82(11), 667-680.

Rinaldi P, Polidori MC, Metastasio A, Mariani E, Mattioli P, Cherubini A, Mecocci P. (2003). Plasma antioxidants are similarly depleted in mild cognitive impairment and in Alzheimer's disease. *Neurobiology of aging*, 24(7), 915-919.

Robson JG, Graham N. (1981). Probability summation and regional variation in contrast sensitivity across the visual field. *Vision research*, 21(3), 409-418.

Robson AG, Moreland JD, Pauleikhoff D, Morrissey T, Holder GE, Fitzke FW, Bird AC, van Kuijk FJM. (2003). Macular pigment density and distribution: comparison of fundus autofluorescence with minimum motion photometry. *Vision Research,* 43, 1765–1775.

Roumes C, Giraudet G, Plantier J. (2001). Influence of glare eccentricity on contrast sensitivity. *Perception* 30, 81

Rovamo J, Raninen A. (1984). Critical flicker frequency and M-scaling of stimulus size and retinal illuminance. *Vision research*, 24(10), 1127-1131.

Sandberg MA, Johnson EJ, Berson EL (2010). The relationship of macular pigment optical density to serum lutein in retinitis pigmentosa. *Investigative Ophthalmology Vision Science,* 51, 1086-1091.

Schalch W, Cohn W, Barker FM, Kopcke W, Mellerio J, Bird AC, Robson AG, Fitzke FF, van Kuijk FJGM (2007). Xanthophyll accumulation in the human retina during supplementation with lutein or zeaxanthin - the LUXEA (LUtein Xanthophyll Eye Accumulation) study. *Archives Biochemistry Biophysics,* 458, 128-135.

Schatz H, McDonald HR. (1989). Atrophic macular degeneration. *Ophthalmology*, 96, 1541-51.

Semba RD, Dagnelie G. (2003). Are lutein and zeaxanthin conditionally essential nutrients for eye health?. *Medical hypotheses*, 61(4), 465-472.

Sheehy JB. (1989). *Dazzling glare: Protection criteria versus visual performance. Interim report, September 1985-August 1990*. Naval Air Development Center, Warminster, PA (USA). Air Vehicle and Crew Systems Technology Dept..

Snodderly DM, Auran JD, Delori FC (1984a). The macular pigment. II. Spatial distribution in primate retinas. *Invest Ophthalmol Vis Sci* 25: 674-685.

Snodderly DM, Brown PK, Delori FC, Auran JD (1984b). The macular pigment. I. Absorbance spectra, localization, and discrimination from other yellow pigments in primate retinas. *Investigative Ophthalmology Vision Science,* 25, 660-673.

Sommerburg O, Siems WG, Hurst JS, Lewis JW, Kliger DS, van Kuijk FJGM (1999). Lutein and zeaxanthin are associated with photoreceptors in the human retina. *Current Eye Research,* 19, 491-495.

Stahl W, Ale-Agha N, Polidori MC. (2002). Non-antioxidant properties of carotenoids. *Biological chemistry*, *383*(3-4), 553-558.

Stahl W, Sies H. (2003). Antioxidant activity of carotenoids. *Molecular aspects of medicine*, *24*(6), 345-351.

Stahl W, Sies H. (2005). Bioactivity and protective effects of natural carotenoids. *Biochimica et Biophysica Acta-Molecular Basis of Disease*, *1740*(2), 101-107.

Stringham JM, Bovier ER, Wong JC, Hammond BR. (2010). The influence of dietary lutein and zeaxanthin on visual performance. *Journal of food science*, 75(1): 24-29.

Stringham JM, Fuld K, Wenzel AJ. (2003). Action spectrum for photophobia. *Journal Optical Society America A*, *20*(10), 1852-1858.

Stringham JM, Fuld K, Wenzel AJ. (2004). Spatial properties of photophobia. *Investigative ophthalmology visual science*, *45*(10), 3838-3848.

Stringham JM, Hammond BR (2007). The glare hypothesis of macular pigment function. *Optometry Vision Science,* 84, 859-864.

Stringham JM, Hammond BR (2008). Macular pigment and visual performance under glare conditions. *Optometry Vision Science,* 85, 82-88.

Stringham JM, Garcia PV, Smith PA, McLin LN, Foutch, B K (2011). Macular pigment and visual performance in glare: benefits for photostress recovery, disability   glare, and visual discomfort. *Investigative ophthalmology visual science*, 52(10), 7406-7415.

Sujak A, Gabrielska J, Grudziński W, Borc R, Mazurek P, Gruszecki WI. (1999). Lutein and zeaxanthin as protectors of lipid membranes against oxidative damage: the structural aspects. *Archives of Biochemistry and Biophysics*, 371(2), 301-307.

Sujak A, Okulski W, Gruszecki WI. (2000). Organisation of xanthophyll pigments lutein and zeaxanthin in lipid membranes formed with dipalmitoylphosphatidylcholine. *Biochimica et Biophysica Acta-Biomembranes*, *1509*(1), 255-263.

Sundelin SP, Nilsson SEG. (2001). Lipofuscin-formation in retinal pigment epithelial cells is reduced by antioxidants. *Free Radical Biology and Medicine*, 31(2), 217-225.

Sunness JS, Gonzalez-Baron J, Applegate CA, Bressler NM, Tian Y, Hawkins B, Bergman, A. (1999). Enlargement of atrophy and visual acuity loss in the geographic atrophy form of age-related macular degeneration. *Ophthalmology*, 106(9), 1768-1779.

Thibos LN. (1987). Calculation of the influence of lateral chromatic aberration on image quality across the visual field. *Journal Optical Society America A*, 4(8), 1673-1680.

Thibos LN, Cheney FE, Walsh DJ. (1987). Retinal limits to the detection and resolution of gratings. *Journal Optical Society America A*, 4(8), 1524-1529.

Thibos LN. (1998). Acuity perimetry and the sampling theory of visual resolution. *Optometry Vision Science*, 75(6), 399-406.

Thibos LN, Bradly A, Still DL, Zhang X, Howarth PA. (1990). Theory and measurement of ocular chromatic aberration. *Vision Research, 30*, 33-49.

Thibos LN, Bradley A, Zhang XX. (1991). Effect of ocular chromatic aberration on monocular visual performance. *Optometry Vision Science, 68*(8), 599.

Thibos LN, Still DL,Bradley A. (1996). Characterization of spatial aliasing and contrast sensitivity in peripheral vision. *Vision Research*, 36(2), 249-258.

Trieschmann M, Heimes B, Hense HW, Pauleikhoff D. (2006). Macular pigment optical density measurement in autofluorescence imaging: comparison of one and two- wavelength methods. *Graefe's Archive for Clinical and Experimental Ophthalmology*, 244(12), 1565-1574.

Trieschmann M, Beatty S, Nolan JM, Hense HW, Heimes B, Austermann U, Pauleikhoff D. (2007). Changes in macular pigment optical density and serum concentrations of its constituent carotenoids following supplemental lutein and zeaxanthin: the LUNA study. *Experimental eye research*. 84(4), 718-728.

Trieschmann M, van Kuijk F, Alexander R, Hermans P, Luthert P, Bird AC, Pauleikhoff   D (2008). Macular pigment in the human retina: histological evaluation of localization and distribution. *Eye,* 22, 132-137.

van den Berg TJTP, Ijspeert JK, De Waard PWT. (1991). Dependence of intraocular straylight on pigmentation and light transmission through the ocular wall. *Vision research*. 31(7), 1361-1367.

van den Berg TJTP. (1995). Analysis of intraocular straylight, especially in relation to age. *Optometry Vision Science*, 72(2), 52-59.

van den Berg TJTP. (1997). Light scattering by donor lenses as a function of depth and wavelength. *Investigative ophthalmology visual science*, 38(7), 1321-1332.

van den Berg TJTP, Franssen L, Kruijt B, Coppens JE. (2011). Psychophysics, reliability, and norm values for temporal contrast sensitivity implemented on the two alternative forced choice C-Quant device. *Journal of biomedical optics*, 16(8), 85004-1-85004-7.

van Nes FL, Bouman MA. (1967). Spatial modulation transfer in the human eye. *Journal Optical Society America*, 57(3), 401-406.

Vaney DI, Nelson JC, Pow DV. (1998). Neurotransmitter coupling through gap junctions in the retina. *Journal of Neuroscience,* 18, 10594-10602.

Virsu V, Rovamo J. (1979). Visual resolution, contrast sensitivity, and the cortical magnification factor. *Experimental Brain Research*, *37*(3), 475-494.

Vishwanathan R, Neuringer M, Snodderly DM, Schalch W, Johnson EJ. (2012). Macular lutein and zeaxanthin are related to brain lutein and zeaxanthin in primates. *Nutritional Neuroscience*. 16(1), 21-29.

Vos JJ. (1984). Disability glare-a state of the art report. *Commision Internationale de L'Eclairage Journal*, 3(2), 39-53.

Vos JJ. (2003). On the cause of disability glare and its dependence on glare angle, age and ocular pigmentation. *Clinical and Experimental Optometry*, 86(6), 363-370.

Walls G, Judd HD. (1933). Intra-ocular colour filters of vertebrates. *British Journal of Ophthalmology, 17*, 641-705.

Weiter JJ, Delori F, Dorey CK (1988). Central sparing in annular macular degeneration. *American Journal Ophthalmol,* 106, 286-292.

Wenzel AJ, Fuld K, Stringham JM, Curran-Celentano J. (2006). Macular pigment optical density and photophobia light threshold. *Vision research*, 46(28), 4615-4622.

Werner JS, Bieber ML, Schefrin BE (2000). Senescence of foveal and parafoveal cone sensitivities and their relations to macular pigment density. *Journal Optical Society America A Optical Image Science Vision,* 17, 1918-1932.

Westheimer G. (1964). Pupil size and visual resolution. *Vision Research, 4*, 39-45.

Westheimer G. (1982). The spatial grain of the perifoveal visual field. *Vision research*, 22(1), 157-162.

Westheimer G. (2001). Updating the classical approach to visual acuity. *Clinical Experimental Optometry, 84*, 258-263.

Westheimer G. (2003). Visual acuity with reversed-contrast charts: 1. Theoretical and psychophysical investigations. *Optometry and Vision Science, 80*, 745-748.

Westrup VKM, Dietzel M, Pauleikhoff D, Hense HW. (2014) The association of retinal structure and macular pigment distribution. *Investigative ophthalmology visual science*, 13

Whitehead AJ, Mares JA, Danis RP. (2006). Macular pigment: a review of current knowledge. *Archives Ophthalmology,* 124, 1038-1045

Wieslaw I. (2004) Carotenoid orientation: role in membranestabilization. In: Carotenoids in Health and Disease (eds N. I.Krinsky, S. T. Mayne and H. Sies), CRC Press Inc, BocaRaton, FL, 151–163.

Wolffsohn JS, Cochrane AL, Watt NA. (2000). Implementation methods for vision related quality of life questionnaires. *British Journal Ophthalmology*, 84(9), 1035-1040.

Wooten BR, Hammond BR, Land RI, Snodderly DM (1999). A practical method for measuring macular pigment optical density. *Investigative Ophthalmology Vision Science,* 40, 2481-2489.

Wooten BR, Hammond BR. (2002). Macular pigment: Influences on visual acuity and visibility. *Progress in Retinal Eye Research.* 21, 225-240.

Wooten BR, Hammond BR. (2005). Spectral absorbance and spatial distribution of macular pigment using heterochromatic flicker photometry. *Optometry Vision Science*, 82(5), 378-386.

Wyszecki G, Stiles WS (1982). The eye. In: *Color Science: Concepts and Methods,Quantitative Data and Formulae.* Wiley-Interscience, New York, 112-114.

Yeum KJ, Russell RM, Krinsky NI, Aldini G. (2004). Biomarkers of antioxidant capacity in the hydrophilic and lipophilic compartments of human plasma. *Archives of biochemistry and biophysics*, 430(1), 97-103.

Yoon GY, Williams DR. (2002). Visual performance after correcting the monochromatic and chromatic aberrations of the eye. *Journal Optical Society America A*, 19(2), 266-275.

Zimmer JP, Hammond, BR. (2007). Possible influences of lutein and zeaxanthin on the developing retina. *Clinical ophthalmology,* 1(1), 25.

Appendix 1
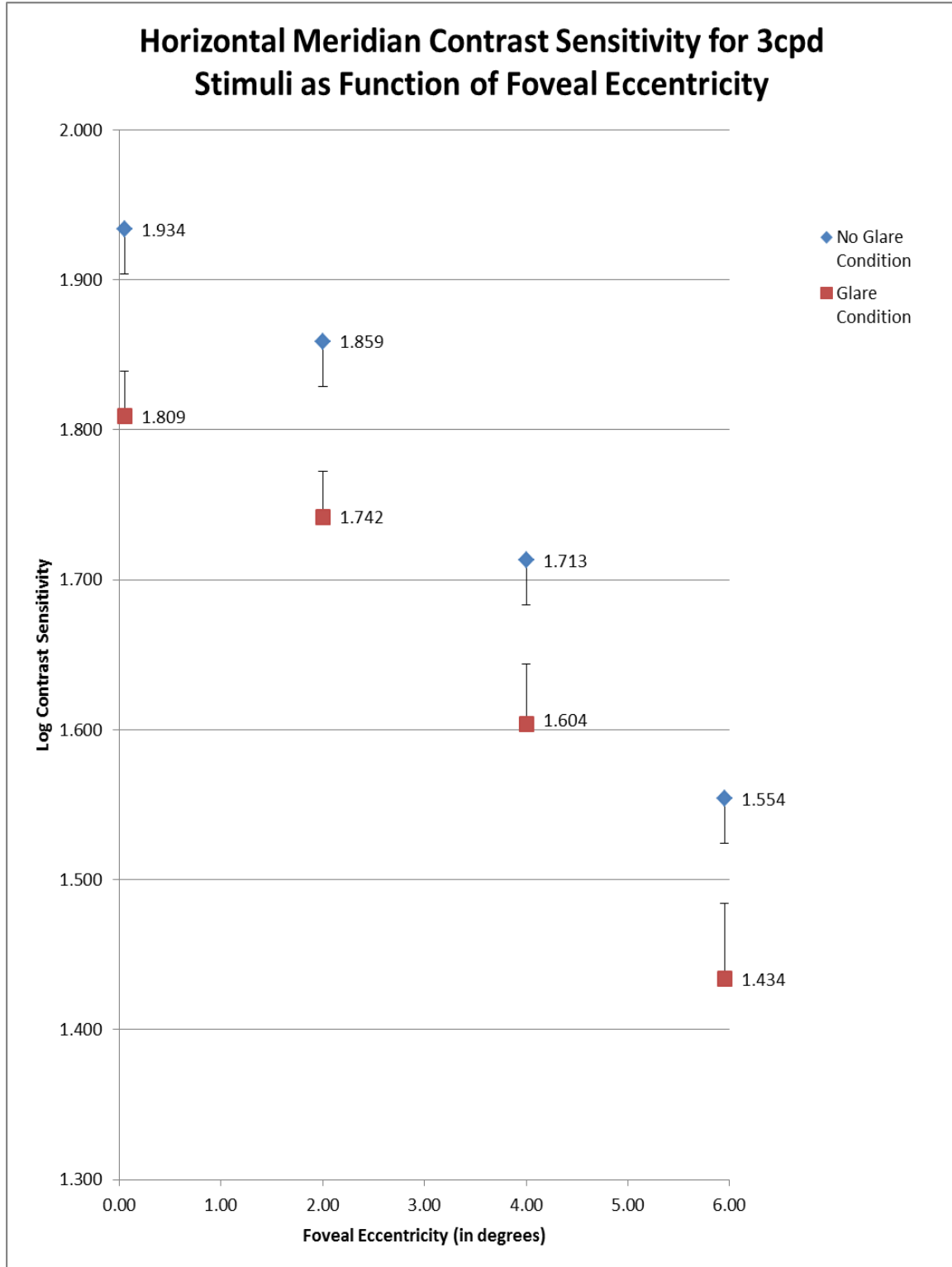
Figure 13

Mean contrast sensitivity values 3cpd stimuli along the horizontal meridian for the 33 subject sample as a function of foveal eccentricity. Blue diamonds indicate contrast sensitivity without flanking glare and red squares represent contrast sensitivity with flanking glare. Error bars indicate a 95% confidence interval.
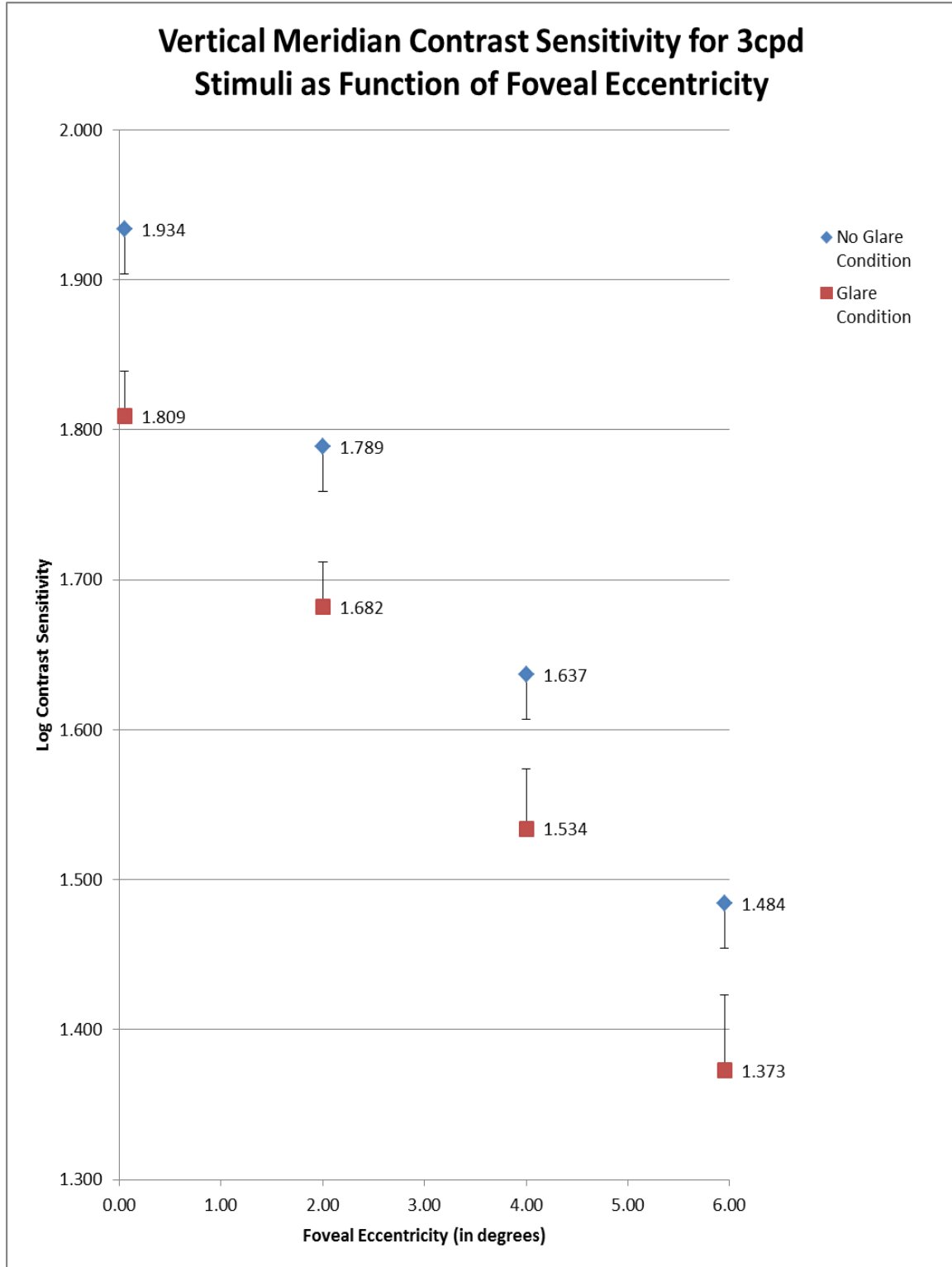
Figure 14
Mean contrast sensitivity values 3cpd stimuli along the vertical meridian for the 33 subject sample as a function of foveal eccentricity. Blue diamonds indicate contrast sensitivity without flanking glare and red squares represent contrast sensitivity with flanking glare. Error bars indicate a 95% confidence interval.
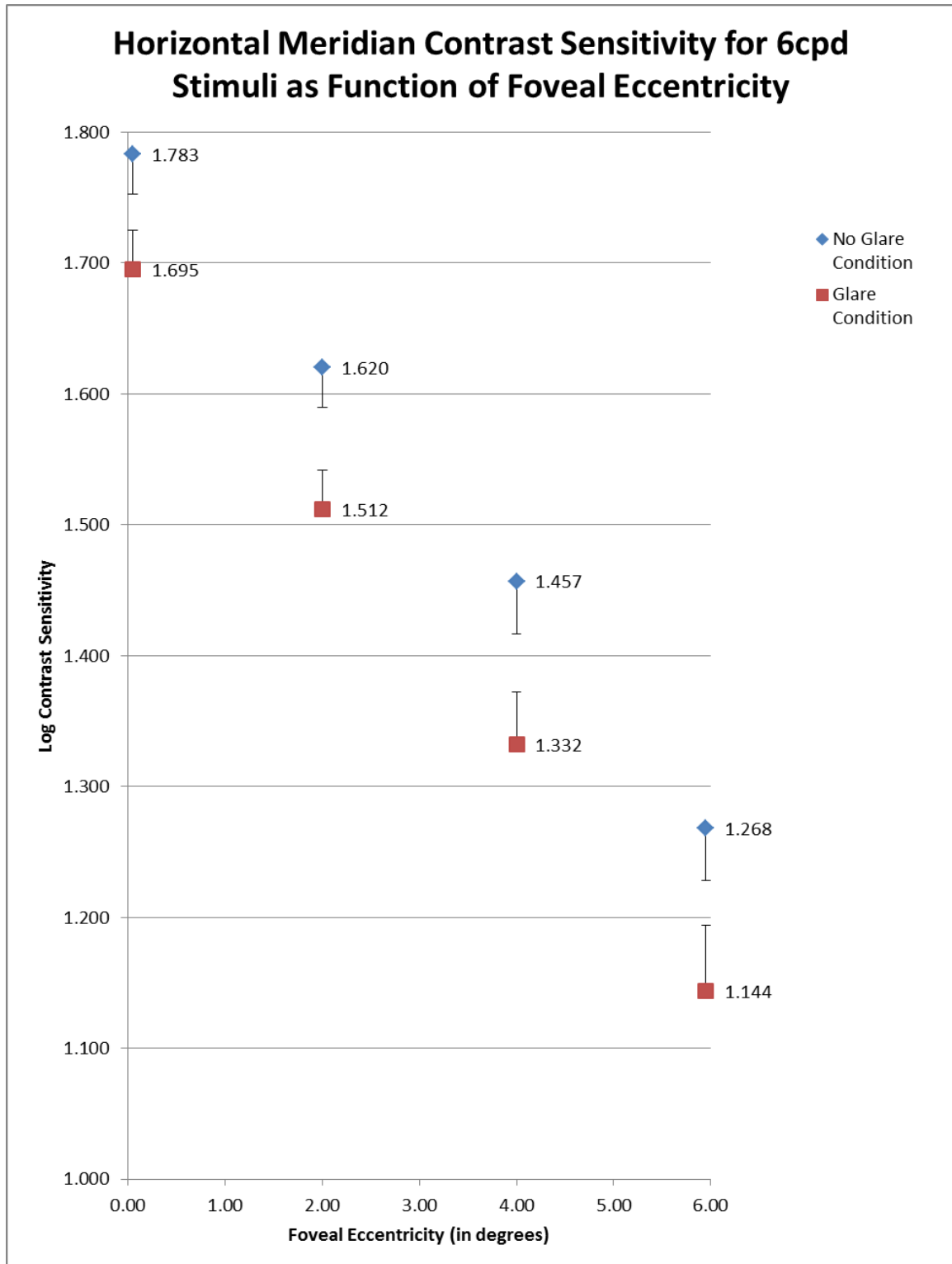
Figure 15
Mean contrast sensitivity values 6cpd stimuli along the horizontal meridian for the 33 subject sample as a function of foveal eccentricity. Blue diamonds indicate contrast sensitivity without flanking glare and red squares represent contrast sensitivity with flanking glare. Error bars indicate a 95% confidence interval.
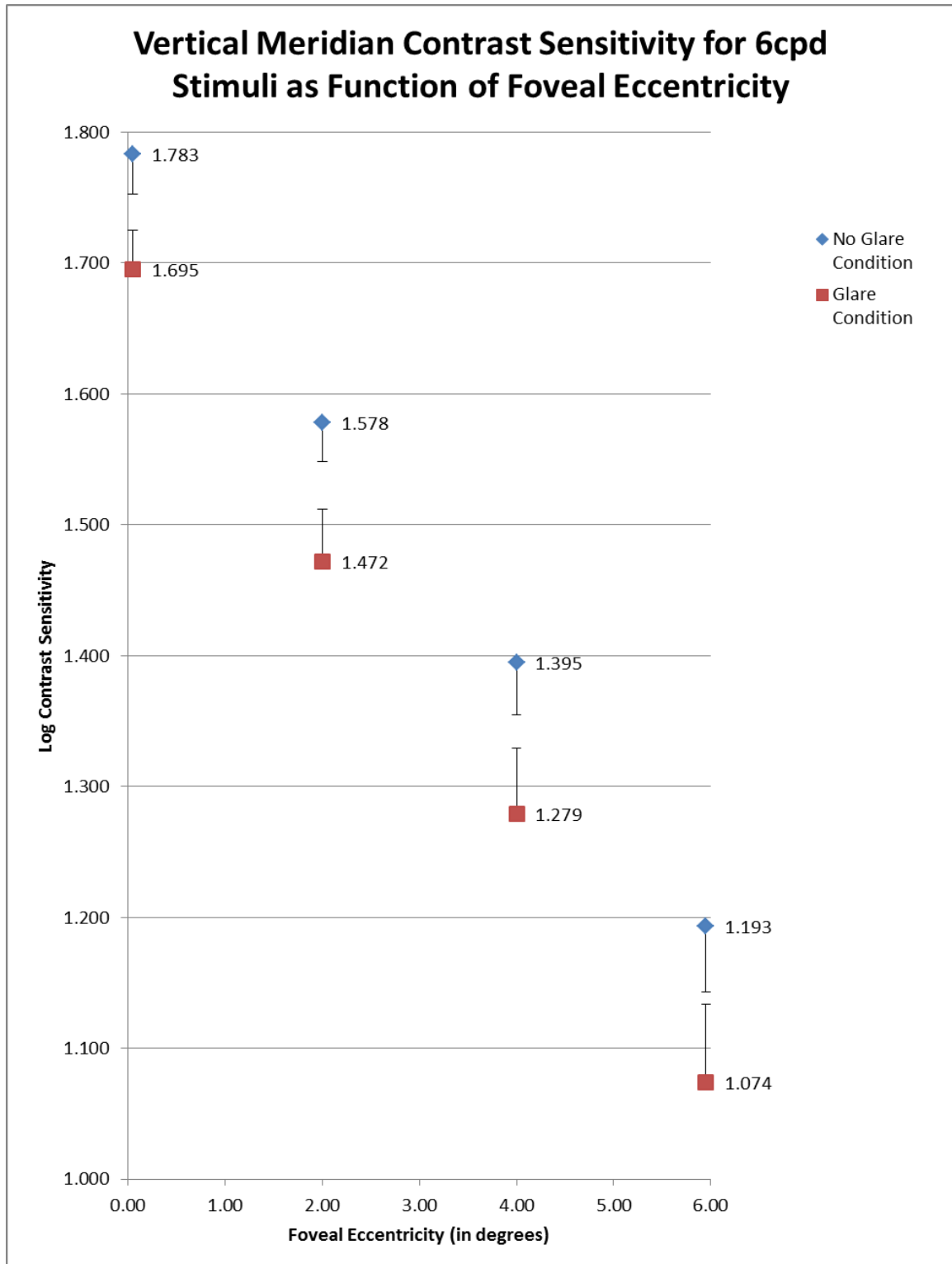
Figure 16
Mean contrast sensitivity values 6cpd stimuli along the vertical meridian for the 33 subject sample
as a function of foveal eccentricity. Blue diamonds indicate contrast sensitivity without flanking glare and red squares
represent contrast sensitivity with flanking glare. Error bars indicate a 95% confidence interval.
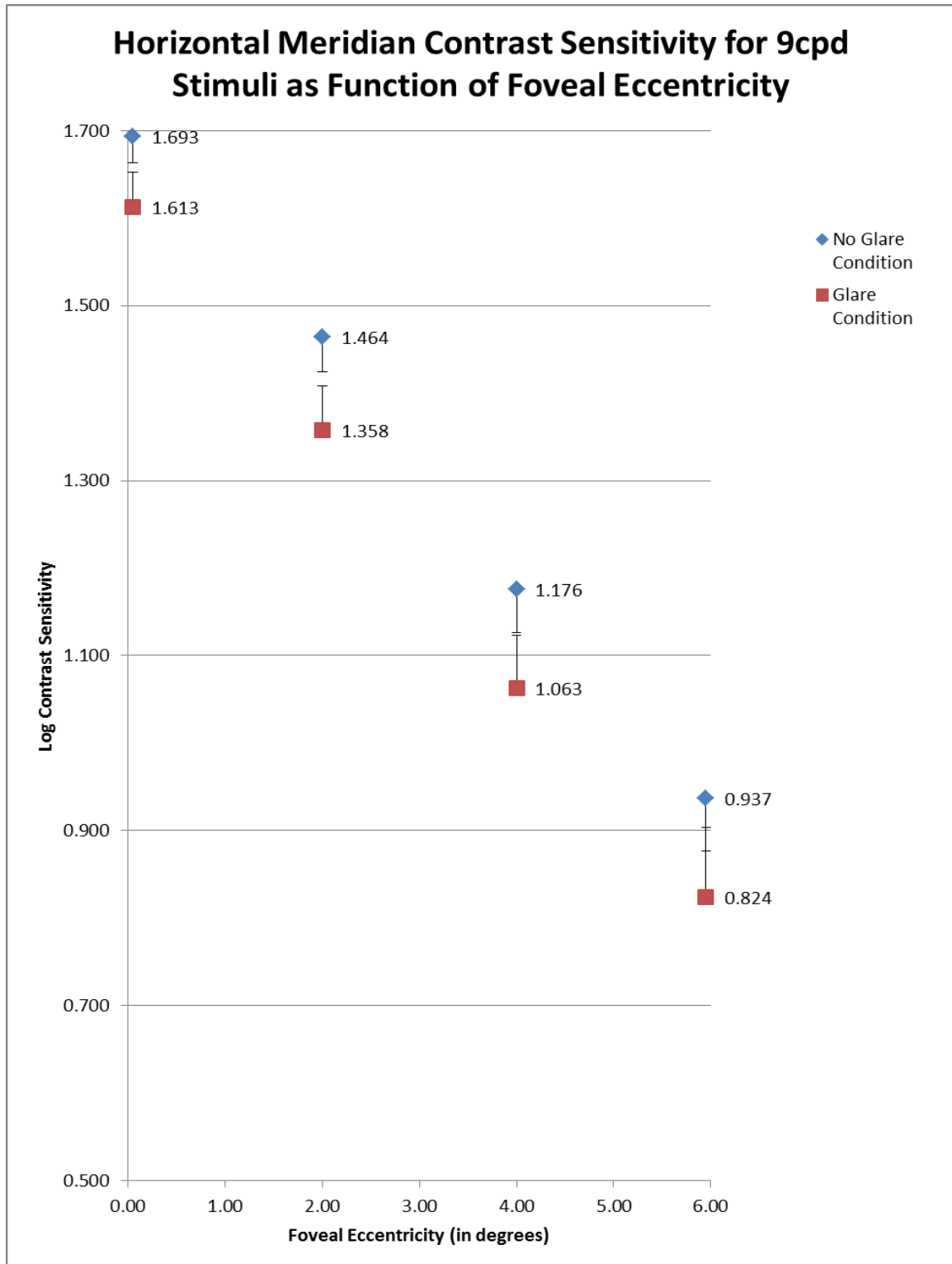
Figure 17
Mean contrast sensitivity values 9cpd stimuli along the horizontal meridian for the 33 subject sample as a function of foveal eccentricity. Blue diamonds indicate contrast sensitivity without flanking glare and red squares represent contrast sensitivity with flanking glare. Error bars indicate a 95% confidence interval.
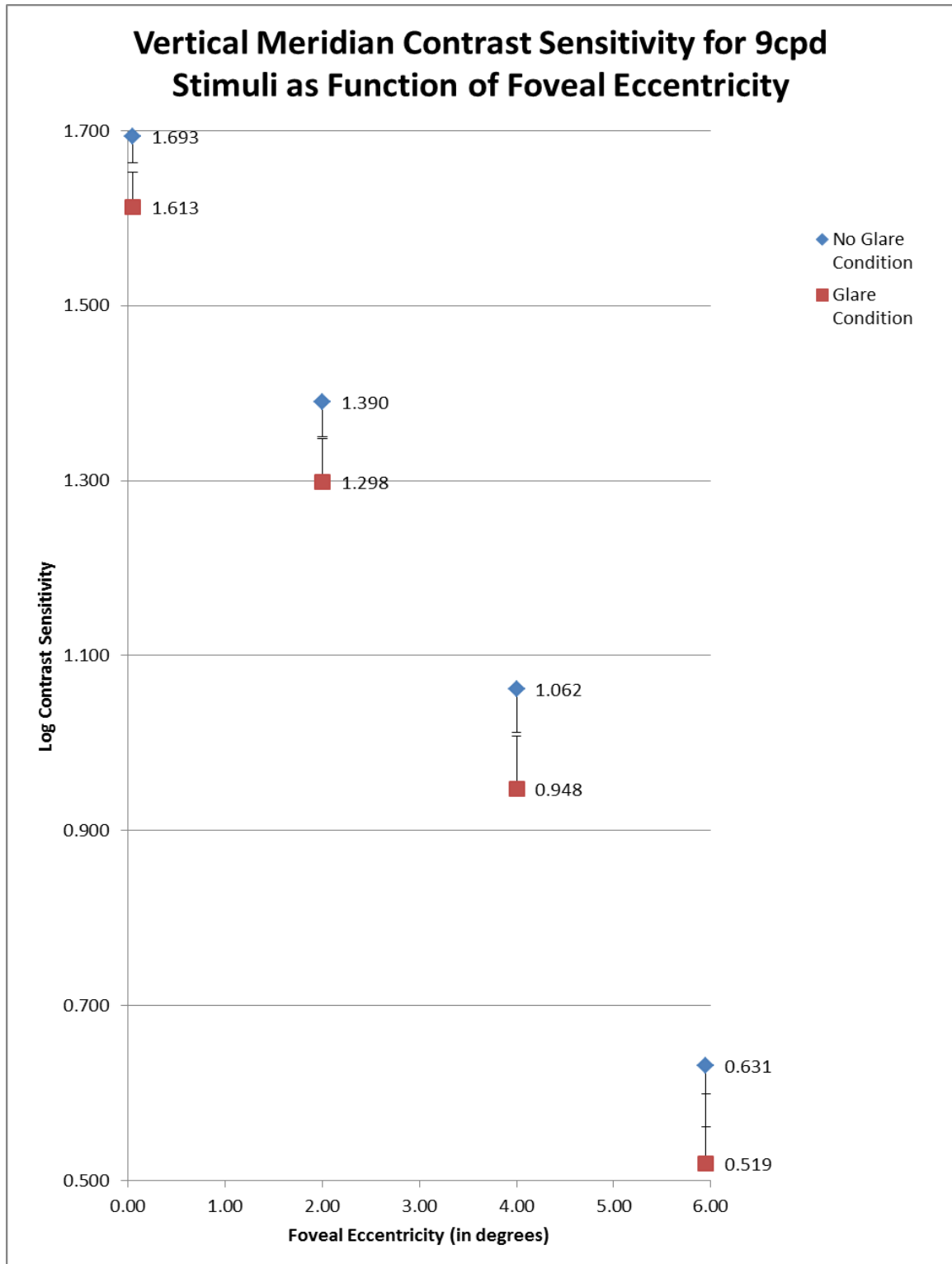
Figure 18
Mean contrast sensitivity values 9cpd stimuli along the vertical meridian for the 33 subject sample
as a function of foveal eccentricity. Blue diamonds indicate contrast sensitivity without flanking glare and red squares
represent contrast sensitivity with flanking glare. Error bars indicate a 95% confidence interval.
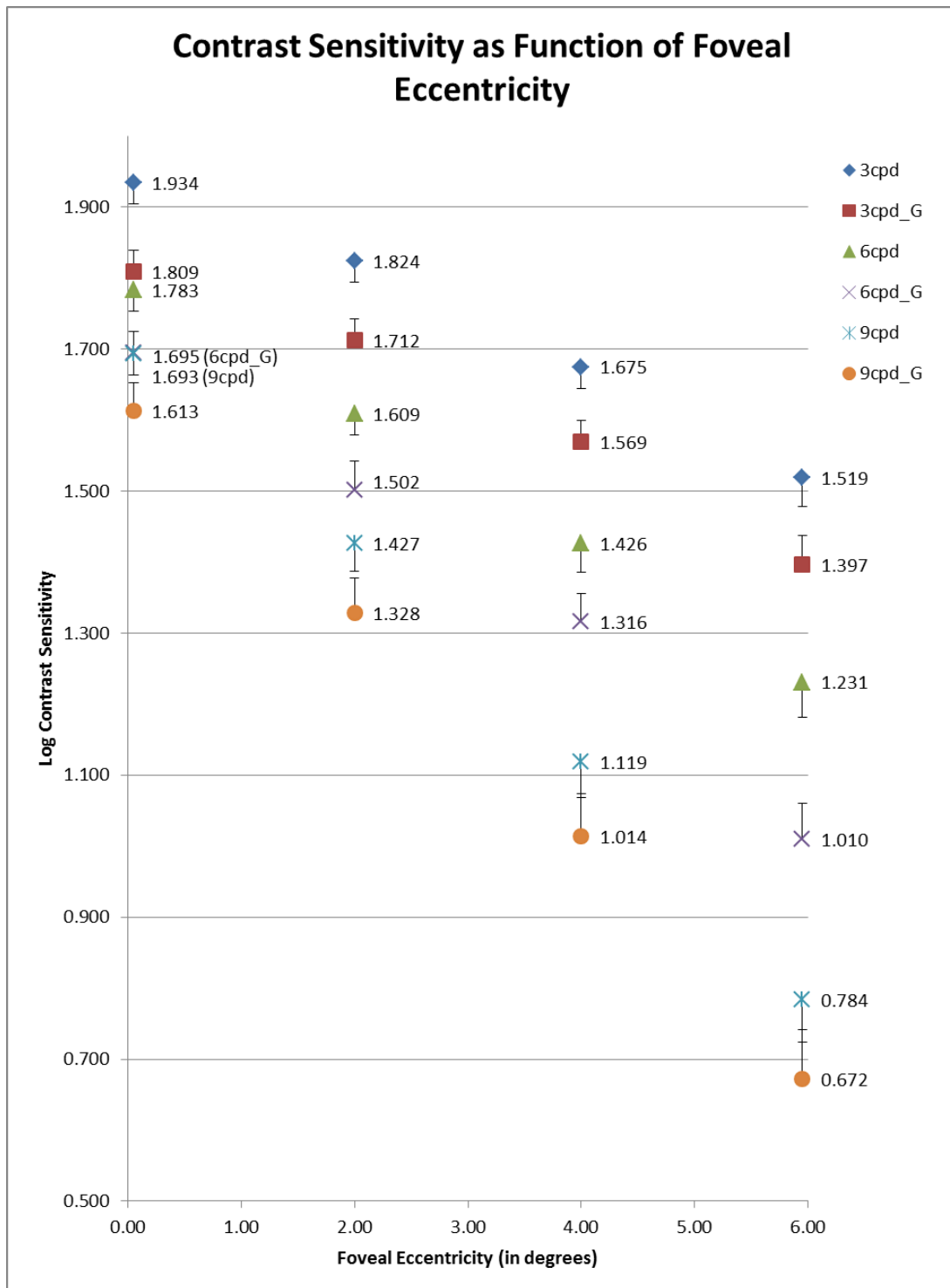
Figure 19
Mean contrast sensitivity values for all targets (3,6,9cpd) along all meridians (horizontal and vertical) for the 33 subject sample as a function of foveal eccentricity. Blue diamonds indicate contrast sensitivity without flanking glare for 3cpd stimuli, red squares indicate contrast sensitivity with flanking glare for 3cpd stimuli , green triangles indicate contrast sensitivity without flanking glare for 6cpd stimuli, lavender X indicates contrast sensitivity with flanking glare for 6cpd stimuli, blue X indicates contrast sensitivity without flanking glare for 9cpd stimuli and orange circles indicate contrast sensitivity with flanking glare for 9cpd stimuli.

Appendix 2

		Temporal	Superior	Nasal	Inferior
Temporal	Pearson Correlation	1.000	0.962	0.964	0.957
	Sig. (2-tailed)	-------	p<0.001	p<0.001	p<0.001
Superior	Pearson Correlation	0.962	1.000	0.955	0.965
	Sig. (2-tailed)	p<0.001	-------	p<0.001	p<0.001
Nasal	Pearson Correlation	0.964	0.955	1.000	0.968
	Sig. (2-tailed)	p<0.001	p<0.001	-------	p<0.001
Inferior	Pearson Correlation	0.957	0.965	0.968	1.000
	Sig. (2-tailed)	p<0.001	p<0.001	p<0.001	-------

Table 1
Table indicating correlation and significance measures for MPOD at 2° of eccentricity along the 4 principle meridians

		Temporal	Superior	Nasal	Inferior
Temporal	Pearson Correlation	1.000	0.931	0.942	0.930
	Sig. (2-tailed)	-------	p<0.001	p<0.001	p<0.001
Superior	Pearson Correlation	0.931	1.000	0.938	0.947
	Sig. (2-tailed)	p<0.001	-------	p<0.001	p<0.001
Nasal	Pearson Correlation	0.942	0.938	1.000	0.928
	Sig. (2-tailed)	p<0.001	p<0.001	-------	p<0.001
Inferior	Pearson Correlation	0.930	0.947	0.928	1.000
	Sig. (2-tailed)	p<0.001	p<0.001	p<0.001	-------

Table 2
Table indicating correlation and significance measures for MPOD at 4° of eccentricity along the 4 principle meridians

		Temporal	Superior	Nasal	Inferior
Temporal	Pearson Correlation	1.000	0.894	0.915	0.929
	Sig. (2-tailed)	-------	p<0.001	p<0.001	p<0.001
Superior	Pearson Correlation	0.894	1.000	0.875	0.893
	Sig. (2-tailed)	p<0.001	-------	p<0.001	p<0.001
Nasal	Pearson Correlation	0.925	0.875	1.000	0.911
	Sig. (2-tailed)	p<0.001	p<0.001	-------	p<0.001
Inferior	Pearson Correlation	0.929	0.893	0.911	1.000
	Sig. (2-tailed)	p<0.001	p<0.001	p<0.001	-------

Table 3
Table indicating correlation and significance measures for MPOD at 6° of eccentricity along the 4 principle meridians

	Kurtosis Value	Integrated AUC Stimuli Center	Integrated AUC Stimuli Highest Sensitivity Point
Subject 1	5.166	1.762	1.467
Subject 2	2.554	1.879	1.577
Subject 3	4.577	2.133	1.772
Subject 4	4.308	1.765	1.457
Subject 5	3.042	2.098	1.734
Subject 6	2.175	1.912	1.598
Subject 7	3.363	2.448	2.051
Subject 8	1.704	1.954	1.649
Subject 9	1.837	1.988	1.671
Subject 10	2.271	1.781	1.501
Subject 11	5.313	1.551	1.279
Subject 12	5.215	1.881	1.534
Subject 13	0.399	1.831	1.581
Subject 14	4.312	1.498	1.251
Subject 15	2.731	2.571	2.142
Subject 16	5.395	1.633	1.358
Subject 17	0.806	2.018	1.722
Subject 18	3.302	1.505	1.255
Subject 19	2.392	1.638	1.375
Subject 20	7.154	1.513	1.223
Subject 21	-0.763	1.705	1.524
Subject 22	1.627	2.371	2.003
Subject 23	4.603	1.666	1.392
Subject 24	1.937	1.579	1.313
Subject 25	2.112	2.135	1.789
Subject 26	2.246	0.851	0.703
Subject 27	0.825	1.245	1.051
Subject 28	1.222	1.087	0.913
Subject 29	3.719	1.346	1.109
Subject 30	2.591	2.587	2.154
Subject 31	1.049	1.693	1.436
Subject 32	3.102	1.566	1.296
Subject 33	-0.503	1.487	1.258
Mean	**2.781**	**1.778**	**1.489**
Std Dev	**1.809**	**0.393**	**0.331**

Table 4
Calculated values for kurtosis, integrated AUC assuming stimulus center and integrated AUC assuming stimulus point of highest retinal sensitivity for the 33 subject sample using MPOD values measured at 0°, 2°, 4°, 6° and 8° eccentricity.

3cpd		CS_0^o	Horiz_CS_2^o	Horiz_CS_4^o	Horiz_CS_6^o
Foveal MPOD Discrete Point	Pearson Correlation	0.087	0.054	0.285	0.154
	Sig. (2-tailed)	0.629	0.765	0.108	0.391
Foveal MPOD Integrated Stimulus Center	Pearson Correlation	0.081	0.054	0.285	0.162
	Sig. (2-tailed)	0.652	0.765	0.108	0.369
Foveal MPOD Integrated Stimulus Highest Sensitivity	Pearson Correlation	0.076	0.052	0.283	0.163
	Sig. (2-tailed)	0.675	0.775	0.110	0.364

Table 8

Correlation coefficients for MPOD at 0° and horizontal meridian contrast sensitivity at 0°, 2°, 4° and 6° for 3cpd grating targets.

3cpd		CS_0^o	Vert_CS_2^o	Vert_CS_4^o	Vert_CS_6^o
Peak Foveal MPOD Discrete Point	Pearson Correlation	0.087	0.013	0.117	0.040
	Sig. (2-tailed)	0.629	0.944	0.518	0.823
Foveal MPOD Integrated Stimulus Center	Pearson Correlation	0.081	0.018	0.127	0.053
	Sig. (2-tailed)	0.652	0.919	0.481	0.771
Foveal MPOD Integrated Stimulus Highest Sensitivity	Pearson Correlation	0.076	0.019	0.127	0.057
	Sig. (2-tailed)	0.675	0.917	0.482	0.753

Table 9

Correlation coefficients for MPOD at 0° and vertical meridian contrast sensitivity at 0°, 2°, 4° and 6° for 3cpd grating targets.

3cpd		CS_0^o	CS_2^o	CS_4^o	CS_6^o
Foveal MPOD Discrete Point	Pearson Correlation	0.087	-0.013	0.180	0.076
	Sig. (2-tailed)	0.629	0.944	0.316	0.673
Foveal MPOD Integrated Stimulus Center	Pearson Correlation	0.081	-0.014	0.185	0.088
	Sig. (2-tailed)	0.652	0.938	0.303	0.627
Foveal MPOD Integrated Stimulus Highest Sensitivity	Pearson Correlation	0.076	-0.017	0.185	0.092
	Sig. (2-tailed)	0.675	0.924	0.304	0.611

Table 10

Correlation coefficients for MPOD at 0° and mean contrast sensitivity at 0°, 2°, 4° and 6° for 3cpd grating targets.

3cpd		Horiz_CS_2^o
2° MPOD Discrete Point	Pearson Correlation	-0.215
	Sig. (2-tailed)	0.229
2° MPOD Integrated Stimulus Center	Pearson Correlation	-0.222
	Sig. (2-tailed)	0.213
2° MPOD Integrated Stimulus Highest Sensitivity	Pearson Correlation	-0.278
	Sig. (2-tailed)	0.117

Table 11

Correlation coefficients for MPOD at 2° and horizontal meridian contrast sensitivity at 2° for 3cpd grating targets.

3cpd		Vert_CS_2^o
2° MPOD Discrete Point	Pearson Correlation	-0.202
	Sig. (2-tailed)	0.260
2° MPOD Integrated Stimulus Center	Pearson Correlation	-0.214
	Sig. (2-tailed)	0.232
2° MPOD Integrated Stimulus Highest Sensitivity	Pearson Correlation	-0.276
	Sig. (2-tailed)	0.120

Table 12

Correlation coefficients for MPOD at 2° and vertical meridian contrast sensitivity at 2° for 3cpd grating targets.

3cpd		CS_2^o
2° MPOD Discrete Point	Pearson Correlation	-0.214
	Sig. (2-tailed)	0.232
2° MPOD Integrated Stimulus Center	Pearson Correlation	-0.285
	Sig. (2-tailed)	0.108
2° MPOD Integrated Stimulus Highest Sensitivity	Pearson Correlation	-0.328
	Sig. (2-tailed)	0.062

Table 13

Correlation coefficients for MPOD at 2° and contrast sensitivity at 2° for 3cpd grating targets.

3cpd		Horiz_CS_4^o
4° MPOD Discrete Point	Pearson Correlation	-0.099
	Sig. (2-tailed)	0.583
4° MPOD Integrated Stimulus Center	Pearson Correlation	-0.120
	Sig. (2-tailed)	0.506
4° MPOD Integrated Stimulus Highest Sensitivity	Pearson Correlation	-0.105
	Sig. (2-tailed)	0.560

Table 14

Correlation coefficients for MPOD at 4° and horizontal meridian contrast sensitivity at 4° for 3cpd grating targets.

3cpd		Vert_CS_4^o
4° MPOD Discrete Point	Pearson Correlation	-0.197
	Sig. (2-tailed)	0.272
4° MPOD Integrated Stimulus Center	Pearson Correlation	-0.228
	Sig. (2-tailed)	0.202
4° MPOD Integrated Stimulus Highest Sensitivity	Pearson Correlation	-0.245
	Sig. (2-tailed)	0.170

Table 15

Correlation coefficients for MPOD at 4° and vertical meridian contrast sensitivity at 4° for 3cpd grating targets.

3cpd		CS_4^o
4° MPOD Discrete Point	Pearson Correlation	-0.129
	Sig. (2-tailed)	0.474
4° MPOD Integrated Stimulus Center	Pearson Correlation	-0.138
	Sig. (2-tailed)	0.444
4° MPOD Integrated Stimulus Highest Sensitivity	Pearson Correlation	-0.132
	Sig. (2-tailed)	0.463

Table 16

Correlation coefficients for MPOD at 4° and contrast sensitivity at 4° for 3cpd grating targets.

3cpd		Horiz_CS_6^o
6° MPOD Discrete Point	Pearson Correlation	-0.113
	Sig. (2-tailed)	0.531
6° MPOD Integrated Stimulus Center	Pearson Correlation	-0.179
	Sig. (2-tailed)	0.319
6° MPOD Integrated Stimulus Highest Sensitivity	Pearson Correlation	-0.057
	Sig. (2-tailed)	0.752

Table 17

Correlation coefficients for MPOD at 6° and horizontal meridian contrast sensitivity at 6° for 3cpd grating targets.

3cpd		Vert_CS_6^o
6° MPOD Discrete Point	Pearson Correlation	-0.191
	Sig. (2-tailed)	0.288
6° MPOD Integrated Stimulus Center	Pearson Correlation	-0.250
	Sig. (2-tailed)	0.160
6° MPOD Integrated Stimulus Highest Sensitivity	Pearson Correlation	-0.139
	Sig. (2-tailed)	0.441

Table 18

Correlation coefficients for MPOD at 6° and vertical meridian contrast sensitivity at 6° for 3cpd grating targets.

3cpd		CS_6^o
6° MPOD Discrete Point	Pearson Correlation	-0.148
	Sig. (2-tailed)	0.412
6° MPOD Integrated Stimulus Center	Pearson Correlation	-0.207
	Sig. (2-tailed)	0.248
6° MPOD Integrated Stimulus Highest Sensitivity	Pearson Correlation	-0.089
	Sig. (2-tailed)	0.622

Table 19

Correlation coefficients for MPOD at 6° and contrast sensitivity at 6° for 3cpd grating targets.

Independent Samples t-test		
3cpd	**t-value**	**Sig.**
CS_0^o	0.299	0.769
CS_2^o	0.416	0.683
CS_4^o	0.475	0.641
CS_6^o	0.713	0.486

Table 20

Independent samples t-test for contrast sensitivity at 0°, 2°, 4° and 6° for 6cpd grating targets between the highest and lowest quartiles of peak foveal MPOD integrated across 1° assuming stimulus point at highest retinal sensitivity. Levene's Test for Equal Variances was non-significant so equal variances were assumed.

6cpd		**CS_0^o**	**Horiz_CS_2^o**	**Horiz_CS_4^o**	**Horiz_CS_6^o**
Foveal MPOD Discrete Point	Pearson Correlation	0.237	0.027	0.222	0.202
	Sig. (2-tailed)	0.183	0.883	0.214	0.260
Foveal MPOD Integrated Stimulus Center	Pearson Correlation	0.227	0.031	0.230	0.214
	Sig. (2-tailed)	0.204	0.864	0.198	0.231
Foveal MPOD Integrated Stimulus Highest Sensitivity	Pearson Correlation	0.215	0.024	0.230	0.216
	Sig. (2-tailed)	0.229	0.894	0.197	0.227

Table 21

Correlation coefficients for MPOD at 0° and horizontal meridian contrast sensitivity at 0°, 2°, 4° and 6° for 6cpd grating targets.

6cpd		**CS_0^o**	**Vert_CS_2^o**	**Vert_CS_4^o**	**Vert_CS_6^o**
Foveal MPOD Discrete Point	Pearson Correlation	0.237	0.228	0.186	0.240
	Sig. (2-tailed)	0.183	0.202	0.301	0.179
Foveal MPOD Integrated Stimulus Center	Pearson Correlation	0.227	0.236	0.205	0.254
	Sig. (2-tailed)	0.204	0.186	0.253	0.154
Foveal MPOD Integrated Stimulus Highest Sensitivity	Pearson Correlation	0.215	0.232	0.214	0.263
	Sig. (2-tailed)	0.229	0.194	0.232	0.140

Table 22

Correlation coefficients for MPOD at 0° and horizontal meridian contrast sensitivity at 0°, 2°, 4° and 6° for 6cpd grating targets.

6cpd		CS_0^0	CS_2^0	CS_4^0	CS_6^0
Foveal MPOD Discrete Point	Pearson Correlation	0.237	0.192	0.213	0.228
	Sig. (2-tailed)	0.183	0.285	0.235	0.203
Foveal MPOD Integrated Stimulus Center	Pearson Correlation	0.227	0.200	0.226	0.238
	Sig. (2-tailed)	0.204	0.265	0.206	0.183
Foveal MPOD Integrated Stimulus Highest Sensitivity	Pearson Correlation	0.215	0.193	0.228	0.239
	Sig. (2-tailed)	0.229	0.281	0.201	0.180

Table 23

Correlation coefficients for MPOD at 0° and mean contrast sensitivity at 0°, 2°, 4° and 6° for 6cpd grating targets.

6cpd		Horiz_CS_2^o
2° MPOD Discrete Point	Pearson Correlation	-0.234
	Sig. (2-tailed)	0.190
2° MPOD Integrated Stimulus Center	Pearson Correlation	-0.254
	Sig. (2-tailed)	0.154
2° MPOD Integrated Stimulus Highest Sensitivity	Pearson Correlation	-0.300
	Sig. (2-tailed)	0.090

Table 24

Correlation coefficients for MPOD at 2° and horizontal meridian contrast sensitivity at 2° for 6cpd grating targets.

6cpd		Vert_CS_2^o
2° MPOD Discrete Point	Pearson Correlation	-0.134
	Sig. (2-tailed)	0.456
2° MPOD Integrated Stimulus Center	Pearson Correlation	-0.149
	Sig. (2-tailed)	0.408
2° MPOD Integrated Stimulus Highest Sensitivity	Pearson Correlation	-0.262
	Sig. (2-tailed)	0.141

Table 25

Correlation coefficients for MPOD at 2° and vertical meridian contrast sensitivity at 2° for 6cpd grating targets.

6cpd		CS_2^o
2° MPOD Discrete Point	Pearson Correlation	-0.074
	Sig. (2-tailed)	0.681
2° MPOD Integrated Stimulus Center	Pearson Correlation	-0.180
	Sig. (2-tailed)	0.317
2° MPOD Integrated Stimulus Highest Sensitivity	Pearson Correlation	-0.271
	Sig. (2-tailed)	0.127

Table 26
Correlation coefficients for MPOD at 2° and mean contrast sensitivity at 2° for 6cpd grating targets.

6cpd		Horiz_CS_4^o
4° MPOD Discrete Point	Pearson Correlation	0.001
	Sig. (2-tailed)	0.997
4° MPOD Integrated Stimulus Center	Pearson Correlation	-0.024
	Sig. (2-tailed)	0.895
4° MPOD Integrated Stimulus Highest Sensitivity	Pearson Correlation	-0.016
	Sig. (2-tailed)	0.932

Table 27
Correlation coefficients for MPOD at 4° and horizontal meridian contrast sensitivity at 4° for 6cpd grating targets.

6cpd		Vert_CS_4^o
4° MPOD Discrete Point	Pearson Correlation	0.023
	Sig. (2-tailed)	0.897
4° MPOD Integrated Stimulus Center	Pearson Correlation	-0.008
	Sig. (2-tailed)	0.964
4° MPOD Integrated Stimulus Highest Sensitivity	Pearson Correlation	-0.070
	Sig. (2-tailed)	0.699

Table 28
Correlation coefficients for MPOD at 4° and horizontal meridian contrast sensitivity at 4° for 6cpd grating targets.

6cpd		CS_4^o
4° MPOD Discrete Point	Pearson Correlation	-0.023
	Sig. (2-tailed)	0.899
4° MPOD Integrated Stimulus Center	Pearson Correlation	-0.066
	Sig. (2-tailed)	0.713
4° MPOD Integrated Stimulus Highest Sensitivity	Pearson Correlation	-0.091
	Sig. (2-tailed)	0.616

Table 29
Correlation coefficients for MPOD at 4° and mean contrast sensitivity at 4° for 6cpd grating targets.

6cpd		Horiz_CS_6^o
6° MPOD Discrete Point	Pearson Correlation	0.024
	Sig. (2-tailed)	0.896
6° MPOD Integrated Stimulus Center	Pearson Correlation	-0.073
	Sig. (2-tailed)	0.687
6° MPOD Integrated Stimulus Highest Sensitivity	Pearson Correlation	0.016
	Sig. (2-tailed)	0.931

Table 30
Correlation coefficients for MPOD at 6° and horizontal meridian contrast sensitivity at 6° for 6cpd grating targets.

6cpd		Vert_CS_6^o
6° MPOD Discrete Point	Pearson Correlation	0.182
	Sig. (2-tailed)	0.310
6° MPOD Integrated Stimulus Center	Pearson Correlation	0.145
	Sig. (2-tailed)	0.421
6° MPOD Integrated Stimulus Highest Sensitivity	Pearson Correlation	0.205
	Sig. (2-tailed)	0.252

Table 31
Correlation coefficients for MPOD at 6° and vertical meridian contrast sensitivity at 6° for 6cpd grating targets.

6cpd		CS_6^o
6° MPOD Discrete Point	Pearson Correlation	0.011
	Sig. (2-tailed)	0.954
6° MPOD Integrated Stimulus Center	Pearson Correlation	0.074
	Sig. (2-tailed)	0.684
6° MPOD Integrated Stimulus Highest Sensitivity	Pearson Correlation	0.131
	Sig. (2-tailed)	0.467

Table 32
Correlation coefficients for MPOD at 6° and contrast sensitivity at 6° for 6cpd grating targets.

Independent Samples t-test		
6cpd	**t-value**	**Sig.**
CS_0^o	0.995	0.355
CS_2^o	0.947	0.358
CS_4^o	1.130	0.275
CS_6^o	1.137	0.272

Table 33
Independent samples t-test for contrast sensitivity at 0°, 2°, 4° and 6° for 6cpd grating targets between the highest and lowest quartiles of peak foveal MPOD integrated across 1° assuming stimulus point at highest retinal sensitivity. Levene's Test for Equal Variances was non-significant so equal variances were assumed.

9cpd		CS_0^o	Horiz_CS_2^o	Horiz_CS_4^o	Horiz_CS_6^o
Foveal MPOD Discrete Point	Pearson Correlation	0.148	0.099	0.103	0.167
	Sig. (2-tailed)	0.412	0.583	0.567	0.354
Foveal MPOD Integrated Stimulus Center	Pearson Correlation	0.143	0.107	0.114	0.175
	Sig. (2-tailed)	0.428	0.554	0.526	0.331
Foveal MPOD Integrated Stimulus Highest Sensitivity	Pearson Correlation	0.133	0.103	0.114	0.175
	Sig. (2-tailed)	0.461	0.570	0.526	0.331

Table 34
Correlation coefficients for MPOD at 0° and horizontal meridian contrast sensitivity at 0°, 2°, 4° and 6° for 9cpd grating targets.

9cpd		CS_0^o	Vert_CS_2^o	Vert_CS_4^o	Vert_CS_6^o
Foveal MPOD Discrete Point	Pearson Correlation	0.148	-0.188	-0.020	-0.015
	Sig. (2-tailed)	0.412	0.294	0.910	0.934
Foveal MPOD Integrated Stimulus Center	Pearson Correlation	0.143	-0.171	-0.005	-0.006
	Sig. (2-tailed)	0.428	0.342	0.978	0.974
Foveal MPOD Integrated Stimulus Highest Sensitivity	Pearson Correlation	0.133	-0.165	-0.001	-0.001
	Sig. (2-tailed)	0.461	0.360	0.997	0.998

Table 35

Correlation coefficients for MPOD at 0° and vertical meridian contrast sensitivity at 0°, 2°, 4° and 6° for 9cpd grating targets.

9cpd		CS_0^o	CS_2^o	CS_4^o	CS_6^o
Foveal MPOD Discrete Point	Pearson Correlation	0.148	-0.106	-0.021	0.067
	Sig. (2-tailed)	0.412	0.558	0.908	0.713
Foveal MPOD Integrated Stimulus Center	Pearson Correlation	0.143	-0.089	-0.005	0.075
	Sig. (2-tailed)	0.428	0.622	0.979	0.678
Foveal MPOD Integrated Stimulus Highest Sensitivity	Pearson Correlation	0.133	-0.090	-0.004	0.077
	Sig. (2-tailed)	0.461	0.620	0.982	0.669

Table 36

Correlation coefficients for MPOD at 0° and mean contrast sensitivity at 0°, 2°, 4° and 6° for 9cpd grating targets

9cpd		Horiz_CS_2^o
2° MPOD Discrete Point	Pearson Correlation	-0.156
	Sig. (2-tailed)	0.386
2° MPOD Integrated Stimulus Center	Pearson Correlation	-0.184
	Sig. (2-tailed)	0.306
2° MPOD Integrated Stimulus Highest Sensitivity	Pearson Correlation	-0.248
	Sig. (2-tailed)	0.165

Table 37

Correlation coefficients for MPOD at 2° and horizontal meridian contrast sensitivity at 2° for 9cpd grating targets.

9cpd		Vert_CS_2^o
2° MPOD Discrete Point	Pearson Correlation	-0.278
	Sig. (2-tailed)	0.117
2° MPOD Integrated Stimulus Center	Pearson Correlation	-0.290
	Sig. (2-tailed)	0.102
2° MPOD Integrated Stimulus Highest Sensitivity	Pearson Correlation	-0.340
	Sig. (2-tailed)	0.053

Table 38
Correlation coefficients for MPOD at 2° and vertical meridian contrast sensitivity at 2° for 9cpd grating targets.

9cpd		CS_2^o
2° MPOD Discrete Point	Pearson Correlation	-0.220
	Sig. (2-tailed)	0.219
2° MPOD Integrated Stimulus Center	Pearson Correlation	-0.262
	Sig. (2-tailed)	0.141
2° MPOD Integrated Stimulus Highest Sensitivity	Pearson Correlation	-0.297
	Sig. (2-tailed)	0.093

Table 39
Correlation coefficients for MPOD at 2° and contrast sensitivity at 2° for 9cpd grating targets.

9cpd		Horiz_CS_4^o
4° MPOD Discrete Point	Pearson Correlation	-0.163
	Sig. (2-tailed)	0.366
4° MPOD Integrated Stimulus Center	Pearson Correlation	-0.174
	Sig. (2-tailed)	0.332
4° MPOD Integrated Stimulus Highest Sensitivity	Pearson Correlation	-0.179
	Sig. (2-tailed)	0.318

Table 40
Correlation coefficients for MPOD at 4° and horizontal meridian contrast sensitivity at 4° for 9cpd grating targets.

9cpd		Vert_CS_4^o
4° MPOD Discrete Point	Pearson Correlation	-0.223
	Sig. (2-tailed)	0.213
4° MPOD Integrated Stimulus Center	Pearson Correlation	-0.294
	Sig. (2-tailed)	0.096
4° MPOD Integrated Stimulus Highest Sensitivity	Pearson Correlation	-0.309
	Sig. (2-tailed)	0.081

Table 41
Correlation coefficients for MPOD at 4° and vertical meridian contrast sensitivity at 4° for 9cpd grating targets.

9cpd		CS_4^o
4° MPOD Discrete Point	Pearson Correlation	-0.271
	Sig. (2-tailed)	0.127
4° MPOD Integrated Stimulus Center	Pearson Correlation	-0.292
	Sig. (2-tailed)	0.099
4° MPOD Integrated Stimulus Highest Sensitivity	Pearson Correlation	-0.301
	Sig. (2-tailed)	0.088

Table 42
Correlation coefficients for MPOD at 4° and mean contrast sensitivity at 4° for 9cpd grating targets.

9cpd		Horiz_CS_6^o
6° MPOD Discrete Point	Pearson Correlation	-0.013
	Sig. (2-tailed)	0.943
6° MPOD Integrated Stimulus Center	Pearson Correlation	-0.062
	Sig. (2-tailed)	0.730
6° MPOD Integrated Stimulus Highest Sensitivity	Pearson Correlation	-0.022
	Sig. (2-tailed)	0.902

Table 43
Correlation coefficients for MPOD at 6° and horizontal meridian contrast sensitivity at 6° for 9cpd grating targets.

9cpd		Vert_CS_6^o
6° MPOD Discrete Point	Pearson Correlation	-0.110
	Sig. (2-tailed)	0.543
6° MPOD Integrated Stimulus Center	Pearson Correlation	-0.128
	Sig. (2-tailed)	0.479
6° MPOD Integrated Stimulus Highest Sensitivity	Pearson Correlation	-0.055
	Sig. (2-tailed)	0.763

Table 44

Correlation coefficients for MPOD at 6° and vertical meridian contrast sensitivity at 6° for 9cpd grating targets.

9cpd		CS_6^o
6° MPOD Discrete Point	Pearson Correlation	-0.109
	Sig. (2-tailed)	0.547
6° MPOD Integrated Stimulus Center	Pearson Correlation	-0.128
	Sig. (2-tailed)	0.477
6° MPOD Integrated Stimulus Highest Sensitivity	Pearson Correlation	-0.067
	Sig. (2-tailed)	0.710

Table 45

Correlation coefficients for MPOD at 6° and contrast sensitivity at 6° for 9cpd grating targets.

Independent Samples t-test		
9cpd	**t-value**	**Sig.**
CS_0^0	0.792	0.440
CS_2^0	0.669	0.494
CS_4^0	0.141	0.890
CS_6^0	0.442	0.665

Table 46

Independent samples t-test for contrast sensitivity at 0°, 2°, 4° and, 4° for 6cpd grating targets between the highest and lowest quartiles of peak foveal MPOD integrated across 1^0 assuming stimulus point at highest retinal sensitivity. Levene's Test for Equal Variances was non-significant so equal variances were assumed.

3cpd		GD_0^o	RGD_0^o	GD_2^o	RGD_2^o	GD_4^o	RGD_4^o	GD_6^o	RGD_6^o
Peak Foveal MPOD Discrete Point	Pearson Correlation	-0.079	-0.205	-0.327	-0.335	-0.205	-0.261	-0.219	-0.254
	Sig. (2-tailed)	0.663	0.252	0.063	0.058	0.253	0.143	0.222	0.150
Peak Foveal MPOD Integrated Stimulus Center	Pearson Correlation	-0.101	-0.217	-0.333	-0.342	-0.208	-0.266	-0.210	-0.251
	Sig. (2-tailed)	0.575	0.226	0.058	0.056	0.245	0.134	0.241	0.155
Peak Foveal MPOD Integrated Stimulus Highest Sensitivity	Pearson Correlation	-0.083	-0.228	-0.331	-0.340	-0.205	-0.264	-0.204	-0.249
	Sig. (2-tailed)	0.646	0.203	0.060	0.055	0.253	0.138	0.256	0.159

Table 47

Correlation coefficients for MPOD at 0° and glare disability and relative glare disability at 0°, 2°, 4° and 6° for 3cpd grating targets.

3cpd		GD_2^o	RGD_2^o
2° MPOD Discrete Point	Pearson Correlation	-0.240	-0.138
	Sig. (2-tailed)	0.179	0.445
2° MPOD Integrated Stimulus Center	Pearson Correlation	-0.217	-0.113
	Sig. (2-tailed)	0.225	0.530
2° MPOD Integrated Stimulus Highest Sensitivity	Pearson Correlation	-0.331	-0.340
	Sig. (2-tailed)	0.060	0.053

Table 48

Correlation coefficients for MPOD at 2° and glare disability and relative glare disability at 2° for 3cpd grating targets.

3cpd		GD_4^o	RGD_4^o
4° MPOD Discrete Point	Pearson Correlation	-0.022	0.046
	Sig. (2-tailed)	0.904	0.801
4° MPOD Integrated Stimulus Center	Pearson Correlation	0.052	-0.142
	Sig. (2-tailed)	0.774	0.432
4° MPOD Integrated Stimulus Highest Sensitivity	Pearson Correlation	0.027	0.112
	Sig. (2-tailed)	0.880	0.534

Table 49

Correlation coefficients for MPOD at 4° and glare disability and relative glare disability at 4° for 3cpd grating targets.

3cpd		GD_6^o	RGD_6^o
6° MPOD Discrete Point	Pearson Correlation	-0.176	-0.116
	Sig. (2-tailed)	0.326	0.521
6° MPOD Integrated Stimulus Center	Pearson Correlation	-0.243	-0.166
	Sig. (2-tailed)	0.173	0.357
6° MPOD Integrated Stimulus Highest Sensitivity	Pearson Correlation	-0.224	-0.208
	Sig. (2-tailed)	0.210	0.244

Table 50
Correlation coefficients for MPOD at 6° and glare disability and relative glare disability at 6° for 3cpd grating targets.

Regression Fit for 3cpd Stimuli		
Integrated Foveal MPOD	**F**	**Significance**
RGD_0^o	1.368	0.251
RGD_2^o	4.073	0.052
RGD_4^o	2.309	0.139
RGD_6^o	2.567	0.119

Table 53
Regression fit significance table for foveal MPOD integrated across 1° assuming stimulus point at highest retinal sensitivity and relative glare disability at 0°, 2°, 4° and 6° using 3cpd grating targets.

Multiple Regression Fit for 3cpd Stimuli		
Integrated Foveal MPOD and Kurtosis as Predictors	**F**	**Significance**
RGD_0^o	0.720	0.495
RGD_2^o	1.992	0.154
RGD_4^o	1.912	0.165
RGD_6^o	1.659	0.207

Table 54
Multiple regression fit significance table for foveal MPOD integrated across 1° assuming stimulus point at highest retinal sensitivity and kurtosis values as predictors for relative glare disability at 0°, 2°, 4° and 6° using 3cpd grating targets.

6cpd		GD_2^o	RGD_2^o
2° MPOD Discrete Point	Pearson Correlation	-0.294	-0.299
	Sig. (2-tailed)	0.096	0.091
2° MPOD Integrated Stimulus Center	Pearson Correlation	-0.288	-0.298
	Sig. (2-tailed)	0.104	0.092
2° MPOD Integrated Stimulus Highest Sensitivity	Pearson Correlation	-0.232	-0.267
	Sig. (2-tailed)	0.194	0.133

Table 56
Correlation coefficients for MPOD at 2° and glare disability and relative glare disability at 2° for 6cpd grating targets.

6cpd		GD_4^o	RGD_4^o
4° MPOD Discrete Point	Pearson Correlation	-0.095	-0.149
	Sig. (2-tailed)	0.600	0.408
4° MPOD Integrated Stimulus Center	Pearson Correlation	-0.115	-0.138
	Sig. (2-tailed)	0.525	0.444
4° MPOD Integrated Stimulus Highest Sensitivity	Pearson Correlation	-0.127	-0.151
	Sig. (2-tailed)	0.481	0.401

Table 57
Correlation coefficients for MPOD at 4° and glare disability and relative glare disability at 4° for 6cpd grating targets.

6cpd		GD_6^o	RGD_6^o
6° MPOD Discrete Point	Pearson Correlation	0.020	-0.053
	Sig. (2-tailed)	0.914	0.770
6° MPOD Integrated Stimulus Center	Pearson Correlation	-0.061	-0.142
	Sig. (2-tailed)	0.735	0.431
6° MPOD Integrated Stimulus Highest Sensitivity	Pearson Correlation	-0.017	-0.113
	Sig. (2-tailed)	0.924	0.530

Table 58
Correlation coefficients for MPOD at 6° and glare disability and relative glare disability at 6° for 6cpd grating targets.

Multiple Regression Fit for 6cpd Stimuli		
Integrated Foveal MPOD and Kurtosis as Predictors	**F**	**Significance**
RGD_0^o	3.211	0.054
RGD_2^o	2.207	0.128
RGD_4^o	1.140	0.333
RGD_6^o	0.503	0.610

Table 61
Multiple regression fit significance table for foveal MPOD integrated across 1° assuming stimulus point at highest retinal sensitivity and kurtosis values as predictors for relative glare disability at 0°, 2°, 4° and 6° using 6cpd grating targets.

9cpd		**GD_6^o**	**RGD_6^o**
6° MPOD Discrete Point	Pearson Correlation	-0.103	-0.078
	Sig. (2-tailed)	0.567	0.667
6° MPOD Integrated Stimulus Center	Pearson Correlation	-0.141	-0.124
	Sig. (2-tailed)	0.432	0.493
6° MPOD Integrated Stimulus Highest Sensitivity	Pearson Correlation	-0.087	-0.126
	Sig. (2-tailed)	0.629	0.485

Table 65
Correlation coefficients for MPOD at 6° and glare disability and relative glare disability at 6° for 9cpd grating targets.